Ulm University Hospital

Clinic for Internal Medicine II

Medical director: Prof. Rottbauer

Generation of an isogenic human induced pluripotent stem cell line for characterization of the SCN5A-mediated long QT syndrome

Dissertation zur Erlangung des Doktorgrades der Medizin der Medizinischen Fakultät der Universität Ulm

Ricarda Schmid

born in Ravensburg

2025

Amtierender Dekan: Prof. Dr. Thomas Wirth

1. Berichterstatter: Prof. Dr. rer. nat. Steffen Just

2. Berichterstatter: Prof. Dr. Leda Dimou

Tag der Promotion: 26.02.2026

Table of content

List of abbreviations III

1. Introduction 1

1.1. Sudden cardiac death and diseases caused by cardiac channelopathies. 1

1.2. History, clinical presentation and genetic background of long QT syndrome (LQTS) 1,2,3 2

1.3. SCN5A and long QT syndrome 3 3

1.4. Induced pluripotent stem cells (iPSC) as an in vitro model to investigate cardiovascular diseases 5

1.5. CRISPR/Cas9 technologies to generate an isogenic control of patient-derived iPSC 7

1.6. Zebrafish (Dan rerio) as an *in vivo* model to investigate cardiovascular diseases 9

1.7. Zebrafish heart and electrophysiological similarities between zebrafish and human heart 11

1.8. From benchside to bedside and personalizend medicine 13

1.9. Aim of the work 15

2. Materials and Methods 16

2.1. Materials 16

2.2. Methods 28

3. Results 39

3.1. Novel SCN5A mutation in a patient with LQTS and generation of first in-silico models 39

3.2. Generating an induced pluripotent stem cell (iPSC) line from a patient with SCN5A mutation 41

3.3. Successful correction of the mutated patient iPSC to obtain an isogenic control 42

3.4. Differentiation of patient-derived iPSC, and isogenic control cells into ventricular cardiomyocytes 47

3.5. The maturity of iPSC-derived ventricular CMs from wildtype control, isogenic control and patient was proved by immunostaining 49

3.6. Isogenic control iPSC- and patient iPSC-derived ventricular cardiomyocytes do not show differences in protein expression levels of SCN5A 50

3.7. Wildtype control, isogenic control, and patient iPSC-derived ventricular cardiomyocytes do not show differences in SCN5A localization in immunostaining 52

3.8. Isogenic control iPSC and SCN5A$^{1072T>C}$ iPSC-derived ventricular cardiomyocytes do not show differences in SCN5A, RYR and SERCA2a mRNA expression 54

3.9. Calcium dynamics are altered in SCN5A$^{1072T>C}$ iPSC-derived ventricular cardiomyocytes compared to wildtype control and isogenic control iPSC-derived cardiomyocytes 55

3.10. Electrophysiological analysis of beating period shows no difference between isogenic control and SCN5A$^{1072T>C}$ cells 60

3.11. SCN5A$^{1072T>C}$ iPSC-derived cardiomyocytes show an impaired conduction velocity in comparison to isogenic control cells 61

3.12. ECG signals from zebrafish embryos can be effectively recorded and exhibit a morphology comparable to human 63

3.13. TgSCN5A$^{1072T>C}$ zebrafish embryos do not show QT-prolongation at 48hpf compared to TÜAB wildtype fish 65

3.14. TgSCN5A$^{1072T>C}$ zebrafish embryos show QT prolongation at 72hpf 66

3.15. TgSCN5A$^{1072T>C}$ +MO injected zebrafish show a long QT phenotype already at 48hpf 68

4. Discussion 72

4.1. Clinical and experimental background of a known SCN5A mutation in comparison to the novel SCN5A$^{1072T>C}$ mutation 72

4.2. SCN5A$^{1072T>C}$ mutated patient iPSC-derived ventricular cardiomyocytes do not show structural abnormalities 73

4.3. Patient iPSC-derived ventricular CMs do not show major electrophysiological abnormalities but altered Ca^{2+} dynamics 75

4.4. SCN5A$^{1072T>C}$ mutation causes QT-prolongation in embryo zebrafish at 72hpf 78

4.5. Conclusion and comparative analysis of *in vitro* and *in vivo* results 79

5. Summary 80

6. Bibliography 82

7. Acknowledgements 91

8. Curriculum Vitae 92

List of abbreviations

ALPM	anterior lateral plate mesoderm
APD	action potential duration
CALM	Calmodulin
CAR-T	Chimeric Antigen Receptor-T-cell
CMs	cardiomyocytes
CRISPR/Cas9	Clustered Regularly Interspaced Short Palindromic Repeats/CRISPR-associated protein 9
crRNA	CRISPR RNA
ctrl	control
DAPI	4′,6-Diamidin-2-phenylindol
DMEM/F12	Dulbecco's Modified Eagle Medium F-12
DMSO	Dimethyl sulfoxide
E3	Embryo Medium
ECG	electrocardiography
E.coli	Escherichia coli
ENU	Ethyl-Nitrosurea
FACS	Fluorescence Activated Cell Sorting
FBS	fetal bovine serum
FDA	Food and Drug Administration
FPD	field potential duration
GBD	Global Burden of Disease
GFP	green fluorescent protein
HDR	homology-directed repair
hESC	human embryonic stem cells
hpf	hours post fertilization
HR-arm	homologous recombination arm
ICD	implantable cardioverter defibrillator
iPSC	induced pluripotent stem cells
KCl	potassium chloride
KCNQ1	potassium voltage-gated channel subfamily Q member1
KO-DMEM	KnockOut Dulbecco's Modified Eagle Medium

KPQ	deletion of lysine-proline-glutamine (KPQ) between domains III and IV of NaV1.5
LB	lysogeny broth
LEU	leucine
LQTS	long QT syndrome
MEA	multiwell microelectrode array
MEF	mouse embryonic fibroblasts
MO	morpholino
MOI	multiplicity of infection
myh6/amch	atrial myosin heavy chain
myl7	myosin light chain polypeptide 7
NaV1.5	voltage-gated sodium channel subtype 1.5
NGS	next generation sequencing
NHEJ	nonhomologous end joining
NKX-2.5	Homeobox protein Nkx-2.5
Oct4	Octamer-binding transcription factor 4
PAM	Protospacer Adjacent Motif
PBS	phosphate buffered saline
PCR	polymerase chain reaction
PHE	Phenylalanine
Pou5f1	POU domain, class 5, transcription factor 1
PVDF	polyvinylidene fluoride
qRT-PCR	quantitative reverse transcription polymerase chain reaction
ROCK-inhibitor	rho-associated protein kinase inhibitor
ROI	regions of interest
RT	room temperature
RYR	ryanodine receptor
SADS	sudden arrythmic death syndrome
SCD	sudden cardiac death
SCN5A	sodium voltage-gated channel alpha subunit 5
SDS	sodium dodecyl sulfate
SERCA2a	Sarcoplasmic/endoplasmic reticulum calcium ATPase 2a

sgRNA	single-guide RNA
tracrRNA	trans-acting RNA
TBE buffer	tris-borate-EDTA buffer
TgSCN5A$^{1072T>C}$	transgenic SCN5A$^{1072T>C}$ zebrafish line
TRPM4	transient receptor potential cation channel subfamily M member 4
vmhc	ventricle myosin heavy chain

1. Introduction

1.1. Sudden cardiac death and diseases caused by cardiac channelopathies

Cardiovascular disease remains the leading cause of death worldwide. The Global Burden of Disease (GBD) study estimates that there were 17.8 million deaths worldwide due to cardiovascular disease in 2017 [27].

Sudden cardiac death (SCD) is responsible for a large proportion of cardiovascular deaths and accounts for approximately 20% of all deaths in western societies [105]. Most commonly, coronary artery disease but also cardiomyopathies, valvular heart disease and inherited arrhythmias such as long QT syndrome are possible causes for sudden cardiac death [41, 105]. The definition of SCD is not always consistent. Usually, it is defined as sudden death from a cardiovascular cause, such as coronary artery disease, cardiomyopathies, or arrhythmias, occurring within one hour of the onset of symptoms (if observed) or, if not observed, as unexpected death from a cardiovascular cause where the person was known to be alive within the previous 24 hours [109]. In 40% of cases of sudden cardiac death in persons between 1 and 35 years of age, the autopsy is inconclusive [6]. SCD with negative autopsy and no toxicological cause is defined as sudden arrhythmic death syndrome (SADS), which accounts for approximately 30% of SCD in persons from 0-40 years [80]. One main reason of SADS are cardiac channelopathies, caused by gene mutations in genes encoding for cardiac ion channels or proteins that interact with these channels [43]. Mutations in ion channels can cause the channels to become dysfunctional, hypoactive or hyperactive.

Since the cellular action potential and thus the correct electrical excitation of the heart depends on the correct functions of ion channels, disturbances in the ion currents lead to disturbed action potentials and increased susceptibility to arrhythmias [83]. Diseases caused by cardiac channelopathies include, among others, long QT syndrome, short QT syndrome, Brugada syndrome, and catecholaminergic polymorphic ventricular tachycardia [43].

1.2. History, clinical presentation and genetic background of long QT syndrome (LQTS) 1,2,3

Congenital long QT syndrome (LQTS) is a life-threatening syndrome of cardiac arrhythmia and is a frequent cause of sudden cardiac death in young people with a suggested prevalence of around 1:2000 among Caucasian infants [75, 78]. The rare autosomal-recessive form of LQTS, associated with congenital neural deafness, was first published in 1957 by Jervell and Lange-Nielsen, in an article about 4 siblings who showed prolonged QT time on ECG and died at a young age [37].

In 1963 and 1964, the more common autosomal-dominant form of LQTS, not associated with other abnormalities, was described by Romano and Ward [101]. The characteristic clinical presentation of LQTS are syncope, anoxic seizures, or palpitations and QT time prolongation on ECG with the occurrence of life-threatening tachyarrhythmias, especially in the context of stress, which may be physical or psychological [76, 99]. QT time duration depends on the heart rate. Therefore, the measured QT time must be corrected depending on the heart rate, for which the most common formula is the Bazett formula. The suggested cutoffs for corrected QT time calculated with the Bazett formula, to make the diagnosis of long QT syndrome are >460ms in young people, >470 in adult women, and >450 in adult men [29].

Ventricular tachyarrhythmias resulting from LQTS are typically torsade de pointes tachycardias (TdP). These are specific to diseases that cause QT time prolongations and are often self-limiting. However, TdP can also trigger ventricular fibrillation, causing sudden cardiac death [74]. Currently, 17 genes are suspected to lead to LQTS. However, the evidence for the different genes varies and only 3 genes are known to lead to LQTS with definitive evidence. These genes are KCNQ1, KCNH2, and SCN5A [1]. These three genes cause three different types of LQTS. KCNQ1 mutations are classified as LQTS1, KCNH2 mutations cause LQTS2 and SCN5A mutations are responsible for LQTS3. LQTS1-3 cause 75% of all LQTS while other genes cause 5% and 20% remain genetically unclear [74].

In LQTS1 and LQTS2, loss-of-function mutations in KCNQ1 (LQTS1) and KCNH2 (LQTS2) cause around 35% and 30% of LQTS, respectively. Gain-of-function mutations in SCN5A (LQTS3) are responsible for around 10% [95]. Furthermore, the triggers for cardiac events differ between the LQTS forms. While most events in

LQTS1 and LQTS2 occur mainly during physical activity and emotional stress, in LQTS3 they occur mainly during rest and sleep [77]. The basis of therapy for LQTS is the administration of ß-blockers, which have an antiarrhythmic effect by preventing early after depolarizations. Additional options for treatment depend on the type of LQTS. Whereas in LQTS2 the supplementation of potassium has shown to be effective, sodium channel blockers are used in LQTS3 [103].

1.3. SCN5A and long QT syndrome 3

SCN5A, located on chromosome 3p21 (~220kDa), encodes for the alpha subunit of NaV1.5 sodium channel, which is the pore forming region of the channel, known to be important for the sodium influx in the beginning of the cardiomyocyte action potential (I_{Na}) and thus the initiation of the excitation-contraction coupling [4, 45, 102]. The pore-forming alpha subunit of the NaV1.5 voltage-dependent sodium channel is associated with a small modulatory ß subunit. The alpha subunit consists of a cytoplasmic N-terminus, 4 homologous domains (D I-IV), consisting of six transmembrane alpha helices each (S1-S6) and a cytoplasmatic C terminal domain (Figure 1). The four domains are connected by intracellular peptide chains. Segment S5 and S6 build the pore and the loop between S5 and S6 is responsible for the selectivity of the channel [72]. The outward movement of the positively charged S4 segments, which work as voltage sensors and move when the membrane depolarizes, activates the channel and opens the pore for sodium influx.

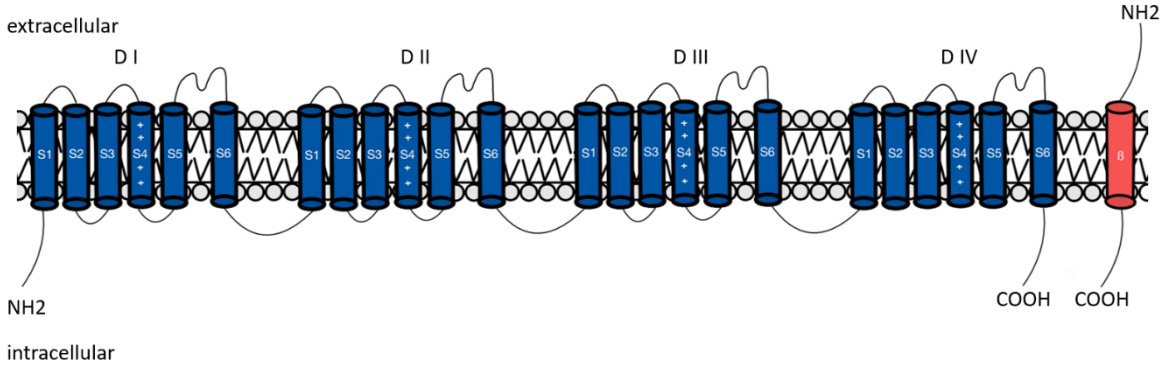

Figure 1: Schematic representation of the cardiac voltage-gated sodium channel subtype 1.5 (NaV1.5). Alpha-subunit (blue) and its associated β-subunit (red). DI-IV=Domains I-IV, S1-6=membrane-spanning segments

NaV1.5 is mainly located in the intercalated disk in the heart.

Previous studies suggested that SCN5A is mainly expressed in the heart, but more recent studies found expression also in other tissues such as the brain and gastrointestinal tract [65, 97].

It is known that besides LQTS, SCN5A mutations can lead to other diseases such as Brugada syndrome, sick sinus syndrome and dilated cardiomyopathy [104]. Not only SCN5A itself is responsible for these diseases, but also a large number of regulatory proteins that interact with NaV1.5. Below ß-subunits, NaV1.5 interacts with anchoring proteins, enzymes such as kinases and modulating proteins of the biophysical properties of Nav1.5 upon binding, where disruptions in the interacting proteins can lead to the same disease patterns as SCN5A mutations themselves [42].

In the cardiomyocyte action potential, 99% of sodium channels usually are inactivated after the rapid depolarization. The channels that remain open under physiological conditions, are responsible for a small window current during the plateau phase [85].

Gain of function mutations in SCN5A, associated with LQTS3, result in increased sodium influx and defective inactivation of the early sodium current into the cell. Increased sodium influx currents can be caused either by increased late sodium influx (I_{Na}) or increased window current, or by increased sodium influx and impaired inactivation of early sodium influx into the cell [102]. This leads to a substantial sodium influx also during plateau phase and thus to a prolonged plateau phase which causes a prolongation of the QT time in the ECG [11] (Figure 2). Due to the prolonged action potential duration, the cardiomyocytes develop a tendency to early afterdepolarization, which in turn can trigger torsade de pointes tachycardia [85].

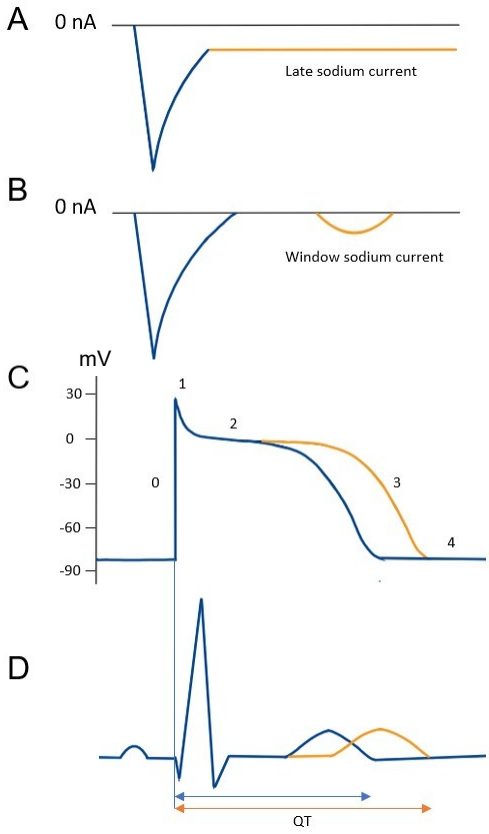

Figure 2: Effects due to gain of function mutations in the sodium voltage-gated channel alpha subunit 5 (SCN5A) gene. (A) Schematic representation of cardiomyocytes membrane conductivity for sodium with increased late sodium current trough cardiac voltage-gated sodium channel subtype 1.5 (NaV1.5). (B) Increased window sodium current. (C) Prolongation of cardiomyocyte action potential duration 0: Depolarisation, 1: Overshoot, 2: Plateau, 3: Repolarisation, 4: Resting membrane potential. (D) Prolongating effect on QT time in electrocardiogram (ECG). mV=millivolt, nA=nanoampere

1.4. Induced pluripotent stem cells (iPSC) as an in vitro model to investigate cardiovascular diseases

Disease models are essential for elucidating disease pathogenesis and developing innovative therapeutic interventions. In the fields of stem cell biology and regenerative medicine, patient-specific induced pluripotent stem cells (iPSCs) represent a promising platform for modeling cardiac diseases, thereby paving the way for the advancement of personalized medicine [100].

In 2006, Yamanaka and Takahashi first generated embryonic pluripotent stem cells from mouse fibroblasts by introducing four transcription factors (Oct4, Sox2, Klf4 and c-Myc), called Yamanaka factors, into mouse somatic cells [92]. Shortly

thereafter, the first iPSCs were produced from human fibroblasts [91, 108]. In addition to animal models, which have proven to be valuable disease models, another new opportunity has arisen to work specifically with human disease-relevant cells.

This offers new opportunities for research, especially with cardiomyocytes, as their limited proliferative capacity and the lack of substantial endogenous regeneration in the adult human heart severely restrict the acquisition of viable cardiac tissue for research purposes directly from a human heart.

Because of their human origin, the many possibilities for differentiation, the ease of propagation and accessibility, iPSCs have rapidly become a "disease-in-a-dish" model [81]. Patient derived iPSC are among the best methods to model disease *in vitro*, as fibroblasts are isolated directly from the patient and thus iPSC, generated from patient fibroblasts exhibit the same genetic background as the patient [26].

Besides the numerous possibilities and advantages of iPSC, nevertheless, there are problems and limitations that are faced in the work with iPSC. For example, a well-known problem is the immaturity of iPSC-induced cardiomyocytes, which show more embryonic morphology, organization and function [82]. For this reason, attempts must be made to allow the cells to become as mature as possible *in vitro* before performing experiments [9].

Initial approaches with iPSC-derived cardiomyocytes to understand the causes of heart disease and evaluate therapeutic potential were conducted in animal studies. These studies demonstrated that implanted iPSC-derived cardiomyocytes integrated well into the surrounding host tissue and, following myocardial infarction, reduced the infarct size and improved parameters of cardiac function, such as the left ventricular ejection fraction and ventricular wall movement in echocardiography [17, 107]. Despite significant challenges associated with iPSC-based therapies, such as the risk of tumor formation (tumorigenicity), immune rejection (immunogenicity), and cell variability (heterogeneity), which complicate therapeutic applications, treatments using iPSC or human embryonic stem cells (hESC) for more than 14 different diseases are currently being investigated or have already been investigated in clinical trials [106].

1.5. CRISPR/Cas9 technologies to generate an isogenic control of patient-derived iPSC

CRISPR/Cas9 (Clustered Regularly Interspaced Short Palindromic Repeats/CRISPR-associated protein 9) -mediated genome editing, with its capacity for targeted mutagenesis at the single-base pair level, offers a powerful platform for dissecting the molecular mechanisms underlying monogenic diseases.

There are two approaches for precise genome editing in iPSC. On the one hand, there is the possibility to insert a suspicious pathogenic mutation into healthy iPSC and compare it against the healthy controls. On the other hand, it is possible to take cells from a diseased patient and replace a point mutation with the wildtype base. The different cells can thus each be compared in an experimental setting, and conclusions about the mutation can be drawn. Mostly, the second approach is used. However, the first approach is particularly useful in very rare diseases, when it is difficult to obtain cells from a diseased patient or when the mutation affects the reprogramming into iPSC. Isogenic controls are cell lines that differ from patient-derived cells exclusively at a single, defined genetic locus and are useful to reveal the exact pathophysiological mechanisms of a mutation [70], and through the individuality of the patient-specific cells, the approach to develop a personalized therapy, for example patient-specific drug screening can be pursued [71]. Moreover, isogenic control cells open up a large field in regenerative medicine and the isogenic cellular therapy is a long-term goal. After differentiating corrected iPSC into the desired cell type they can be transplanted without risk of immune rejection, by the fact that the cells originate from the patient himself [10].

CRISPR-Cas systems are present in almost all archea and about half of bacteria. CRISPR (clustered regularly interspaced short palindromic repeats) and Cas (CRISPR-associated) genes are RNA-based defense systems that confer adaptive immunity to genetic elements such as viruses and plasmids [94].

There are three CRISPR systems that interact with many different Cas proteins. CRISPR II requires only one Cas protein, Cas 9, an endonuclease. To form a functioning DNA-targeting complex, Cas 9 requires a CRISPR RNA (crRNA) and a trans-acting CRISPR RNA (tracrRNA), which can be combined into a functional duplex, a single-guide RNA (sgRNA), guiding the complex to a specific site in the genome [15, 33, 38]. Versions of Cas9, originally derived from the bacterium

Streptococcus pyogenes, were generated that allowed activity to be achieved in the nucleus of human cells [16, 18, 51].

Cas9 targeting requires a PAM sequence (Protospacer Adjacent Motif) in the target DNA as well as complementary binding between the target DNA and the 20nt long crRNA sequence [38]. The PAM sequence is specific to the particular species of Cas9 protein and for Streptococcus pyogenes it is 5'NGG3'.

Cas9 induces a double-strand break at a specific site in DNA, which induces endogenous DNA repair processes. Two distinct pathways exist for precise genome editing using CRISPR/Cas9: non-homologous end joining (NHEJ) and homology-directed repair (HDR). In the NHEJ pathway, the ends are rejoined without using a template, which frequently results in loss of a few nucleotides (deletions) but can also lead to addition of new nucleotides (insertions). These deletions or insertions cause a frameshift mutation, typically resulting in loss of function of the affected gene (knockout). This pathway is highly efficient to knockout genes, but has a limited significance in precise genome editing. The HDR pathway is less efficient than the NHEJ pathway, but enables targeted DNA repair by using a homologous DNA sequence as a template for DNA repair. As a template an exogenously supplied DNA can be used, for example a plasmid. Through homologous recombination using the template DNA, the damaged DNA sequence of the cell is repaired by precise gene editing, such as the knock-in of specific base sequences or the correction of point mutations [2, 3, 35] (Figure 3).

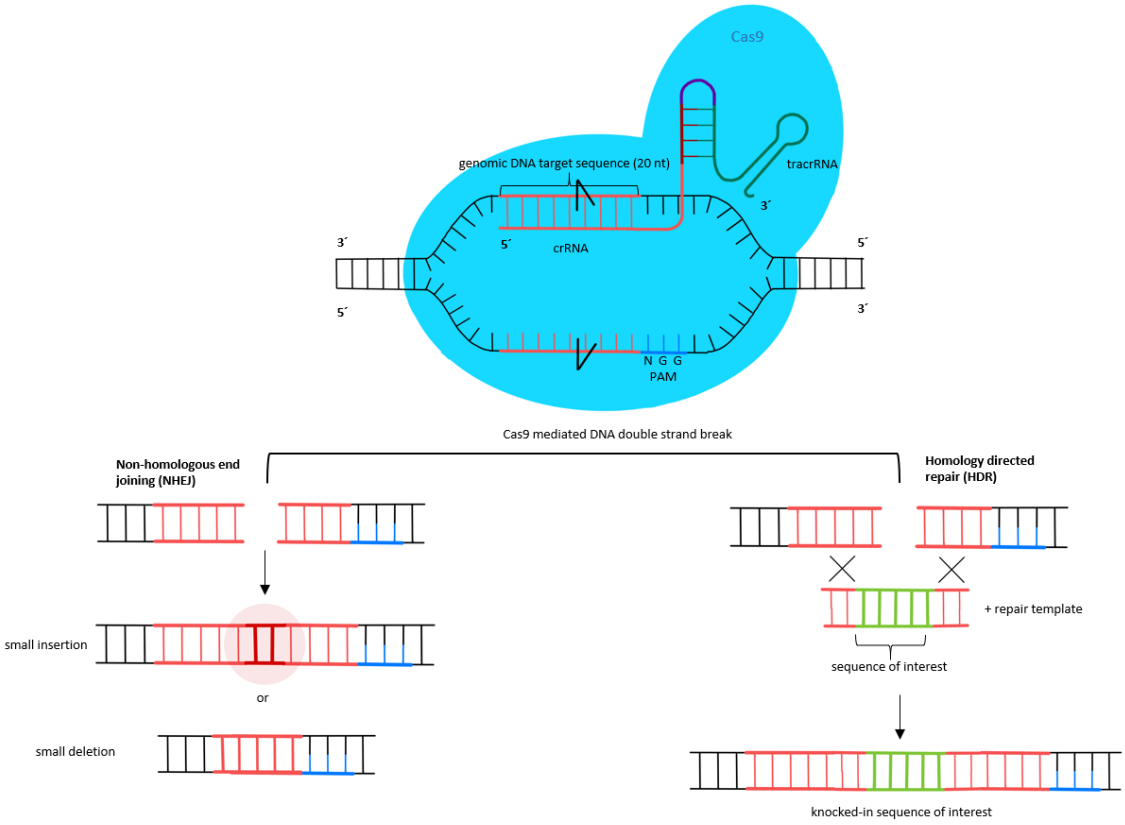

Figure 3: Schematic representation of Clustered Regularly Interspaced Short Palindromic Repeats/CRISPR-associated protein 9 (CRISPR/Cas9) complex. Non-homologous end joining (NHEJ) and Homology directed repair (HDR) pathway for DNA reparation are shown. (Adapted from [2, 21]). crRNA=CRISPR RNA, tracrRNA=trans-activating CRISPR RNA, PAM=protospacer adjacent motif, N=variable nucleotide, G=guanine

1.6. Zebrafish (Dan rerio) as an *in vivo* model to investigate cardiovascular diseases

In the last years, the zebrafish (Danio rerio), as a non-mammalian vertebrate model, has gained importance as a model organism in research for human diseases.

The zebrafish has a number of characteristics that make it interesting for research. It is a small (3-5cm), robust fish that can be kept under simple conditions. The female fish produce a large number of eggs (up to 200 per week) that are fertilized after spawning by the male zebrafish. Due to the extracorporeal development of zebrafish embryos, it is possible to observe the development from the 1-cell stage. The fish are fully grown and sexually mature after 3-4 months, so it does not take long to breed a new generation [86].

Especially in cardiovascular research it has a great significance, since genes that are important for cardiovascular development show high conservation between human and zebrafish, making it a valuable model for human heart diseases [61].

Beneath the rapid development of the cardiovascular system, during early embryogenesis, zebrafish embryos can survive up to a week without an efficiently functioning cardiovascular system because of their capacity for passive diffusion of oxygen and nutrients across the integument. This physiological adaptation contrasts sharply with mammalian embryogenesis, where a functional circulatory system is essential for early development. Consequently zebrafish embryos can tolerate mutations that profoundly impair cardiovascular function for a while, which gives the opportunity to investigate the developmental consequences of severe cardiovascular defects in this model system [7, 88].

There are several methods to study genes in zebrafish. A distinction is made between a forward-genetics and a reverse-genetics approach. The forward genetics approach aims to identify novel genes, that are responsible for a specific phenotype, i.e. the pathway from phenotype to genotype. In this approach, single base pair mutations are randomly induced into the male zebrafish genome, using mutagenic substances, especially Ethyl-Nitrosurea (ENU). This method creates a population of zebrafish with diverse mutations. Stable mutations in the germ line are transmitted to the next generation. There are different breeding schemes that can be used in a forward genetic screen. For instance, ENU-treated males are out-crossed to generate a population of F1 individuals. F1 individuals are out-crossed with wildtype fish, leading to F2 generation. In-cross of heterozygote F2 generation leads to F3 generation with a genetic distribution following the Mendelian rules. F3 embryos are screened for special phenotypes. Afterwards the induced mutations are identified. In the reverse-genetics approach, the aim is to analyze a specific gene. The way from genotype to phenotype is investigated. The gene of interest must be known and can be knocked-out, knocked-down or overexpressed to investigate the various effects on the phenotype. An easy way to knock down genes is using Morpholinos (MOs), which are synthetic antisense oligonucleotides, similar to DNA and RNA oligonucleotides, with around 25 nucleotides. MOs are complementary to the target mRNA and have a high binding affinity. They bind to the translational start site of mRNA or interfere with pre-mRNA splicing, which leads to the block the translation of a particular mRNA. To knock down a gene *in* vivo, MOs are injected into a zebrafish oocyte in one cell state.

1.7. Zebrafish heart and electrophysiological similarities between zebrafish and human heart

The zebrafish heart consists of a tubular structure and two contractile chambers. A single atrium and single ventricle, separated by the atrioventricular junction and valves. Adjacent to the atrium and ventricle are the sinus venosus, an inflow reservoir, and the bulbus arteriosus as an outflow tract, respectively [12]. The heart is a venous heart, which means that it receives the deoxygenated blood from the body and pumps it to the gills. Zebrafish possess a specialized conduction system that is very similar to that of humans, despite the anatomical differences of the fish heart, with the sinus node located in the sinus venosus [12] (Figure 4).
The action potential propagates to the atrium and is then slowed at the atrioventricular canal before it excites the ventricle [44, 79].

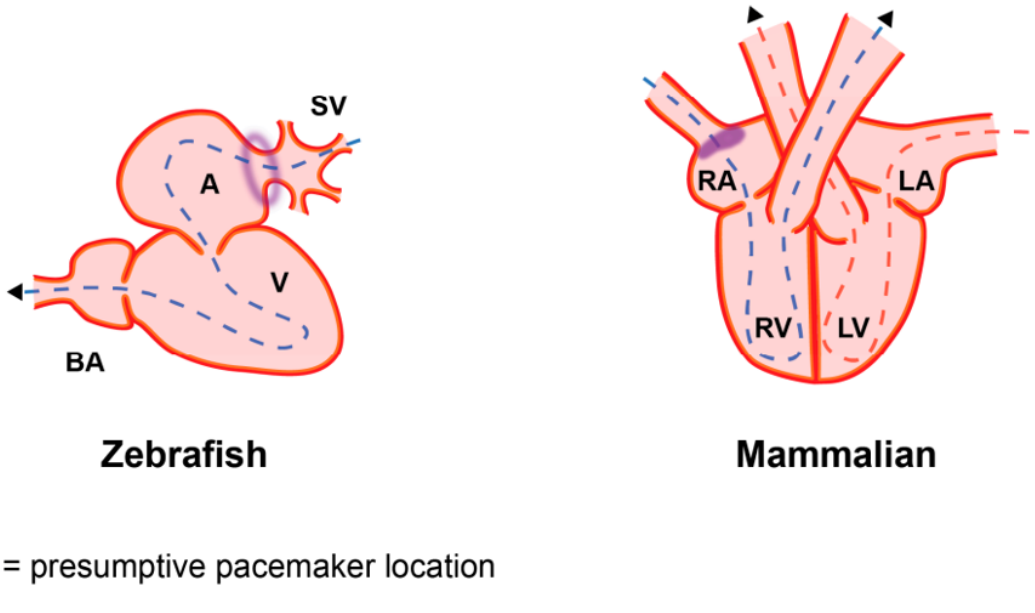

Figure 4: Two chambered heart of zebrafish (Danio rerio) in comparison to four chambered mammalian heart. Sinoatrial node is the primary pacemaker in both (purple). Arrows demonstrate the direction of the blood flow. Red=myocardial/muscle layer; orange=endocardium; A=atrium; RA=right atrium; LA=left atrium; V=ventricle; SV=sinus venosus; BA=bulbus arteriosus [12].

In zebrafish heart development, during the cardiac looping (36-48hpf), called chamber ballooning, the ventricle and atrium become morphologically distinct. Blood flow through the developing ventricle contributes to form the later shape of the heart [5]. The first contractions of the heart occur as soon as the cardiac tube is

formed. The first contractions of the heart are uncoordinated, but appear peristaltic because of the slow conduction through the heart tube [7]. When the cells, that form the sinus node appear, they have a higher contraction frequency than the rest of the heart tube [59]. During looping, a delay in conduction occurs in the AV canal. At 24hpf, uncoordinated peristaltic movements develop into coordinated contractions, that begin in the atrium, and then continue through the AV canal into the ventricle [89].

After 72hpf, the cardiovascular system of zebrafish embryos is quite mature and fully functional. The heart valves continue to undergo complete formation after 105hpf.

Many genes are highly conserved between humans and zebrafish. Zebrafish genome sequencing showed that approximately 70% of the human genome has at least one orthologous gene in zebrafish [34].

Zebrafish hearts are increasingly being used as a model for the human heart, in part because of the similar heart rate and electrophysiology reflected in the action potential shape and duration, which show several similarities to human ones [55].

The conduction system of zebrafish contains only the essential elements and is relatively simple. Nevertheless, similarities between humans and zebrafish in the electrophysiology of the heart have been shown. There are clear similarities between a human ECG and an ECG of a zebrafish, which make the zebrafish a good model organism also for the study of diseases of the conduction system [61].

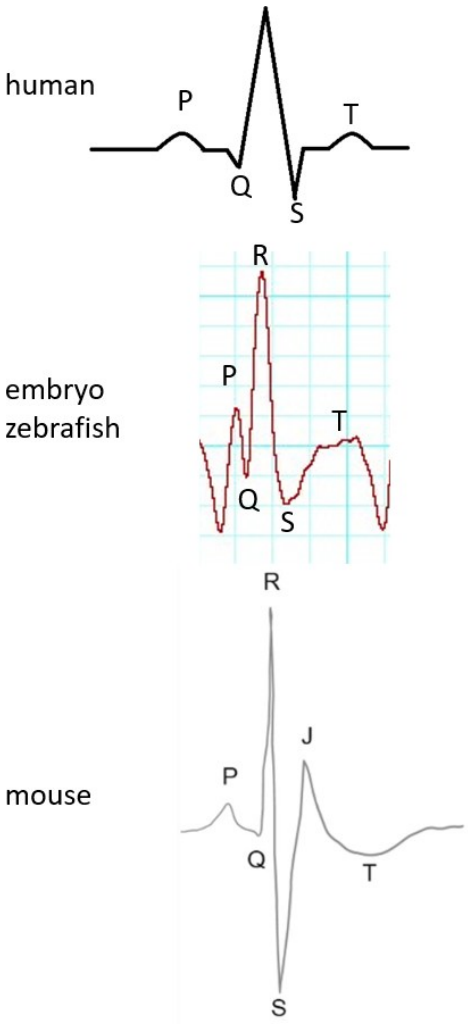

Figure 5: Comparison of human, embryo zebrafish and mouse electrocardiogram (ECG). Different components of the ECG are labeled (P wave, QRS complex, T wave, J point). Mouse ECG taken from [13].

For example, in the modeling of conduction disturbances, the zebrafish is electrophysiological closer to humans than the mouse and there are several things to consider when comparing a mouse ECG to a human ECG [13, 98] (Figure 5). This is due to the different mechanisms that lead to depolarization in the mouse, making it more difficult to detect the T wave in the mouse ECG, which can be easily detected in zebrafish ECG. Furthermore, the heart rate and QT-interval in zebrafish is more similar to human than mouse ones [44, 47].

1.8. From benchside to bedside and personalizend medicine

The current approach for developing new drugs and treatment options follows a “one-size-fits-all” approach, which assumes that all people with the same disease

are responding to the same drugs. Therefore, most patients receive first-line therapy, although this is only effective in 30-60% according to NHS England [57, 64]. For this reason, exploration of new approaches to pathophysiological understanding and therapy that are more responsive to patient individuality, are necessary. This approach is followed by “personalized medicine”, recently referred to as “precision medicine”, due to the fact that physicians have always tried to respond to the personal situation of the patient, some say that personalized medicine is not really a new approach. However, the two names are currently used in a similar way [53]. The Food and Drug Administration (FDA) defined personalized medicine as “an innovative approach to tailoring disease prevention and treatment that takes into account differences in people's genes, environments, and lifestyles” [23]. As a goal they name “to target the right treatments to the right patients at the right time” [23].

Science has made great progress, especially in the field of genetics. While the sequencing of the first human DNA took 13 years, currently it is possible to sequence an entire human genome in one day thanks to next generation sequencing (NGS).

In combination with the generation of iPSC, there are promising possibilities of generating "disease-in-a-dish" models of patient's individual genetic conditions [73]. This approach allows to identify the individual cause of a genetic disease and thus to find the best option for an individual therapy. Genetic correction of potential disease-causing mutations in these patient-specific iPSCs using CRISPR, enables the generation of an isogenic control group [84]. Analysis and comparison between the mutated and corrected cells allows conclusions to be drawn about the specific effects of the mutation without regard to the genetic background of the individual patient [84]. In order to investigate individual disease patterns and increasingly implement individualized types of therapy procedures in practice, translational research, bridging the gap between basic research and clinical research, is needed to establish a strong link from bedside to benchside and from benchside to bedside [28].

1.9. Aim of the work

It is known that some mutations in the SCN5A gene can lead to long QT syndrome, but also to other cardiac diseases such as dilated cardiomyopathy or Brugada syndrome [104].

The aim of this work was to determine whether the SCN5A$^{1072T>C}$ mutation, identified in a patient with long QT syndrome, is responsible for the clinical manifestation of the disease.

To address this question, patient-specific ventricular cardiomyocytes were generated and an isogenic control cell-line was established, serving as a comparison. To establish representative cell lines for these research purpose, fibroblasts obtained from the patient were reprogrammed into induced pluripotent stem cells (iPSCs) and subsequently differentiated into ventricular cardiomyocytes (CMs). To implement an appropriately matching control, the patient-specific iPSCs were corrected to the wild type genotype by using CRISPR/Cas9 and reversing the point mutation.

To determine whether the mutation induces any alterations, the phenotypes of the SCN5A$^{1072T>C}$ mutated and wildtype iPSC-derived CMs were analyzed and various parameters were inspected. The analysis included the examination of gene expression, possible structural effects on sarcomere morphology and NaV1.5 ion channel localization, calcium dynamics during contraction and field potential measurements. To elucidate potential structural and functional impacts of the mutation, the parameters were compared between SCN5A$^{1072T>C}$ mutated and CRISPR/Cas9 corrected iPSC-derived CMs.

Furthermore, the purpose was to evaluate the mutation also in an *in vivo* model. Given that long QT syndrome is most effectively diagnosed by ECG, the electrical cardiac currents of TgSCN5A$^{1072T>C}$ zebrafish embryos were recorded by ECG and compared to those of with wild-type embryos.

2. Materials and Methods

2.1. Materials

Technical instruments

Cameras

Leica DFC400	Leica Microsystems; Wetzlar, Germany

Centrifuges

Centrifuge 5418	Eppendorf AG; Hamburg, Germany
Multifuge 3 S-R	Heraeus; Hanau, Germany
Centrifuge Compact star CS4	Peqlab; VWR; Radnor, PA, US
Centrifuge 5424 R	Eppendorf AG; Hamburg, Germany
Megafuge 1.0R	Heraeus; Hanau, Germany
Centrifuge 5417R	Eppendorf AG; Hamburg, Germany
MiniStar Silverline	VWR; Radnor, PA, US

Incubators

Incubator Hera cell (cells)	Heraeus; Hanau, Germany
Incubator B6200 (fish)	Thermo Fisher Scientific; Waltham, MA, US

Scales

Scale Sartorius ED124S	Sartorius; Göttingen, Germany
Scale Adventurer AR 5120	Ohaus; Parsippany-Troy Hills, NJ, US

Shaking platforms

Heidolph Duomax 1030	Heidolph; Schwabach, Germany
IKA® Roller 10 basic	IKA; Staufen, Germany

Amaxa Nucleofector™ I	Lonza; Basel, Swizerland
Gel combs and chambers	Peqlab; VWR; Radnor, PA, US
PowerPac™ Basic	Bio-Rad; Hercules, California, US
Nano Drop 2000	Thermo Fisher Scientific; Waltham, MA, US
Hybridization Oven OV5	Biometra; Göttingen, Germany
UV light BioDocAnalyze Darkhood	Biometra; Göttingen, Germany
Injection apparatus FemtoJet	Eppendorf AG; Hamburg, Germany
Capillary puller PC-10	Narishige CO. Ltd.; Tokyo, Japan
PCR mastercycler ProS	Eppendorf; Hamburg, Germany
Image Quant LAS 4000 mini	Cytiva Life Sciences; Marlborough, MA, US
PowerLab 4/35	AD instruments; Dunedin, New Zealand
Extracellular Amplifier EXT 10-2F	NPI Electronic; Tamm, Germany
LightCycler® 480	Roche; Mannheim, Germany
Vortex VV3	VWR; Radnor, PA, US
Fridges and Freezers	Liebherr; Biberach a.d. Riß, Germany
Thermomixer compact	Eppendorf AG; Hamburg, Germany
External light source EL6000	Leica microsystems; Wetzlar, Germany
Power Pac 300	BIO-RAD; Hercules, CA, US
Plate reader infinite 200 Pro	Tecan; Männedorf, Switzerland
Sealer 4S3™ (4titude)	Brooks Life Sciences; Chelmsford, MA,US
Pipettes Research plus	Eppendorf; Hamburg, Germany
Pipetting aids	BRAND; Wertheim, Germany
Refrigerators and freezers	Liebherr; Bulle, Switzerland
Ultra-low Temperature freezer	PHC corporation; Tokyo, Japan
Trans-Blot Turbo Transfer System	Bio-Rad; Hercules, California, US
Micromanipulator	Narishinge CO.Ltd.; Tokyo, Japan
BD FACSAria™ III Cell Sorter	BD; Franklin Lakes, New Jersey, U.S.
Maestro Edge	Axion Biosystems; Atlanta, GA, US

Microscopes

Leica TCS SP8	Leica microsystems; Wetzlar, Germany
Olympus CKX53	Olympus Europa; Hamburg, Germany
Leica DMIL LED	Leica microsystems; Wetzlar, Germany
Zeiss Axio V.16	Carl Zeiss AG; Oberkochen, Germany
Olympus SZX16	Olympus Europa; Hamburg, Germany

Consumables

Cell culture plates (Falcon® 6/12/24 well)	Corning Life Science; Corning, NY, US
Cell culture plate glass (96-well black uncoated)	Ibidi; Gräfelfing, Germany
Nunclon Delta Surface (96-well cell culture plate)	Thermo Fisher Scientific; Waltham, MA, US
96-well-PCR-plate, Semi-Skirted	STARLAB GmbH; Hamburg, Germany
Multiwell microelectrode array (MEA) plates (24-well)	Axion Biosystems; Atlanta, GA, US
Vacuum filtration	VWR; Radnor, PA, US
Sterile bottle	VWR; Radnor, PA, US
Cryogenic vial	Corning Life Science; Corning, NY, US
Serological pipette (5/10/25/50ml)	Corning Life Science; Corning, NY, US
Sterile filter Millex-GS 0,22µM	Merck KGaA; Darmstadt, Germany
Custom MicroFil 34G	World Precision Instruments; Sarasota, FL, US
Eppendorf Tubes (1,5/2ml)	Eppendorf AG; Hamburg, Germany
Polystyrene Round-Bottom Tube with Cell-Strainer Cap (Falcon)	Corning Life Science; Corning, NY, US
Pipette tips	BRAND; Wertheim, Germany
Conical tubes (Falcon® 15/50ml)	Corning Life Science; Corning, NY, US
NanoSurface Plate (96-well)	Curi Bio; Seattle, WA, US
Silver wire AGW1010	World Precision Instruments; Sarasota, FL, US
Syringe 1ml Luer Lock ™ Tip	BD; Franklin Lakes, NJ

Tip Pre-Pulled Glass Capillaries TIP5TW1-L	World Precision Instruments; Sarasota, FL, US
Matrices for injection ramp	Eppendorf AG; Hamburg, Germany
Microloader	Eppendorf AG; Hamburg, Germany
Pasteur pipettes plastic	BRAND; Wertheim, Germany
Petri dishes plastic (fish)	VWR; Radnor, PA, US
Disposable Reagent Reservoir 25ml	Thermo Fisher Scientific; Waltham, MA, US
Alkaline battery 1604AUP, 9V Plus Ultra	Gold Peak; Hongkong, China
Thin wall glass capillary TW100F-6	World Precision Instruments; Sarasota, FL, US
Pasteur pipettes plastic	BRAND; Wertheim, Germany
Geltrex (Gibco™)	Thermo Fisher Scientific; Waltham, MA, US
Versene (Gibco™)	Thermo Fisher Scientific; Waltham, MA, US
1xTryp LE (Gibco™)	Thermo Fisher Scientific; Waltham, MA, US
Penicillin/Streptomycin (Gibco™)	Sigma-Aldrich; St. Louis, USA
Human Albumin, Recombinant	Sigma-Aldrich; St.Louis, MO, US
B-27 Supplement	Thermo Fisher Scientific; Waltham, MA, US
HEPES Buffer (pH 7.0-7.6)	Sigma-Aldrich; St.Louis, MO, US
Water, sterile filtered	Sigma-Aldrich; St.Louis, MO, US
Gelatin Solution 0,5%	HIMEDIA; Marg, Mumbai - 400 086, India.
PBS (Gibco)	Thermo Fisher Scientific; Waltham, MA, US
FBS superior stabil	Biochrom; Cambridge, UK
mFreSR™ Defined Cryopreservation Medium for hESCs and hiPSCs	Stemcell Technologies; Vancouver, Canada
STEMdiff™ Cardiomyocyte freezing medium	Stemcell Technologies; Vancouver, Canada

GeneRuler DNA Ladder Mix	Thermo Fisher Scientific; Waltham, MA, US
HiMark™ Pre-stained Protein Standard	Thermo Fisher Scientific; Waltham, MA, US
PageRuler™ Prestained Protein Ladder	Thermo Fisher Scientific; Waltham, MA, US
RevitaCell supplement (Gibco™)	Thermo Fisher Scientific; Waltham, MA, US
QIAshredder	QIAGEN; Hilden, Germany
dNTP-Mix 10 mM	Roche Diagnostics Deutschland GmbH; Mannheim, Germany
Recombinant Ribonuclease Inhibitor (Invitrogen™, RNaseOUT™)	Thermo Fisher Scientific; Waltham, MA, US
Cell culture flasks (Cellstar) 250ml	Greiner Bio-one; Kremsmünster Austria
C-CHIP Disposable Hemocytometer	NanoEntek; Waltham, MA, US
Stem Pro Accutase (Gibco™)	Thermo Fisher Scientific; Waltham, MA, US
NuPAGE Tris-Acetate Mini Gels (3-8%, 1mm)	Thermo Fisher Scientific; Waltham, MA, US
Fish Food (dry)	Tetra; Melle, Germany
Fish food Gemma Micro	Skretting; Stavanger, Norway
Nuclease-free-water	QIAGEN; Hilden, Germany
LightCycler®480 SYBR Green	Roche Diagnostics Deutschland GmbH; Mannheim, Germany
Trans-Blot Turbo 0,2µm PVDF membrane	Bio-Rad; Hercules, California, US
6x Loading Dye	Thermo Fisher Scientific; Waltham, MA, US
Universal Blocking Reagent	BioGenex; Fremont, CA, US

Cell lines

Thermo IPSC (Gibco™ Human Episomal A18944)	Thermo Fisher Scientific; Waltham, MA, US
iPSC SCN5A$^{1072T>C}$	mutated patient iPSC-line
iPSC isogenic control	CRISPR/Cas9 corrected control iPSC-line
iPSC derived cardiomyocytes SCN5A$^{1072T>C}$	mutated patient cardiomyocyte line
iPSC derived cardiomyocytes isogenic control	CRISPR/Cas9 corrected cardiomyocyte line
CF1 Mouse Embryonic Fibroblasts, MitC-treated	Thermo Fisher Scientific; Waltham, MA, US
Fibroblasts SCN5A$^{1072T>C}$	extracted from skin biopsy of the patient

Kits

Isolate II PCR and Gel Kit	Meridian Bioscience, OH, US
Human Cardiomyocyte Immunochemistry Kit	Thermo Fisher Scientific; Waltham, MA, US
Subcellular Protein Fractionation Kit	Thermo Fisher Scientific; Waltham, MA, US
RNeasy Mini Kit	QIAGEN; Hilden, Germany
Pierce™ BCA Protein Assay Kit	Thermo Fisher Scientific; Waltham, MA, US
Human Tri-Lineage Multiplex PCR-Kit	abm; Vancouver, Canada
Superscript III Reverse Transcriptase	Thermo Fisher Scientific; Waltham, MA, US
Q5® High-Fidelity DNA Polymerase	NEB Biolabs; Ibswich, MA, US
CTS CytoTune-iPS 2.1 Sendai Reprogramming Kit	Thermo Fisher Scientific; Waltham, MA, US
OneShot™ Chemically Competent E.coli Kit	Thermo Fisher Scientific; Waltham, MA, US

SuperSignal™ West Femto Trial Kit	Thermo Fisher Scientific; Waltham, MA, US
Amaxa™ Human Stem Cell Nucleofector™ Kit 2	Lonza; Basel, Swizerland

CRISPR/Cas9 Plasmids

gRNA plasmid SCN5A (gRNA sequence: ccacaagggacagcaagtgt)	Biocat; Heidelberg, Germany
HR-arm plasmid SCN5A	Biocat; Heidelberg, Germany

Chemical reagents

CHIR 99021	Merck KGaA; Darmstadt, Germany
IWP-2	Merck KGaA; Darmstadt, Germany
Retinoic acid	Sigma-Aldrich; St.Louis, MO, US
Fura-2, AM	Thermo Fisher Scientific; Waltham, MA, US
Pluronic F-127 (20% solution in DMSO)	Thermo Fisher Scientific; Waltham, MA, US
L-ascorbic acid 2-phosphate	Sigma-Aldrich; St.Louis, MO, US
Sodium DL-Lactate Solution	Sigma-Aldrich; St.Louis, MO, US
Thiazovivin	Merck KGaA; Darmstadt, Germany
Potassium chloride solution 3M	Sigma-Aldrich; St.Louis, MO, US
TWEEN 20	Sigma-Aldrich; St.Louis, MO, US
Skim Milk Powder	Sigma-Aldrich; St.Louis, MO, US
Paraformaldehyde (PFA)	Sigma-Aldrich; St.Louis, MO, US
Triton ® X-100	SERVA, Heidelberg, Germany

The rest of chemical reagents was obtained from Amersham, AppliCem, Brown, Fluka, Invitrogen, Lonza, Merck, NEB, Polysciences, QIAGEN, Roche, ROTH, SIGMA-ALDRICH, Stratagene and VWR. Purified water was purchased from BRAUN and is termed as ddH_2O in the following.

Buffers and working solutions

Blocking buffer (Western Blot)	5% milk powder in TBST
E3 Buffer	5 mM NaCl
	0,17 mM KCl
	0,33 mM $CaCl_2$
	0,33 mM $MgSO_4$
Tyrodes Solution	140 mM NaCl
	5 mM KCl
	5 mM HEPES
	1 mM NaH_2PO_4
	1 mM $MgCl_2$
	1,8 mM $CaCl_2$
	10 mM glucose
	adjusted to pH 7,4 with NAOH
MESAB	4 mg/ml Ethyl-3-aminobenzoate-methanesulfonate salt
	1% Na_2HPO_4
	pH 7.0-7.5
3x Laemmli-buffer	187,5 mM Tris HCl (pH 6,8)
	6% SDS
	30% glycerol
	2% beta-mercaptoethanol
	0,03% Bromphenol Blue
	150 mM DTT
TBS 20x (1L)	2,8 M NaCl
	500 mM Tris
	Fill up to 1 L with ddH_2O, pH 7,4
1xTBST	0,05% Tween 20 in 1xTBS
TBE 10x, 1L	purchased from Sigma-Aldrich T4415-10L
NuPAGE™ Tris-Acetate SDS Running Buffer (20X)	purchased from Thermo Fisher Scientific
LB-Agar, 1L	30g LB-Agar
	50mg Kanamycin

	in 1L ddH_2O
LB-Medium	20g LB-Broth
	50mg Kanamycin
	in 1L ddH_2O

Cell culture media

Fibroblast culture medium	DMEM
	10% FBS
	1x L-glutamine
	1x sodium pyruvate
	1x penicillin-streptomycin
MEF-Medium	DMEM
	10% FBS
StemFlex (Gibco™)	Thermo Fisher Scientific; Waltham, MA, US
DMEM/F12 (Gibco™)	Thermo Fisher Scientific; Waltham, MA, US
KO-DMEM	KnockOut DMEM
	15% KnockOut serum replacement
	1x L-glutamine
	1x nonessential amino acids
	1x penicillin-streptomycin
	0,1 mM beta-mercaptoethanol
	10ng/ml basic fibroblast growth factor (bFGF)
Post-Facs Medium	50% StemFlex
	50% sterile filtered conditioned medium (medium already used for other iPSC)
	1:100 penicillin/streptomycin
	1:100 RevitaCell Supplement
Cardio Differentiation Medium	RPMI 1640 (with GlutaMAX and HEPES)

	0,2 mg/ml L-ascorbis acid 2-phosphate 0,5 mg/ml human recombinant albumin
Cardio Culture Medium	RPMI 1640 (with GlutaMAX and HEPES) 1x B-27 Supplement (from 50x)
Cardio Recovery Medium	Cardio Culture Medium 20% Fetal Bovine Serum 2 µM Thioazovivin
Cardio Selection Medium	RPMI 1640 (without glucose and HEPES) 0,2 mg/ml L-ascorbic acid 2-phosphate 0,5 mg/ml human recombinant albumin 4 mM lactate/HEPES
RPMI 1640 with GlutaMAX and HEPES (Gibco™)	Thermo Fisher Scientific; Waltham, MA, US
RPMI 1640 (without glucose and HEPES) (Gibco™)	Thermo Fisher Scientific; Waltham, MA, US

Primary Antibodies

Antibody name	**Working concentration**	**Company/Catalogue number**
Anti-SCN5A	1:100 (Immunostaining) 1:500 (Western Blot)	Origene TA338791
Anti-alpha-Actinin antibody (Mouse IgG1)	1:200 (Immunostaining)	Sigma Aldrich #A7811
Vinculin	1:2000 (Western Blot)	Abcam ab91459

Secondary Antibodies

Antibody name	Working concentration	Company(Catalogue number
Anti-rabbit IgG HRP linked	1:2000	Cell signaling #7074
Goat Anti-rabbit IgG Alexa Fluor 488	1:100	Thermo Fisher #A11034
Goat Anti-mouse IgG1 Alexa Fluor 555	1:100	Thermo Fisher #A21127

Primers

All Primers were purchased from Eurofins Genomics and diluted to a working concentration of 50pM/µL.

Experiment	Primer name	Sequence 5´-3´
Genotyping	SCN5A Exon fw	AACGGCACCTCTGATGTGTT
	SCN5A Exon rev	TCCTCATAGGCCATTGCGAC
qRT-PCR	SERCA2A fw	TTGGCAGGAGCGGAACGCAG
	SERCA2A rev	CAACCCGCAGCGTGGTGGAT
	RYR2 fw	AAGCCCTCTCGTCTGAAACA
	RYR2 rev	CCACCCAGACATTAGCAGGT
	SCN5A fw	ACTGCACAATGACCAGCAGGA
	SCN5A rev	GTGAGAAGTGCTCGATTAGTTCAGACA
	18S fw	AAATCAGTTATGGTTCCTTTGGTC
	18S rev	CCGTCGGCATGTATTAGCTC
	GAPDH fw	CACCCACTCCTCCACCTTTG
	GAPDH rev	ACCACCCTGTTGCTGTAGCC
Sendai loss	Sendai fw	GGATCACTAGGTGATATCGAG
	Sendai rev	ACCAGACAAGAGTTTAAGAGATATGTATC

Morpholino modified antisense oligonucleotides (MO)

Morpholino name	Sequence 5´-3´
MO1-SCN5laa (translation blocking)	CCGCTGGTAAGAGCATGGTCGCCAT
MO2-SCN5lab (splice blocking, splice donor site exon/intron 6)	AGCGGCCTCTCACCTGGGATGACTG

Fish lines

TÜAB	wildtype line
TgSCN5A$^{1072T>C}$	transgenic line with SCN5A$^{1072T>C}$ mutation

Software

Softwares	Application	Supplier
ApE	Program to show sequencing	ApE
Finch TV	Tool to visualize chromatograms	Geospiza
Image J	Program to process scientific images	National Institutes of Health
Microsoft office	Writing application	Microsoft
Citavi	Reference manager	QRS International
Prism 7+9	Statistical data analysis	Graphpad
LAS X	Program to acquire and analyze pictures of confocal microscope	Leica
Image Quant LAS 4000	Program to picture western blots	Cytiva Life Sciences
Gelpro 3.1	Program for analysis of western blots	Media cybernetics
Clampfit 11.2	Program to analyze signals	Molecular devices
Labchart 8	Program to record zebrafish ECG	AD Instruments
ImageJ	Program to process images	Image editor
Turbo SM	Calcium Imaging Software	RedShirtImaging
LAS X	Program to analyze and acquire pictures from confocal microscope	Leica

AxIS Navigator	Program for MEA recording	Axion BioSystems
Cardiac Analysis Tool	Program to analyze MEA recordings	Axion BioSystems
GoodNotes	Tool to draw illustrations	Good Notes Limited

Databases

mCSM-membrane	http://biosig.unimelb.edu.au/mcsm_membrane
PolyPhen-2	http://genetics.bwh.harvard.edu

Statistics

All graphs and statistical analysis were performed using GraphPad Prism 7 and 9. All graphs show means ± standard deviation (SD). Statistical analyses were carried out using the Mann-Whitney test to compare two independent groups, as it does not assume normality and is suitable for comparing central tendencies when normal distribution is questionable. For comparison of more than two independent groups one-way ANOVA was used to identify statistically significant differences, followed by Tukey´s multiple comparison to identify which group means differ significantly from one another. When comparing more than two independent groups with uncertain normality, Kruskal-Wallis test was employed, followed by Dunn´s multiple comparison test to determine which specific groups differed significantly from each other. Value of $p<0,05$ was accepted as statistically significant. The type of statistical analysis used for each experiment is specified in the figure legend.

Ethics vote reference number: 394/19

2.2. Methods

Generation of iPSC

To generate the patient-specific iPSC line, mainly the protocol "Skin Biopsy and Patient-Specific Stem Cell Lines" by Yao Li et al. was used [46].

To create the patient specific iPSC, fibroblasts from the patient were collected by skin biopsy and cultured in fibroblast culture medium. CTS™ CytoTune™-iPS Sendai 2.1 Reprogramming Kit (Thermo Fisher) was used to reprogram the fibroblasts. Cells were infected with a MOI (multiplicity of infection) of 4. Two days post-infection, the medium was changed to KO-DMEM. Seven days after infection, fibroblasts were seeded on a plate with mouse embryonic fibroblasts (MEF), used as feeder cells in KO-DMEM medium containing 10µM ROCK-inhibitor. The medium was changed every other day. As soon as colonies appeared they were transferred to a new culture plate containing MEF cells (plates coated with 0,1% gelatin solution) and transferred a second time to a culture plate without feeder cells, as already established and performed in our lab by Maximiliane Däuwel [19]. From this point on conventional methods for iPSC cultures were used.

Culture of iPSC

IPSC were maintained in a monolayer culture with StemFlex medium in an incubator with 5% CO_2, and 37°C. Cells were seeded in culture plates coated with Geltrex (Thermo Fisher). For coating, Geltrex was used at a ratio of 1:100 in DMEM/F12 (Thermo Fisher) for plastic plates and at a ratio of 1:50 in DMEM/F12 for glass plates. The culture plates were incubated with Geltrex and DMEM/F12 at 37°C for at least 1 hour. When the cells reached approximately 90% confluence, they were detached with Versene for 4 minutes and plated in a lower density on a new plate containing StemFlex medium supplemented with RevitaCell 1:100. One day after splitting, the medium was changed to StemFlex without RevitaCell.

Prove of pluripotency

To prove pluripotency of iPSC, the Human Tri-Lineage Multiplex PCR-Kit (abm) was used according to the manufacturer`s instructions.

Transformation and preparation of CRISPR/Cas9 plasmids

OneShot™ Chemically Competent E.coli Kit (Thermo Fisher) was used to clone the CRISPR/Cas9 plasmids.

First, the plasmids were diluted to 1ng/µl and subsequently the manufacturer´s instructions for transformation were followed. After transformation, bacteria were plated out on LB-agar containing Kanamycin (50mg/ml). The plates were incubated over night at 37°C. The next day, colonies were harvested and incubated with 5ml of LB-medium containing Kanamycin (50mg/ml) over night at 37°C. The following day, 100µl of LB-medium, containing the bacteria, were collected and mixed with 100ml LB-medium with Kanamycin. The suspension was incubated at 37°C, for 12-16 hours.
Afterwards the manufacturer`s instructions for QIAfilter Plasmid Midi and Maxi Kit were followed. The pellet was air dried overnight and was resuspended with 100µl sterile H_2O the next day. Plasmid concentration was measured using the Nano Drop 2000.

Nucleofection

To create the isogenic control, CRISPR/Cas9 plasmids produced by Biocat were transferred into the patient´s iPSC by electroporation to correct the mutation. Stem Cell Nucleofector Kit 2 (Lonza) and the Amaxa Nucleofector™ I were used for nucleofection. Each nucleofection was performed with a total of 800.000 cells, 6-8µg gRNA plasmid, 6-8µg HR-arm Plasmid (GFP labeled) and 100µl Nucleofection solution 2. After detaching cells with StemPro Accutase and resuspending cells with Nucleofection solution 2, containing the appropriate amount of gRNA-plasmid and HR-arm plasmid, the cells were electroporated in the Amaxa Nucleofector™ I by using the program A-23. Around 12 nucleofections were carried out on new iPSC for 5-6 times. 24 hours post-nucleofection, cells that integrated the GFP-labeled HR-arm plasmid could be detected as GFP-positive cells under the fluorescence microscope.
After electroporation, cells were seeded on a culture plate pre-coated with Geltrex (1:100) in Stemflex medium containing Revita cell supplement (1:100).

Preparation and follow up care for FACS sorting

On the second day after nucleofection, GFP^+ cells were selected by FACS sorting and sorted as single cells in Nunclon Delta Surface 96-well cell culture plates. Single

cells were maintained in Post-Facs Medium. The day after nucleofection, medium was changed newly to Post-Facs Medium and 2 days after nucleofection medium was replaced with StemFlex Medium.

Isolation of mRNA from iPSC and cardiomyocytes

After expanding of each individual cell clone, each clone was sequenced to identify the clones, in which the genome editing worked. 91 cell clones had to be sequenced until the first one with the mutation corrected could be detected, so the efficiency of genome editing in the cells, that incorporated the plasmid was quite low around 1-2%.

The RNeasy Mini Kit (QIAGEN) was used to isolate mRNA from iPSC and cardiomyocytes. 10µl of beta-mercaptoethanol were added to 1ml RLT buffer. After washing the cells two times with PBS, cells were scraped in RLT, mixed with beta-mercaptoethanol. Subsequently the cell suspension was centrifuged trough a QIAshredder. An equal volume of 70% ethanol was added to the flow-through and from then on, the manufacturer´s instructions from the protocol were followed. The mRNA concentration was measured using the Nano Drop 2000.

Reverse transcription

For reverse transcription of mRNA into cDNA, 1-2µg mRNA were taken to prepare cDNA by using Sscript® lll Reverse Transcriptase (Life Technologies), according to the manufacturers` instructions. Samples were stored at -20°C prior to use.

Step	**Temperature**	**Time**
cDNA synthesis	65°C	5 min
	4°C	Pause (at least over 1 min)
	50°C	60 min
	70°C	15 min
Hold	4°C	∞

Differentiation into cardiomyocytes

The iPSC were differentiated into cardiomyocytes in 12-well plastic bottom plates, when they covered 80-90% of the well, as described by Kleinsorge and Cyganek [40]. After 8-12 days, the cells started to beat spontaneously and were transferred to a new culture plate on day 14, to obtain a cardiomyocyte monolayer, which started beating again after 1-2 days. Thereafter, cardiomyocytes were purified by providing lactate as the sole energy source. Patient SCN5A$^{1072T>C}$, isogenic control and Thermo Fisher iPSC behaved similarly during differentiation, established the typical cross-linked structure of cardiomyocytes simultaneously, started to beat the same day and looked similar at the same timepoints.

Polymerase chain reaction (PCR)

To determine gene expression or to amplify a gene of interest, PCR was performed using Q5® Hot Start High-Fidelity DNA Polymerase (NEB) according to the manufacturer´s instructions under the following thermocycling conditions:

Step	Temperature	Time
Initial Denaturation	98°C	30 sec
25-35 cycles	98°C	5-10 sec
	50-72°C	10-30 sec
	72°C	20-30 sec/kb
Final extension	72°C2	2 min
Hold	4°C	∞

Agarose gel electrophoresis

To separate and visualize DNA fragments of different size, agarose gel electrophoresis was used. 2% agarose was dissolved in 1x TBE buffer by boiling and 0,5µg/mL ethidium bromide was added to the gel to visualize the DNA fragments under UV-light. Afterwards the gel was poured in the gel tray. The samples were mixed with 6x Loading Dye and for size standard, GeneRuler DNA Ladder was used. After running the gel for 1,5h at 200-250V the DNA bands were pictured under UV light and excised for purification and subsequent sequencing.

DNA gel extraction

To extract the DNA from agarose gels, Isolate II PCR and Gel Kit (Meridian Bioscience) was used by following the manufacturer´s instructions. Purified DNA was used for sequencing.

Quantitative reverse transcription polymerase chain reaction (qRT-PCR)

Quantitative reverse transcription polymerase chain reaction was performed according to standard protocols, using SYBR Green Master Mix (Roche) on a LightCycler 480 II. cDNA was generated from RNA isolated from 31-day-old cardiomyocytes, as previously described in the reverse transcription paragraph. Two housekeeper genes, 18s ribosomal RNA and GAPDH, were used as reference genes. The ΔΔCt method was used to analyze relative gene expression.

Protein extraction from iPSC derived cardiomyocytes

Proteins were extracted on days 36 and 37 after the start of differentiation. Extraction was performed by following the manufacturer´s instructions of Subcellular Protein Fractionation Kit (Thermo Fisher). Subcellular protein fractions were stored at -80°.

BCA-Essay

Protein concentration was measured using the Pierce™ BCA Protein Assay Kit (Thermo Fisher) and the Plate reader infinite 200 Pro by following the manufacturer´s instructions.

Immunoblotting

10µg of protein from 36 or 37-days old cardiomyocytes derived from Thermo Fisher, isogenic control, and patient iPSC were used. Proteins were boiled in 1xLaemmli Buffer at 95°C for 5 min and separated with NuPAGE Tris-Acetate Mini Gels (3-8%, 1mm) for 1h at 150V constant. A denaturing buffer consisting of 50ml 20xNuPAGE Tris-Acetate SDS Running Buffer and 950ml deionized water was used as running

buffer. The gel was blotted onto a polyvinylidene fluoride (PVDF) membrane using the Turbo Blot Machine with high molecular weight setting for 10 min. Afterwards the membrane was blocked by using 5% skim milk powder in TBST for 1h at RT. Subsequently, the membrane was incubated with the primary antibodies over night at 4°C. Anti-SCN5A antibody (Origene TA338791; 1:500) and Anti-Vinculin antibody (Abcam ab91459; 1:2000) in 5% skim milk powder in TBST were used as primary antibodies. After washing the membrane three times for 10min with TBST on the following day, the Anti-rabbit secondary antibody (IgG HRP-linked) was added to TBST (1:2000) and incubated for 1h at RT with gentle shaking. After washing 3 times, membranes were developed by using the SuperSignal West Femto Trial Kit (Thermo Fisher) and a luminescent image analyzer (Image Quant Las4000 mini). Quantification was performed using the Gelpro 3.1 program.

Immunostaining for NKX-2.5 and Troponin T2

Staining of NKX-2.5 and troponin T2 was performed using the Human Cardiomyocyte Immunochemistry Kit according to the manufacturer´s instructions on cells plated on a 96-well glass bottom plate. Afterwards the images were acquired using the Leica TCS SP8 confocal microscope with 40x objective.

Immunostaining for NaV1.5, α-actinin and DAPI

Cardiomyocytes previously plated on a 96-well glass bottom plate were fixed with 4% PFA in PBS for 20 minutes at RT and washed twice with cold PBS. Then, cardiomyocytes were incubated with 0,2% Triton in PBS and washed twice with cold PBS. Afterwards, cardiomyocytes were treated with 1% Universal Blocking Reagent in PBS and were incubated for 1 hour at RT. Primary antibodies were diluted in 1% BSA in PBS and cells were incubated with the primary antibodies over night at 4°C with gentle shaking. Anti-SCN5A from Origene TA338791 (host: rabbit; 1:100) for NaV1.5 staining, and Anti-α-Actinin antibody from Sigma Aldrich #A7811 (host: mouse; 1:200) were used. The next day, cells were washed once at 4°C for a few minutes and then twice at RT for 15 minutes each. After secondary antibodies were diluted in PBS and incubated for 2 hours at RT, cells were washed twice with PBS. Goat Anti-rabbit IgG Alexa Fluor 488 and Goat Anti-mouse IgG1 Alexa Fluor 555

were used as secondary antibodies. Subsequently, cells were stained with 1xDAPI in PBS for 10 minutes at RT and washed again twice with PBS. Images were then acquired using a Leica TCS SP8 confocal microscope with 40x objective and 63x objective.

Calcium Imaging

Calcium imaging was performed on 24 days old cardiomyocytes, derived from Thermo Fisher, isogenic control, and patient iPSC plated onto a 96-well glass plate. To prepare the cardiomyocytes the culture medium was mixed with fura-2 to obtain a 2µM concentration, previously dissolved in Pluronic acid (20% in DMSO) to 1mM stock. Cardiomyocytes were incubated with this mixture for 8 min at RT in the dark. Then, the medium was changed into Tyrodes solution and incubated for 10min at RT in the dark. Medium was changed back to cardiomyocyte culture medium and the cells were maintained at 37°C and 4% CO_2 for 30min. After that, calcium currents were detected with Leica TCS SP8 confocal microscope (40x objective, DAPI filter) using the Turbo SM software (settings: 25ms exposure time (40 frames/second), 1200 frames, camera gain mid low). ImageJ was used to analyze the data, and 16 regions of interest (ROI), including at least one cell each, were selected for each well by visual recognition. Subsequently, the fluorescent intensity of each ROI was converted from fit format to txt, using an Excel sheet specific for 40 frames/second, for further analysis. The txt data were opened using Clampfit software. Clampfit was used to analyze the half width, rise time and decay time of the calcium waves, with a total of 3 complete waves included for each ROI. Time of peak was calculated by summation of rise time and decay time. Further statistics were generated using GraphPad Prism 9.

Microelectrode arrays (MEA)

For MEA experiments fully differentiated and metabolically selected cardiomyocytes were transferred to a MEA plate. The 24-well MEA plates were coated with Geltrex (1:100) in DMEM/F12 and incubated for 1 hour at 37°C. Cardiomyocytes were detached with TrypLE (1x) for 10 minutes, centrifuged at 100G for 10 minutes and resuspended with the appropriate volume of Cardio Recovery Medium, to obtain a

cell suspension with 150.000 cells in 8µl for each well. On the MEA plate, cardiomyocytes were plated only on the recording electrodes, whereas plating on the reference electrodes was avoided as much as possible. After the cells stayed in 8µl for 1 hour and started attaching, 1ml of Cardio Recovery Medium was carefully added to the cells. After plating on the MEA plate, the cardiomyocytes remained on the plate for at least 7 days to recover completely before starting the experiments. For electrophysiological recording the Maestro Edge was used with the AxIS Navigator software, and for subsequent analysis the Cardiac Analysis Tool (Axion BioSystems) was used. The temperature during the recording was set at 37°C and the CO_2 concentration at 5%. Recording was carried out for 2 min.

Zebrafish breeding and husbandry

Adult and embryonic zebrafish were kept and bred as described below.

The fish facility of the working group was built by Aqua Schwarz Aquarienbau. The system contains 10m^3 of deionized water with a constant pH (7,2-7,4) by adding Na_2CO_3 to the water. The temperature of water is constant at 28°C and by adding 200-400µS/cm salt to system water, conductivity of the water is ensured. To mimic the natural circadian rhythm of the zebrafish, a day-night rhythm (13 hours light/11 hours dark) was maintained. Fish were fed as described in the following section: Twice in the morning, fish were fed with ex-capsulated artemia (20-25g of artemia eggs incubated for two days in 10 L deionized water with 360g sea salt at 28°C with constant air supply before the capsuled were washed off with deionized water), and one time in the afternoon with Gemma micro. To increase reproductive capacity, fish were fed with Tetra pro dry food once daily.

To mate the fish, female and male fish were separated in a mating tank with a sieve in between and with a second sieve at the bottom to separate the eggs from the fish. The next morning, the female and male fish were placed together in the first 3 hours after the light period began, so they could mate. After 10-15 minutes, the eggs were collected, washed with E3 buffer supplemented with methylene blue and transferred to a petri dish. Immediately after the eggs were collected, morpholinos were injected. After injection or immediately after collection, embryos were placed in an incubator with 28,5°C for up to five days.

Microinjection in zebrafish eggs

Prior to microinjection, ramps and needles were prepared. The ramps consist of 3% agarose dissolved in E3 medium in a petri dish. A plastic matrix is used to form wells in the agarose gel, into which zebrafish eggs can later be placed and fixed for injection. As injection needles 0,75mm glass capillaries, pulled with a capillary puller and afterwards opened with razor blade, were used. Morpholinos were loaded and injected into the eggs in single cell state in the yolk sac. For injection, the needles were fixed on a FemtoJet microinjection device and injection pressure was set, depending on the specific characteristics of each injection needle, such as the width of the opening. A mixture of 2 morpholinos, 80µM MO1laa and 80µM MO2lab, was used. The mix was injected into fish of the TgSCN5A$^{1072T>C}$ fish line. All morpholinos were dissolved in 0,2M KCl. After injection, eggs were placed into a petri dish containing E3 medium and placed in the incubator. Daily, the dead eggs were removed and the E3 medium was changed.

Embryo zebrafish ECG

ECG recording of the embryonic zebrafish was performed at 48hpf and 72hpf with zebrafish from the TÜAB line and TgSCN5A$^{1072T>C}$ line as well as morpholino injected fish from the TgSCN5A$^{1072T>C}$ line at 48hpf (TgSCN5A$^{1072T>C}$ + MO). For the recording electrode a Tip Pre-Pulled Glass Capillary (TIP5TW1-L) was filled with 3M KCl without air bubbles. A chlorinated silver wire was inserted into the glass capillary. The glass capillary containing the chlorinated silver wire was fixed on a micromanipulator. A second micromanipulator was placed on the other side of the recording site and held a silver wire as a reference electrode. Recording and reference electrodes were connected to the head stage of the extracellular amplifier (EXT-10-2F) (settings: Gain: 1k, high pass: 0,1Hz, low pass: 100Hz, filtered output). The extracellular amplifier was connected to the PowerLab 4/35 and the signals from the PowerLab 4/35 were acquired in the Windows software LabChart 8.1.21 (settings: Channel: 1k/s, 10V, Digital filter: Band pass; High cut off frequency: 30Hz, Low cut off frequency: 4Hz; Auto adjust selected). For anesthesia, zebrafish embryos were placed in MESAB (3mg/ml diluted in E3 medium) for 3 minutes. Then, the embryos were placed in a well of an injection ramp filled with E3 medium for

fixation. The tip of the recording electrode was placed on the embryo, lightly touching the skin surface over the AV-point of the embryos heart. The silver wire of the reference electrode was placed in the surrounding E3 medium. The exact position of the recording electrode was adjusted until the ECG wave looked correct and showed all relevant parameters. From each ECG, the part that showed the signal with the lowest background noise possible was selected and exported as pCLAMP file (abf.). For better analysis, the data were opened in Clampfit, where parameters were measured manually. For heart rate, beats were counted in a 15s interval and multiplied by 4 to obtain beats per minute. QRS-interval and ST-interval were measured 4 times in each ECG and averaged. Qt-time was measured 4 times in each ECG and the average of Qt-time was obtained. QTc was calculated with the Fridericia formula.

QTc (Fridericia)=QT-time/(RR^(1/3))

3. Results

3.1. Novel SCN5A mutation in a patient with LQTS and generation of first in-silico models

Due to a familial history of long QT syndrome (LQTS) and incidents of sudden cardiac death in the family of the index patient, this study aimed to investigate the novel mutation identified in the SCN5A gene (Figure 6). The investigation focused on exploring its potential pathogenetic role and the impact on the clinical phenotype observed in the patient. Next Generation Sequencing showed a heterozygous variant of uncertain significance in SCN5A, with one allele mutated in exon 9 c.1072T>C.

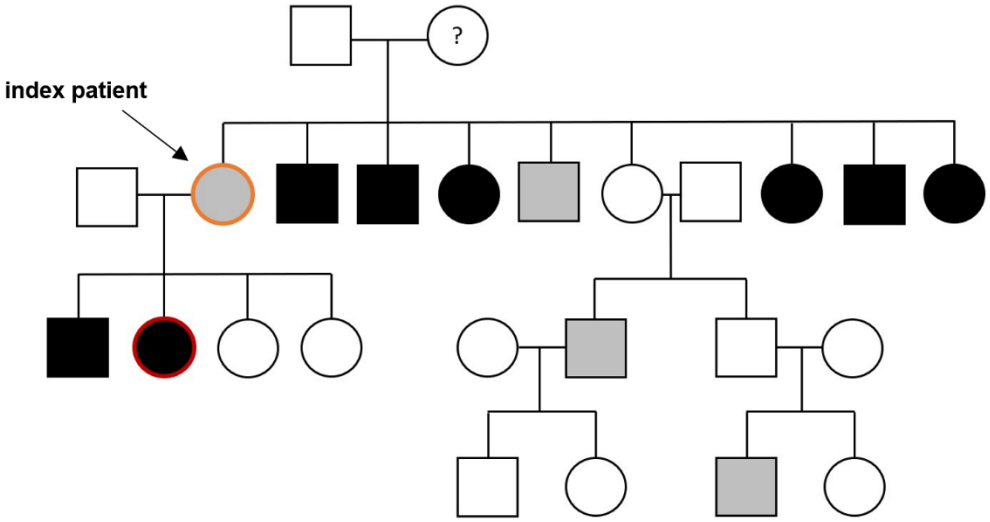

Figure 6: Pedigree of the family. The two persons in red and orange showed the heterozygote SCN5A$^{1072T>C}$ mutation. The person in the orange circle suffers from long QT syndrome. Black individuals have died. Gray individuals suffer from long QT syndrome. Square=male individuals, circle=female individuals.

This mutation results in a predicted amino acid exchange from phenylalanine (PHE) to leucine (LEU) at position 358. In order to gain a preliminary understanding of the potential functional or structural impact of the mutation, various in-silico tools were used (Figure 7). The computational models predicted an amino acid exchange within the intracellular region of chain A, located between transmembrane domains 4 and 5 (Figure 7 A, B). Notably, the mCSM-membrane tool suggested that this mutation could destabilize the protein structure, while the PolyPhen-2 tool indicated that the mutation might be functionally damaging (Figure 7 C). These predictions

provide valuable initial evidence that the mutation may disrupt protein stability and function, which prompted further investigation into the possible effects of the mutation.

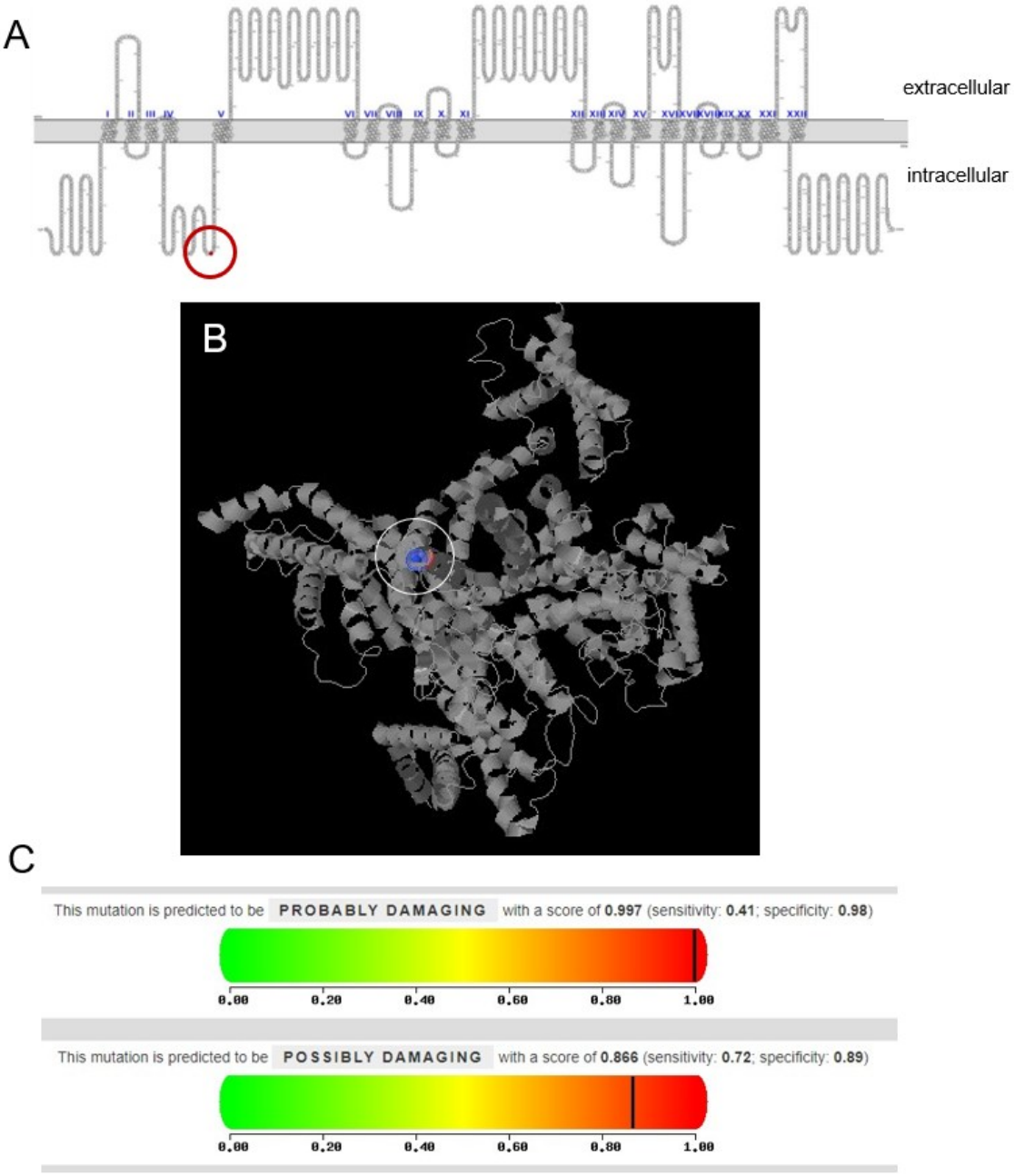

Figure 7: In-silico analysis of the SCN5A$^{1072T>C}$ mutation. (A) Schematic illustration from Biosig mCSM-membrane (http://biosig.unimelb.edu.au) of subunit alpha of voltage-gated sodium channel NaV1.5 with a red circle around the predicted position of the mutation in the intracellular region. (B) 3D structure of subunit alpha of voltage-gated sodium channel NaV1.5 from PolyPhen-2 (http://genetics.bwh.harvard.edu) with a white circle around the predicted position of the mutation. (C) Prediction of the mutation effect by PolyPhen-2 (http://genetics.bwh.harvard.edu).

3.2. Generating an induced pluripotent stem cell (iPSC) line from a patient with SCN5A mutation

To investigate the effects of the identified SCN5A$^{1072T>C}$ mutation on cardiomyocytes *in vitro*, I generated a patient-derived iPSC line and established the isogenic control cell line. Patient iPSC were generated from fibroblasts, obtained from a skin biopsy (Figure 8 A). The fibroblasts were reprogrammed into iPSC transfecting the four Yamanaka factors (Oct3/4, Sox2, Klf4 and L-Myc, a less oncogenic variant of c-Myc) with a Sendai virus. The Sendai virus is non-integrating and remains in the cytoplasm of the cells, reducing the risk of unpredictable disruptions of important genes and integration in the host genome (Figure 8 B-D).

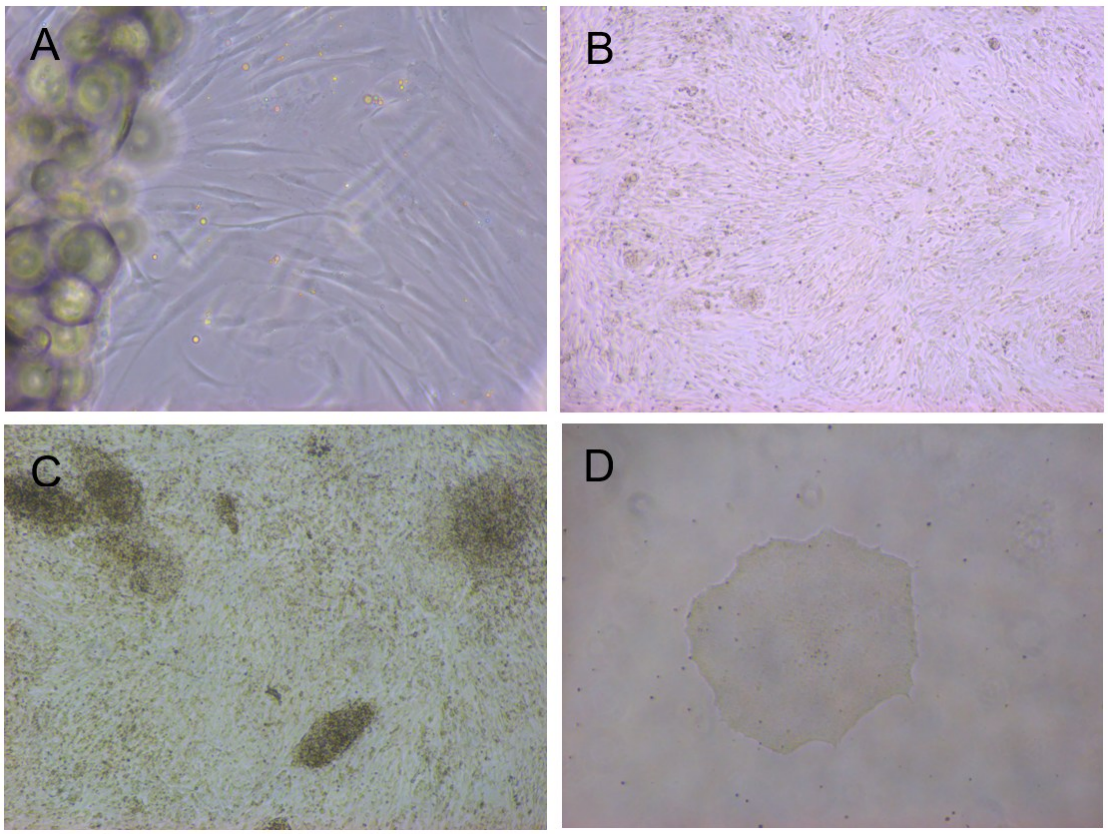

Figure 8: Generation of the patient´s induced pluripotent stem cell (iPSC) SCN5A$^{1072T>C}$ line. (A) Fibroblasts from skin biopsy at day 14. (B) Fibroblasts at day 3 after transfection with Sendai virus. (C) iPSC colonies on the top of mouse embryonic fibroblasts (MEF) at day 11 after transfection. The colonies are beginning to appear. (D) Pure iPSC colony on day 1 after transfer to an empty culture plate.

After 10 passages, the cells successfully lost the non-integrating virus, as evidenced by the results of the Sendai-specific PCR. mRNA was extracted from the cells and

subjected to PCR, which showed that the Sendai-specific band was no longer detectable after gel electrophoresis (Figure 9 A). This confirmed the removal of the virus from the cells. Additionally, the pluripotent state of the cells was confirmed by the expression of Pou5f1/Oct4, a key transcription factor essential for maintaining undifferentiated pluripotency (Figure 9 B). The presence of this gene expression indicated that the cells remained in a pluripotent state.

In conclusion, a Sendai-free, pluripotent iPSC line derived from the index patient was successfully established, which will provide a valuable tool for further investigation of the mutation and its potential impact.

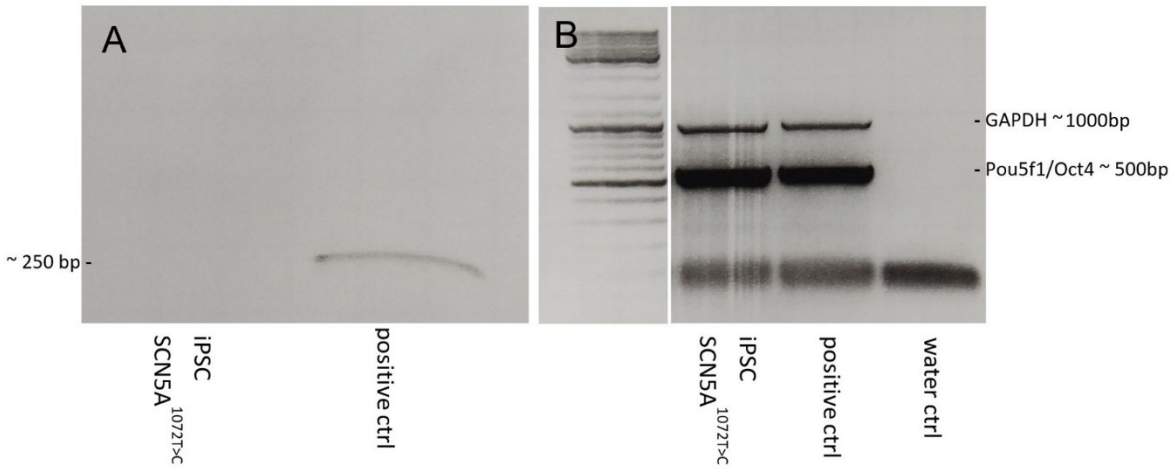

Figure 9: Agarose gels with PCR products. (A) Agarose gel with PCR product from Sendai PCR. On the left cDNA from SCN5A$^{1072T>C}$ cell line (from mRNA extracted after passage 10) and positive control (ctrl) on the right. (B) Agarose gel from proof of pluripotent state by expression of the transcription factor Pou5f1/Oct4 with cDNA from SCN5A$^{1072T>C}$ cell line (from mRNA extracted after passage 10), ladder on the left, positive control and water control. GAPDH=Glycerinaldehyd-3-phosphat-Dehydrogenase, serves as a loading control. bp=base pairs

3.3. Successful correction of the mutated patient iPSC to obtain an isogenic control

Isogenic control cell lines serve as highly valuable tools for studying diseases, particularly those inherited through point mutations. These cell lines are generated using CRISPR/Cas9 genome editing technology, which allows for precise, targeted alterations in the genetic sequence. By introducing specific genetic variations into the genome, isogenic controls enable to isolate and study the effects of a single point mutation, free from the confounding influence of an individual's genetic

background. This approach provides a clearer and more accurate understanding of how particular mutations contribute to disease phenotypes. In this study, I established an isogenic control cell line derived from the index patient's induced pluripotent stem cells (iPSCs) to investigate the specific effects of the SCN5A mutation. The use of this highly precise and controlled model allows for a detailed analysis of the mutation's impact, while minimizing variability from other genetic factors (Figure 10).

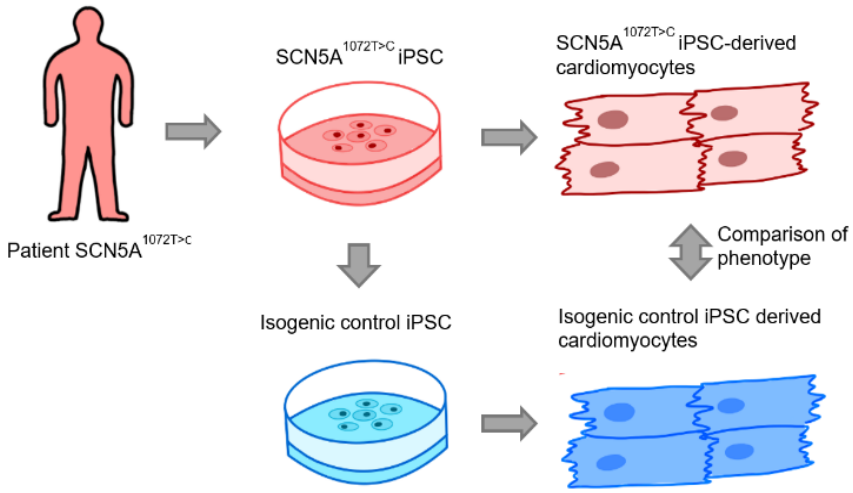

Figure 10: Workflow for the production of cell lines. The iPSC are derived from patient (red). To study the effects of the mutation, the cells were corrected with CRISPR/Cas9 and HDR (homology direct repair) pathway and established as an isogenic control cell line (blue). Both cell lines were differentiated into cardiomyocytes. The phenotypes of the cardiomyocytes were

To generate the isogenic control, precise single nucleotide genome editing was performed. Initially, a double-strand break was induced in the target region using CRISPR/Cas9 technology. Following this, to ensure an accurate correction of the SCN5A$^{1072T>C}$ mutation, the homology-directed repair (HDR) pathway was utilized. This method enables the precise incorporation of the desired genetic sequence at the site of the break. Specifically, two plasmids were introduced into the cells: one containing the guide RNA (gRNA) to direct the Cas9 nuclease to the correct genomic location for editing, and another carrying the wild-type template sequence for the targeted repair of the SCN5A$^{1072T>C}$ mutation (Figure 11 A, B, C).

This strategy allowed for the highly specific replacement of the SCN5A$^{1072T>C}$ point mutation with the corresponding wild-type base, ensuring the correction of the genetic variant at the single-nucleotide level (Figure 13).

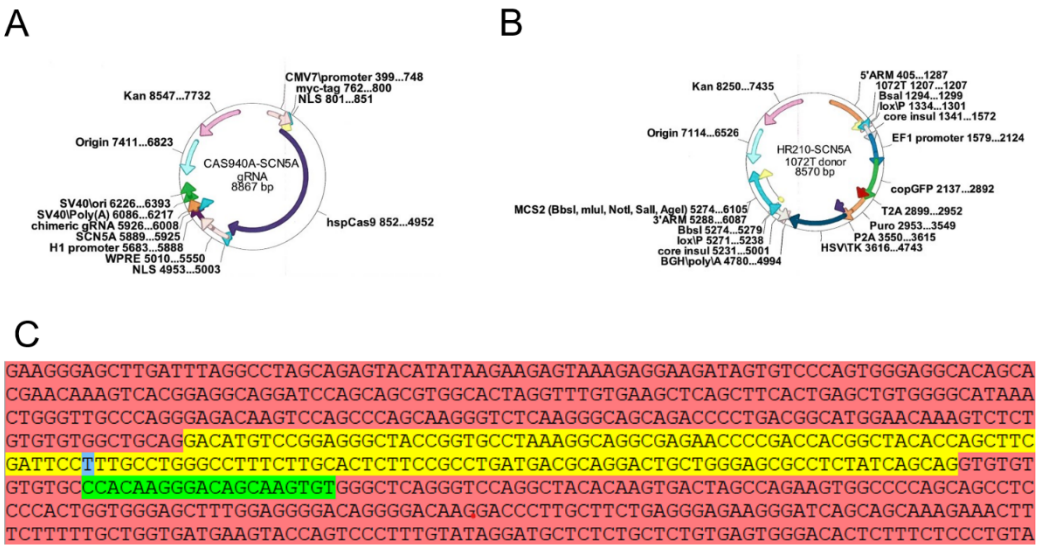

Figure 11: Plasmids for genome editing and gene sequence of SCN5A. (A) gRNA (guide RNA) plasmid, to find the correct place in genome for editing. (B) HR-arm (homologous recombination) plasmid, which gives the template for precise correction from mutation to wildtype. Plasmids were designed and synthetized by Biocat. (C) Exon 9 of SCN5A (yellow), position of mutation (blue) and gRNA (guide RNA) for CRISPR/Cas9 (green).

The index patient´s SCN5A$^{1072T>C}$ iPSC were transfected with the plasmids, as precisely described in materials and methods. Upon microscopic analysis, they showed positive GFP expression (Figure 12 A). The GFP (green fluorescent protein) positive iPSC were sorted out by FACS (Fluorescence-Activated Cell Sorting) (Figure 12 B) and from these single sorted cells, new colonies were grown (Figure 12 C).

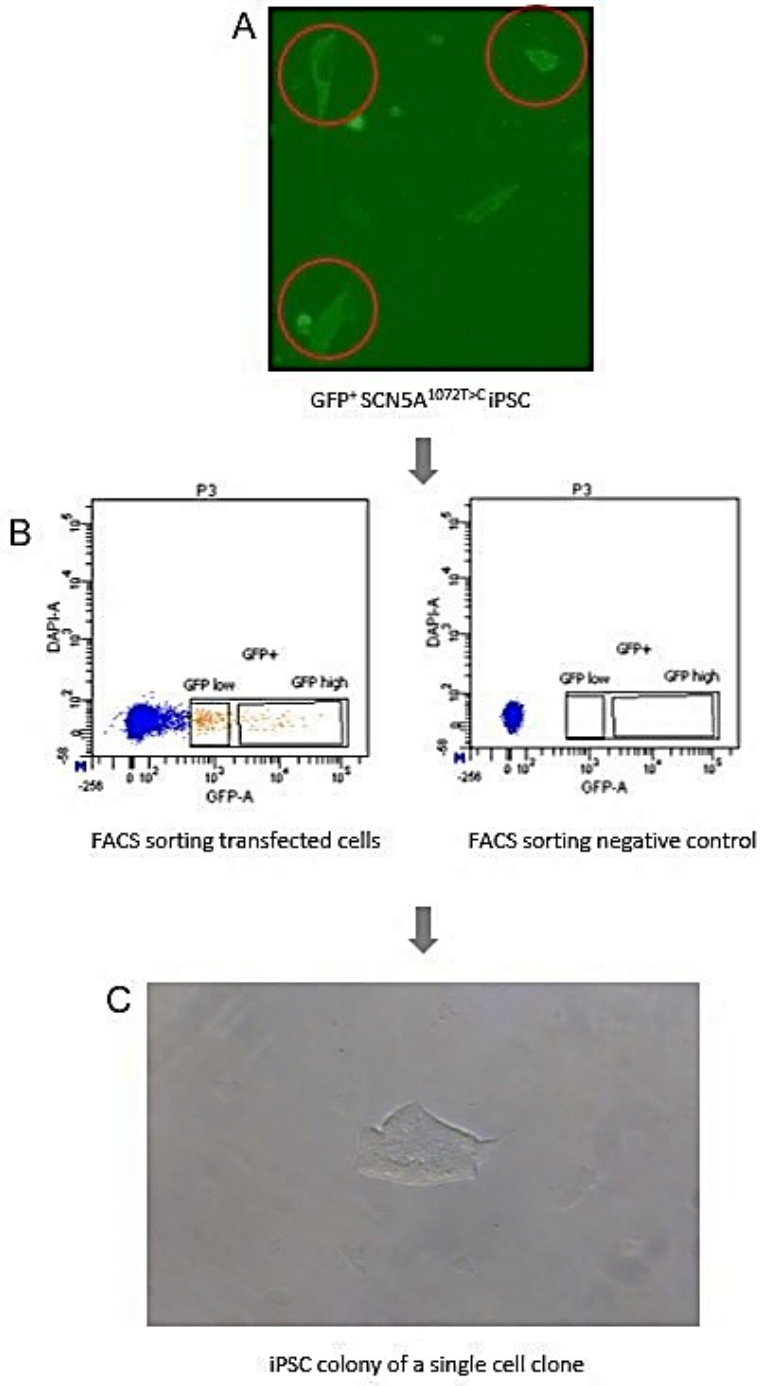

Figure 12: Workflow of CRISPR/Cas9 correction of patient SCN5A$^{1072T>C}$ cells. (A) GFP^{+} (green fluorescent protein) SCN5A$^{1072T>C}$ cells 24 hours after nucleofection. Vital cells are marked with a red circle (B) GFP^{+} cells in FACS (Fluorescence-Activated Cell Sorting) and FACS sorting of GFP^{-} control cells. (C) Single cell colony at day 4 after nucleofection.

Figure 13 presents the sequencing analysis of the index patient's SCN5A$^{1072T>C}$ iPSC and the corresponding isogenic control iPSC. As indicated by the peaks in the sequencing chromatograms, the index patient carries a heterozygous SCN5A variant at position 1072 (Figure 13 A, black arrow), where both thymine (T) and

cytosine (C) are observed at this specific locus, resulting in the appearance of two distinct, smaller peaks (SCN5A c.1072T>C). In contrast, the sequencing of the isogenic control at the identical genomic position (Figure 13 B, black arrow) reveals a single, prominent peak, consistent with the presence of two thymine (T) bases at this locus (SCN5A c.1072>T) which corresponds to a wildtype. The base triplets, highlighted by a black line underneath the respective bases, further elucidate the consequential amino acid substitution at position 358. Specifically, the mutation SCN5A c.1072T>C results in a replacement of phenylalanine (PHE) with leucine (LEU) (p.Phe358Leu) (Figure 13 A, B).

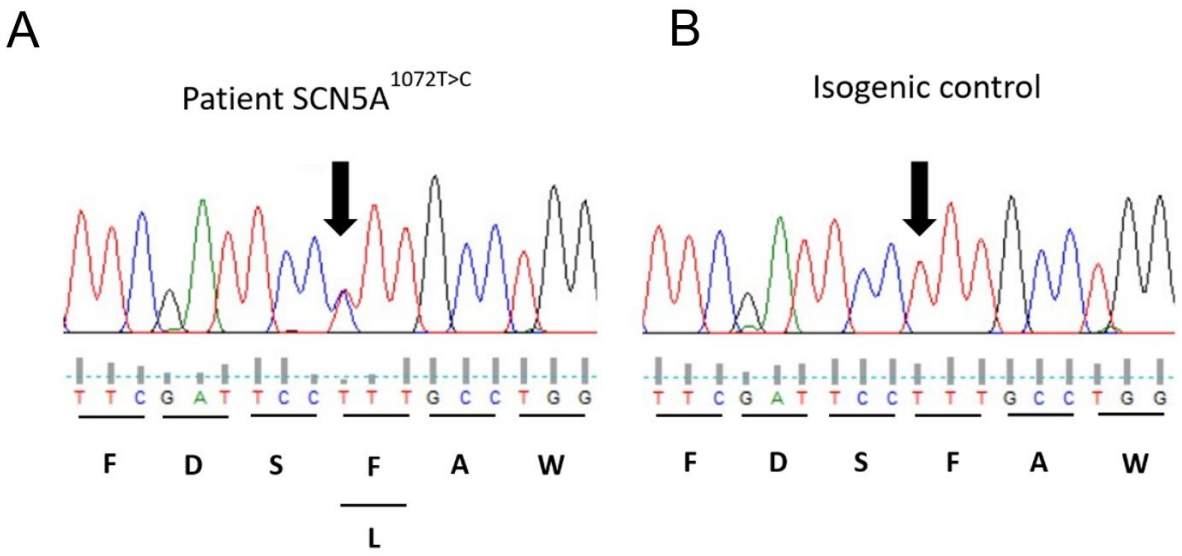

Figure 13: Sequencing of patient SCN5A$^{1072T>C}$ iPSC and isogenic control iPSC. The heterozygote base exchange from thymine to cytosine at position 1072 (black arrow) results in an amino acid exchange from phenylalanine (F) to leucine (L) at position 358. DNA bases: T=Thymine (red), C=Cytosine (blue), A=Adenine (green), G=Guanine (black), Amino acids (black): F=Phenylalanine, D=Aspartic acid, S=Serine, L=Leucine, A=Alanine, W=Tryptophan

With this approach the isogenic control cell line, only differing in the point mutation from the index patient´s SCN5A$^{1072T>C}$ iPSC line was successfully generated, which represents an optimal control (Figure 13 B).

3.4. Differentiation of patient-derived iPSC, and isogenic control cells into ventricular cardiomyocytes

LQTS3, which is predominantly caused by mutations in the SCN5A gene and possibly also by the $SCN5A^{1072T>C}$ mutation, is characterized by alterations in the repolarization phase of the electrocardiogram (ECG). Due to the fact that the repolarization phase in ECG mainly involves the ventricle, we focused on ventricular cardiomyocytes. In the following, all iPSC-derived cardiomyocytes (CMs) always refer to ventricular cells.

Both, patient derived- and isogenic control-iPSC were differentiated into ventricular cardiomyocytes. As an additional control, iPSC produced from a company (Thermo Fisher iPSC), in the following referred to as “wildtype control”, were also differentiated into ventricular cardiomyocytes. This additional wildtype control was established to investigate whether the wildtype cell line and the isogenic control cell line exhibit similar behavior, or whether there are differences between them. This gave me a further opportunity for comparison with my isogenic control cell line and thus better opportunities for classification and comparison of the generated cell lines, to be sure the isogenic control represents a healthy control.

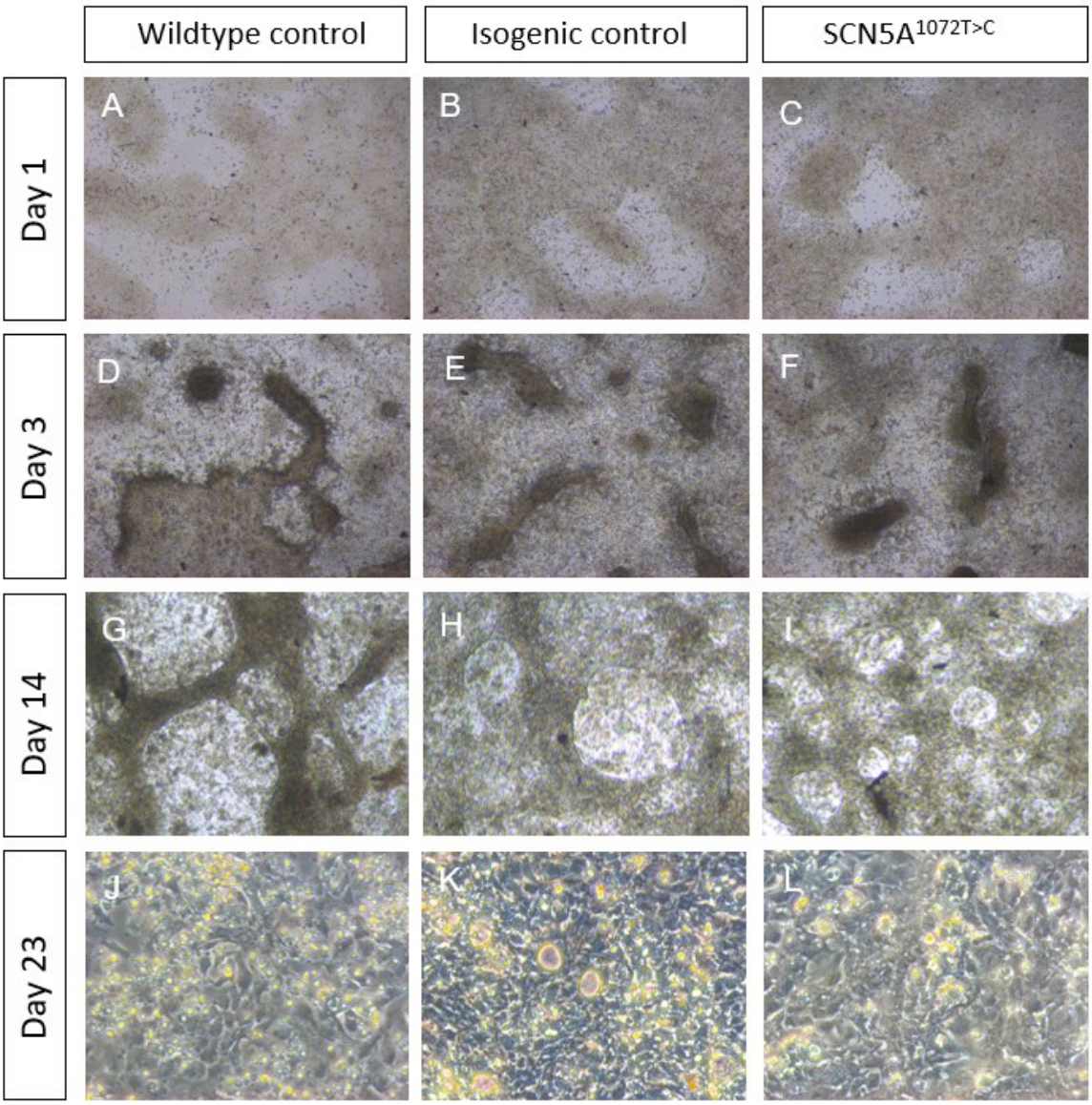

Figure 14: Differentiation of iPSC-derived ventricular cardiomyocytes from wildtype control, isogenic control, and patient SCN5A$^{1072T>C}$ iPSC. The same time points of differentiation are shown for each iPSC line (day 1 (A, B, C), day 3 (D, E, F), day 14 (G, H, I), day 23 (J, K, L)). Day 1-14 show the cells establishing the typical cross-linked structure of cardiomyocytes (acquired with 10x objective). At day 23, the cells are shown in a monolayer after transfer to a new culture plate (acquired with 20x objective).

During differentiation wildtype control, isogenic control and patient SCN5A$^{1072T>C}$ iPSC, showed very similar morphologies on the same days. The first indications of differentiation were already visible on day one, where slight condensed structures started to appear in the homogeneous iPSC colonies (Figure 14 A, B, C). These structures became more pronounced on day 3, where the formation of the typical cardiomyocyte cross-linking structure was already evident (Figure 14 D, E, F), and was very pronounced on day 14 (Figure 14 G, H, I), where the classical

cardiomyocyte syncytium could be well observed. On day 8-12, the cells of wildtype control, isogenic control and patient SCN5A$^{1072T>C}$ began to beat. First uncoordinated and later followed by more and more rhythmic, regular and coordinated contractions of the whole well.

After the cells were seeded to new cell culture plates, allowing them to build a cardiomyocyte monolayer, wildtype control, isogenic control and patient SCN5A$^{1072T>C}$ cardiomyocytes showed similar morphologies again (Figure 14 J, K, L) and all three cardiomyocyte cell lines began to beat simultaneously and rhythmically a 1-2 days after the transfer to the new plate.

3.5. The maturity of iPSC-derived ventricular CMs from wildtype control, isogenic control and patient was proved by immunostaining

It is well known, that iPSC-derived cardiomyocytes at an early developmental stage tend to show an immature rather than mature phenotype, which means that they can show different behavior in contractility, differences in sarcoplasmic reticulum calcium cycling or a different metabolism, compared to mature iPSC-derived cardiomyocytes. Therefore, it is of great importance to provide evidence of cell maturity of the iPSC-derived cardiomyocytes before starting to perform experiments. To prove the maturity in our cells, an immunostaining for NKX-2.5 (Homeobox protein NKX-2.5) was performed. NKX-2.5 is a marker for early cardiac mesoderm and a key transcription factor in early heart development. It serves as a marker for immature cardiomyocytes, as it plays a critical role in cellular differentiation. During the maturation process, the expression of NKX-2.5 is downregulated, leading to the loss of this marker. In mature cardiomyocytes, NKX-2.5 is therefore either no longer detectable or only present at very low levels.

To show the sarcomere structure, an antibody against Troponin T2 was used. Immunostaining was performed on 36-day-old cardiomyocytes with wildtype control, isogenic control and patient SCN5A$^{1072T>C}$ iPSC-derived cardiomyocytes (Figure 15).

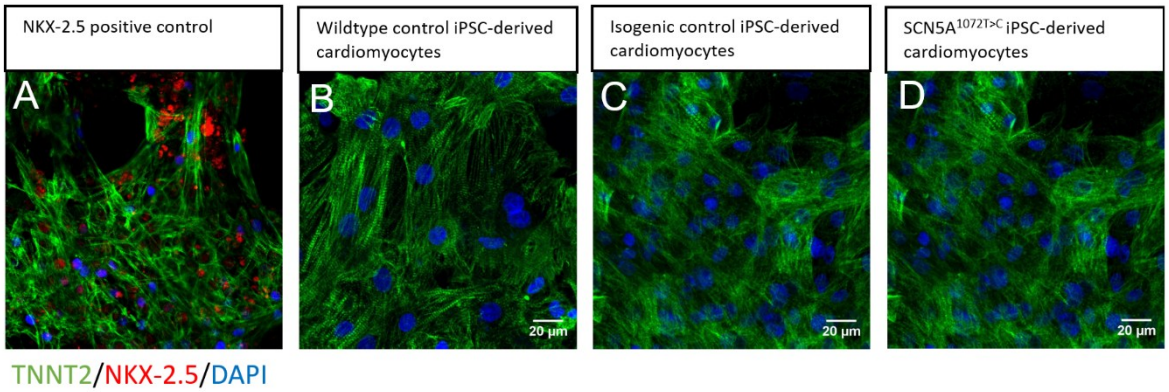

Figure 15: NKX-2.5 (Homeobox protein NKX-2.5) staining. (A) NKX-2.5 positive control iPSC-derived cardiomyocytes, (B) 36-day-old iPSC-derived cardiomyocytes of wildtype control, (C) isogenic control, and (D) patient SCN5A$^{1072T>C}$. Troponin T2 is stained green, NKX-2.5 is stained red and the nucleus is stained blue with DAPI (4′,6-Diamidin-2-phenylindol). All cell lines are mature and show no persistence of NKX-2.5. Images were acquired with a 40x objective.

While in the NKX-2.5 positive control iPSC-derived cardiomyocytes, NKX-2.5 as a marker for immature cardiomyocytes was still detectable (red signal) (Figure 15 A), the wildtype control, isogenic control and patient SCN5A$^{1072T>C}$ iPSC-derived cardiomyocytes (Figure 15 B,C,D) do not show any red signal, indicating the absence of NKX-2.5. This leads to the conclusion that the cells lost the immaturity marker and consequently having reached a mature state.

3.6. Isogenic control iPSC- and patient iPSC-derived ventricular cardiomyocytes do not show differences in protein expression levels of SCN5A

To understand how the SCN5A$^{1072T>C}$ mutation may have an impact on the cardiomyocytes, I started to investigate the protein expression to detect possible differences in the amount of SCN5A protein. For this, proteins were extracted from the membrane and the cytosol of iPSC-derived cardiomyocytes from isogenic control and SCN5A$^{1072T>C}$ cells and a Western Blot (N=3) was performed on each fraction. With this approach I aimed to assess not only differences in the amount of proteins, but also if there is a difference in localization of SCN5A, which is usually mainly localized in the cell membrane. Vinculin was used as a loading control and showed similar intensity in isogenic control and SCN5A$^{1072T>C}$ protein fraction, making sure that the same amount of protein was loaded onto the gel.

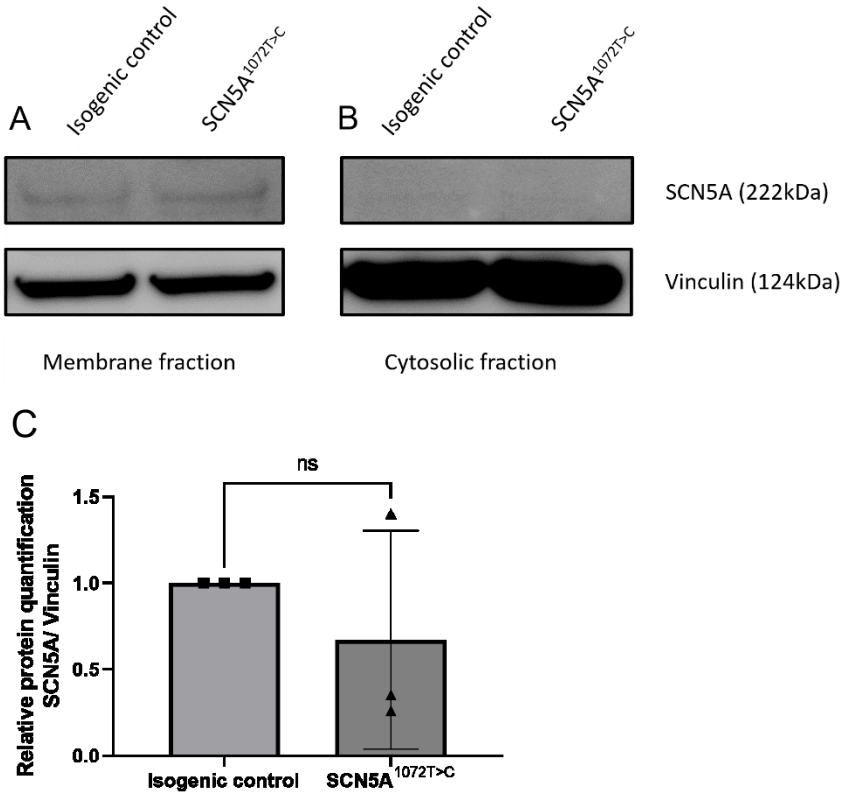

Figure 16: Western Blot of membrane and cytosolic protein fraction of isogenic control and patient iPSC-derived cardiomyocytes. Vinculin is served as a loading control. (A) Western Blot of isogenic control and SCN5A$^{1072T>C}$ from membrane isolated protein. (B) Western Blot of isogenic control and SCN5A$^{1072T>C}$ from cytosolic isolated protein. (C) Relative protein quantification SCN5A/Vinculin of membrane fraction. (N=3, mean±S.D. Mann-Whitney test, p=0,7)

The Western Blot showed SCN5A protein expression only in the membrane fraction (Figure 16A) but not in the cytosolic fraction (Figure 16 B) of the isogenic control and patient SCN5A$^{1072T>C}$ cardiomyocytes. In comparison between the isogenic control and the patient SCN5A$^{1072T>C}$ cardiomyocytes the amount of protein expression of SCN5A does not show a significant difference in the membrane fraction (Figure 16 C).

These results led me to the conclusion, that the SCN5A$^{1072T>C}$ mutation does not lead to a dislocation of the SCN5A protein, and is mainly localized in the cell membrane in both of the cell lines, where it exerts its physiological function. Comparison of protein expression levels between isogenic control and SCN5A$^{1072T>C}$ patient cardiomyocytes revealed no statistically significant difference.

3.7. Wildtype control, isogenic control, and patient iPSC-derived ventricular cardiomyocytes do not show differences in SCN5A localization in immunostaining

To support the hypothesis that the SCN5A$^{1072T>C}$ mutation does not lead to a dislocation of SCN5A, and to get a better impression of the SCN5A protein localization in the cell, I performed immunostainings. Additionally, my objective was to develop an understanding of the cell structure, including sarcomeric structure through this staining. For immunostaining an anti-SCN5A antibody was used to check the localization of the channel and anti-alpha-actinin antibody, to visualize the sarcomere structure and to investigate if there are any structural problems in the sarcomeres.

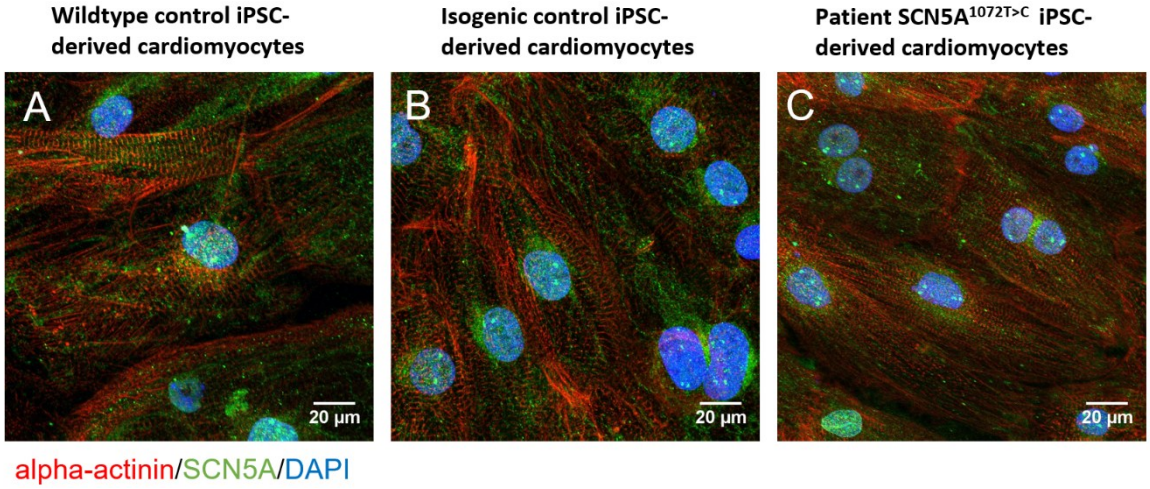

Figure 17: Immunostaining of wildtype control, isogenic control and patient SCN5A$^{1072T>C}$ iPSC-derived cardiomyocytes. SCN5A is stained green, alpha-actinin is stained red and the nucleus is stained blue with DAPI (4′,6-Diamidin-2-phenylindol). Images were acquired with a 63x objective.

Qualitative rather than quantitative conclusions about SCN5A expression can be drawn from the immunostaining analysis. The analysis of Figure 17 A, B and C and Figure 18 D, E and F, revealed that SCN5A is predominantly localized in the cell membrane, which is matching the findings from the Western Blot, where SCN5A protein was also found to be mainly expressed in the cell membrane protein fraction (Figure 16 A). In wildtype control, isogenic control and patient SCN5A$^{1072T>C}$ cardiomyocytes, unspecific binding of the SCN5A antibody in the nucleus could be detected in all cell lines (Figure 17 A, B, C; Figure 18 D, E, F), a phenomenon which is already described previously in literature. These observations suggest that the SCN5A$^{1072T>C}$ mutation is not causing a mislocalization of SCN5A.

Sarcomere structures, shown in alpha-actinin staining, show well organized and less organized parts in all three cell lines (Figure 18 A, B, C), but do not show major differences in structure and organization overall, in comparison between wildtype control, isogenic control and patient SCN5A$^{1072T>C}$ cardiomyocytes. This leads to the assumption that there are no major impairments in sarcomere structure due to the SCN5A mutation.

Taken together, these results suggest that the mutation causes no structural alterations in the iPSC-derived cardiomyocytes, like dislocation of SCN5A protein, the shape of the cardiomyocytes or the sarcomere structure. (Figure 17, 18).

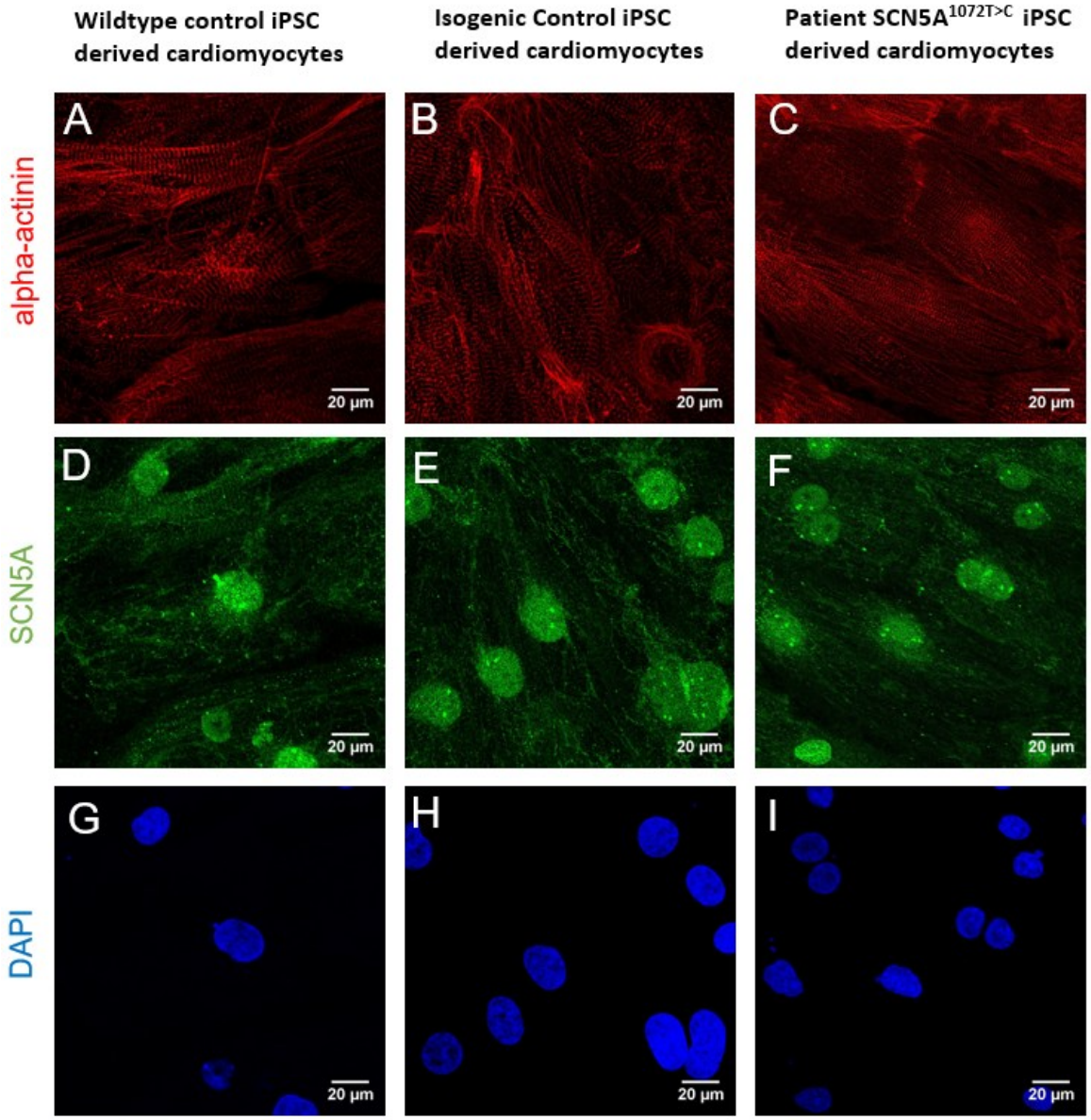

Figure 18: Different split pictures from immunostaining of wildtype control, isogenic control and patient SCN5A$^{1072T>C}$ iPSC-derived cardiomyocytes. SCN5A is stained green, alpha-actinin is stained red and the nucleus (DAPI/4′,6-Diamidin-2-phenylindol) is stained blue. Images were acquired with a 63x objective.

With the results obtained so far, I can summarize that the SCN5A$^{1072T>C}$ mutation does not cause alterations in protein expression levels, localization of SCN5A or in sarcomere structure of the iPSC-derived cardiomyocytes.

3.8. Isogenic control iPSC and SCN5A$^{1072T>C}$ iPSC-derived ventricular cardiomyocytes do not show differences in SCN5A, RYR and SERCA2a mRNA expression

To confirm these findings also on a mRNA level, qRT-PCR (quantitative reverse transcription polymerase chain reaction) was performed with mRNA obtained from adult cardiomyocytes of wildtype control, isogenic control and SCN5A$^{1072T>C}$ iPSC-derived cardiomyocytes. Based on the observed perturbations in calcium current dynamics in SCN5A$^{1072T>C}$ mutant cells (see 3.9), we hypothesized that alterations in the expression of key calcium handling genes may occur. While the functional interplay in excitation-contraction coupling of SCN5A, RyR (ryanodine receptor), and SERCA2a (Sarcoplasmic/Endoplasmic Reticulum Calcium ATPase 2a) is established, direct transcriptional regulation between these genes has not yet been reported. To address this hypothesis, we quantified the mRNA expression of important genes in calcium homeostasis, RyR and SERCA2a, to investigate the potential for direct interaction with SCN5A.

The mRNA levels of the isogenic control showed no significant difference from those of the wildtype control, making it apparent, that gene expression is not significantly different between the commercial wildtype control and self-produced isogenic control iPSCs. This indicates that the isogenic control shows a wildtype gene expression.

SCN5A$^{1072T>C}$ cells (0,6503±0,02859) showed no significant difference in SCN5A mRNA expression, compared to the control cells (N=3, n=3, p=0,9143). In our analysis SERCA2a or RYR mRNA showed no alterations in SCN5A$^{1072T>C}$ cells. No significant difference was observed in SERCA2a mRNA expression (0,8216±0,5118) (N=3, n=3, p=>0,9999) as well as in RyR (ryanodine receptor) mRNA expression (1,061±0,6146) (N=3,n=3, p=>0,9999) (Figure 19). Thus, no major changes in mRNA expression of the examined genes between the control cell lines and the SCN5A$^{1072T>C}$ cell line could be revealed.

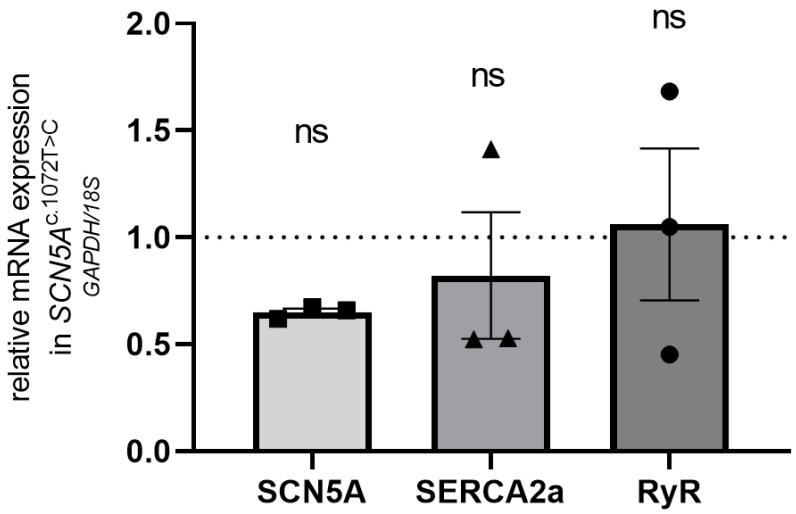

Figure 19: Relative mRNA expression of SCN5A, SERCA2a (Sarcoplasmic/endoplasmic reticulum calcium ATPase 2a), and RyR (ryanodine receptor) in SCN5A$^{1072T>C}$ iPSC-derived cardiomyocytes compared to isogenic control iPSC-derived cardiomyocytes in qRT-PCR (quantitative reverse transcription polymerase chain reaction). (N=3, n=3, mean±S.D. Kruskal-Wallis test, followed by Dunn´s multiple comparison test. SCN5A (0,6503±0,02859) p=0,9143, SERCA2a (0,8216±0,5118) p=>0,9999, RyR (1,061±0,6146) p=>0,9999.

These results support the outcomes from Western Blot where differences in the amount of protein expression of SCN5A could not be detected, supporting the hypothesis that the SCN5A$^{1072T>C}$ mutation does not lead to an altered SCN5A expression. Also, mRNA of the functional closely interacting proteins RYR and SERCA2a did not show differences in gene expression, suggesting that a potential impairment by the SCN5A$^{1072T>C}$ mutation might not affect the expression level of these genes but could manifest as a functional impairment.

3.9. Calcium dynamics are altered in SCN5A$^{1072T>C}$ iPSC-derived ventricular cardiomyocytes compared to wildtype control and isogenic control iPSC-derived cardiomyocytes

Calcium transients, which occur with every heartbeat in cardiomyocytes, are important for cardiac contraction. In cardiomyocytes, Na^+ kinetics closely interact functionally with Ca^{2+} kinetics in the excitation-contraction coupling, which is essential for the transduction of the electrical signal of the cardiac action potential into the subsequent mechanical response of myocardial contraction. To deepen the functional understanding and to determine whether the SCN5A$^{1072T>C}$ mutation

affects Ca^{2+} homeostasis in any way, we aimed to investigate Ca^{2+} dynamics in the iPSC-derived CMs. This was achieved by performing Calcium Imaging, a method in which Ca^{2+} dynamics can be measured during the contraction cycle by using Fura-2. Fura-2, a fluorescent Ca^{2+} indicator with high affinity for calcium ions, undergoes a conformational change upon Ca^{2+} binding, which is detectable as a shift in its fluorescence spectrum. This property allows for the precise measurement of intracellular Ca^{2+} dynamics in various cell types, including cardiomyocytes. Consequently, Fura-2 is a valuable tool for investigating Ca^{2+} transients associated with excitation-contraction coupling in cardiac muscle. Experiments were performed on 24-day-old cardiomyocytes (Figure 20).

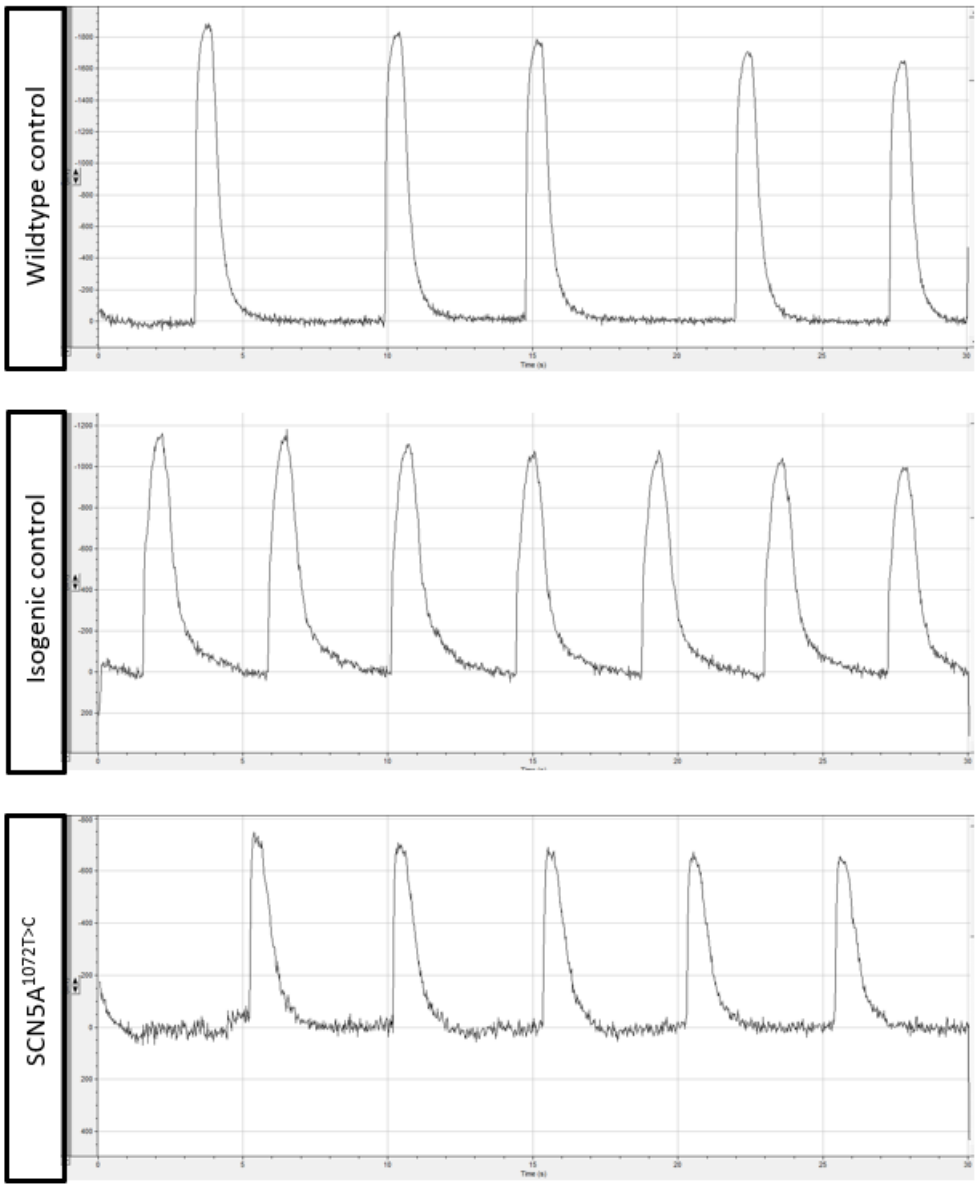

Figure 20: Calcium imaging peaks of beating cardiomyocytes from wildtype control, isogenic control and patient iPSC-derived cardiomyocytes. Images show the peaks in a 30 second interval for each cell line, obtained from 24-day-old cardiomyocytes.

The first set of analyses examined the beating frequency. From the recorded Ca^{2+} peaks, the number of beats in a 30 seconds interval was determined and from these values the beats per minute (bpm) were calculated. Beats per minute were compared between isogenic control and $SCN5A^{1072T>C}$. Beating frequency in Calcium Imaging experiments was decreased in $SCN5A^{1072T>C}$ cardiomyocytes (15,38±4,788) compared to isogenic control cells (20,15±5,257) (n=13, *p=0,0288) (Figure 21).

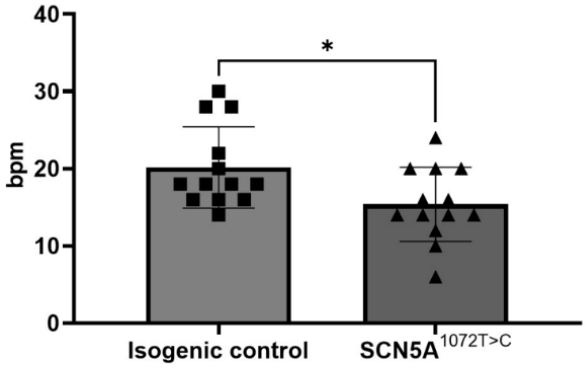

Figure 21: Beating rate (beats per minute). Isogenic control (20,15±5,257) compared to patient iPSC derived cardiomyocytes (15,38±4,788) (N=3 n=13, mean±S.D. Mann-Whitney test, *p=0,0288).

To characterize the Ca^{2+} peaks, the following parameters were measured and compared between the cell lines. Half width, resulting from the mV reached after half of the maximum peak. Rise time, which indicates the time required for the calcium peak to reach 90% of its maximum from 10% of its maximum. Decay time for the required time from 90% of the maximum to 10% of the maximum and the time of peak, which is the duration of the calcium peak, calculated from rise time and decay time (Figure 22).

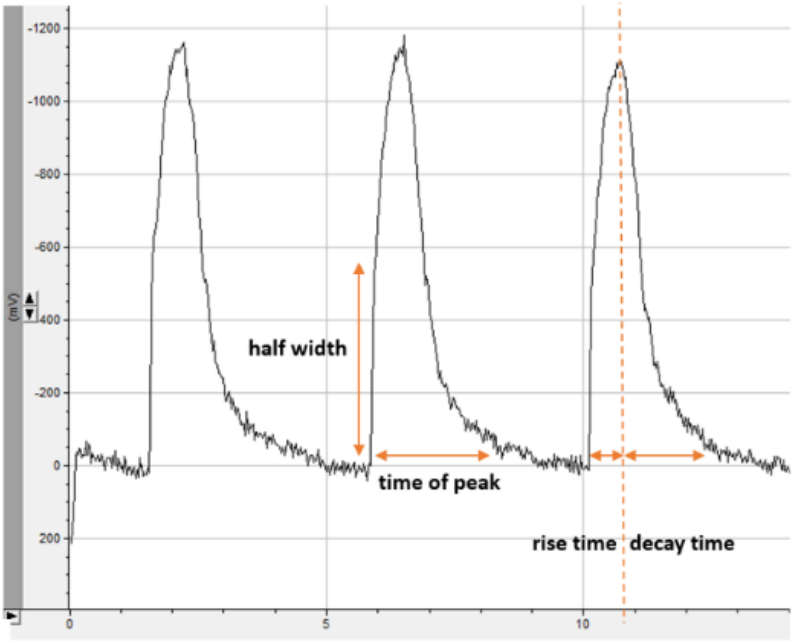

Figure 22: Image to demonstrate the parameters for calcium imaging statistics. The different parameters time of peak, half width, rise time, decay time are shown. mV=millivolt

Statistical analysis and comparison of time of peak, half width, rise time and decay time between the wildtype control and the isogenic control showed no statistical significant difference in all 4 investigated parameters, thus in the following only the statistical differences between isogenic control and SCN5A$^{1072T>C}$ mutated cardiomyocytes are displayed. Time of peak analysis showed a significant difference between and isogenic control (1505±483,1) and SCN5A$^{1072T>C}$ (703,7±230,5) (N=3, n=47/48, Isogenic control vs SCN5A$^{1072T>C}$ ****p=<0,0001) (Figure 23 A). Half width analysis showed a significant difference between isogenic control (957±181,4) and SCN5A$^{1072T>C}$ (701,6±43,8), (N=3, n=48, Isogenic control vs SCN5A$^{1072T>C}$ ****p=<0,0001) (Figure 23 B). Rise time analysis also showed a significant difference between isognenic control (231,8±105,2) and SCN5A$^{1072T>C}$ (147,6±63,03) (N=3, n=47/48, Isogenic control vs SCN5A$^{1072T>C}$ ****p=<0,0001) (Figure 23 C). Statistical analysis of Decay time showed a significant difference between isogenc control (1277±414,7) and SCN5A$^{1072T>C}$ (556,1±198,5), as well (N=3, n=48, Isogenic control vs SCN5A$^{1072T>C}$ ****p=<0,0001) (Figure 23 D).

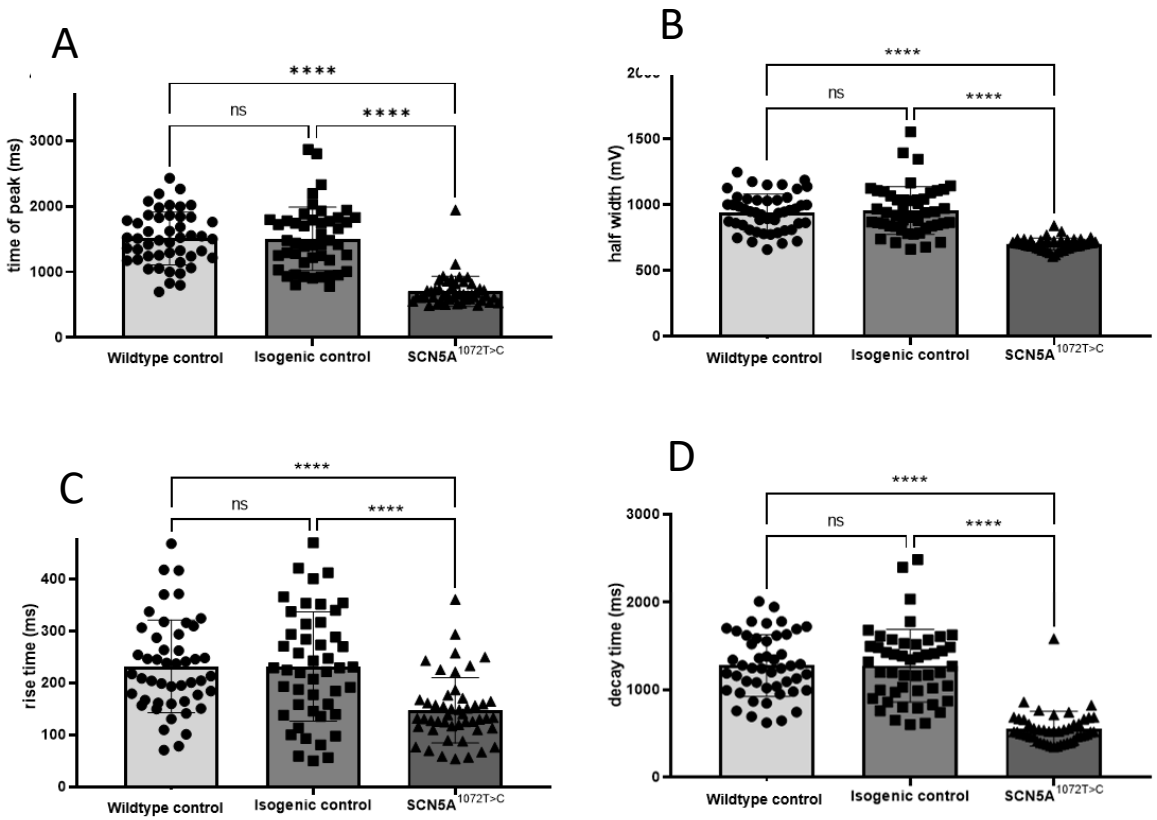

Figure 23: Analysis of Calcium Imaging (time of peak, half width, rise time, decay time). (A) Time of peak comparison between wildtype control (1510±403,1), isogenic control (1505±483,1), and SCN5A$^{1072T>C}$ (703,7±230,5) (N=3, n=48/47/48, mean±S.D. One-way ANOVA followed by tukey´s multiple comparison analysis, wildtype control vs isogenic control p=0,9976; wildtype control vs SCN5A$^{1072T>C}$ ****p=<0,0001; isogenic control vs SCN5A$^{1072T>C}$ ****p=<0,0001). (B) Half width comparison between wildtype control (939,9±142,2), isogenic control (957±181,4), and SCN5A$^{1072T>C}$ (701,6±43,8) (N=3, n=48, mean±S.D. One-way ANOVA followed by tukey´s multiple comparison analysis, wildtype control vs isogenic control p=0,8112; wildtype control vs SCN5A$^{1072T>C}$ ****p=<0,0001; isogenic control vs SCN5A$^{1072T>C}$ ****p=<0,0001). (C) Rise time comparison between wildtype control (232,2±89,06), isogenic control (231,8±105,2), and SCN5A$^{1072T>C}$ (147,6±63,03) (N=3, n=48/47/48, mean±S.D. One-way ANOVA followed by tukey´s multiple comparison analysis, wildtype control vs isogenic control p=0,9996; wildtype control vs SCN5A$^{1072T>C}$ ****p=<0,0001; isogenic control vs SCN5A$^{1072T>C}$ ****p=<0,0001). (D) Decay time comparison between wildtype control (1278±354), isogenic control (1277±414,7), and SCN5A$^{1072T>C}$ (556,1±198,5) (N=3, n=48, mean±S.D. One-way ANOVA followed by tukey´s multiple comparison analysis, wildtype control vs isognic control p=0,9999; wildtype control vs SCN5A$^{1072T>C}$ ****p=<0,0001; isogenic control vs SCN5A$^{1072T>C}$ ****p=<0,0001). ms=milliseconds, mV=millivolt

Finding no significant difference between Wildtype control and Isogenic control cardiomyocytes, I can assume that correcting the mutation of the patient cardiomyocytes has resulted in a wildtype phenotype that behaves the same as the commercial wildtype concerning calcium dynamics. Both, wildtype control and isogenic control show a significant different behavior compared to the patient cardiomyocytes. These results give a strong indication that the mutation is the cause

of the altered values in Calcium Imaging. These findings lead me to assumption, that the SCN5A$^{1072T>C}$ mutation affects Ca^{2+} dynamics in a functional manner. Together with the previous results, these findings support my hypothesis that the SCN5A mutation leads to functional problems, and by correcting the mutation these functional problems regarding calcium dynamics can be solved.

3.10. Electrophysiological analysis of beating period shows no difference between isogenic control and SCN5A$^{1072T>C}$ cells

To deepen the understanding of the functional, electrophysiological behavior of the iPSC-derived cardiomyocytes, experiments were performed with a multi-electrode array (MEA), a cell culture plate, that can derive the extracellular potentials of the cells with electrodes. For this purpose, the cells were placed on the MEA plates and left there for at least one week for recovery before the experiments were performed. For measurements, the cells were paced at 1Hz, which is approximately the usual resting heart rate in adult humans. The isogenic control and SCN5A$^{1072T>C}$ cells beat regularly and followed the pacing rhythmically (Figure 19 A). Signals with the beating rate of 1Hz, following the pacing, could be obtained from both cell lines (Figure 24 B).

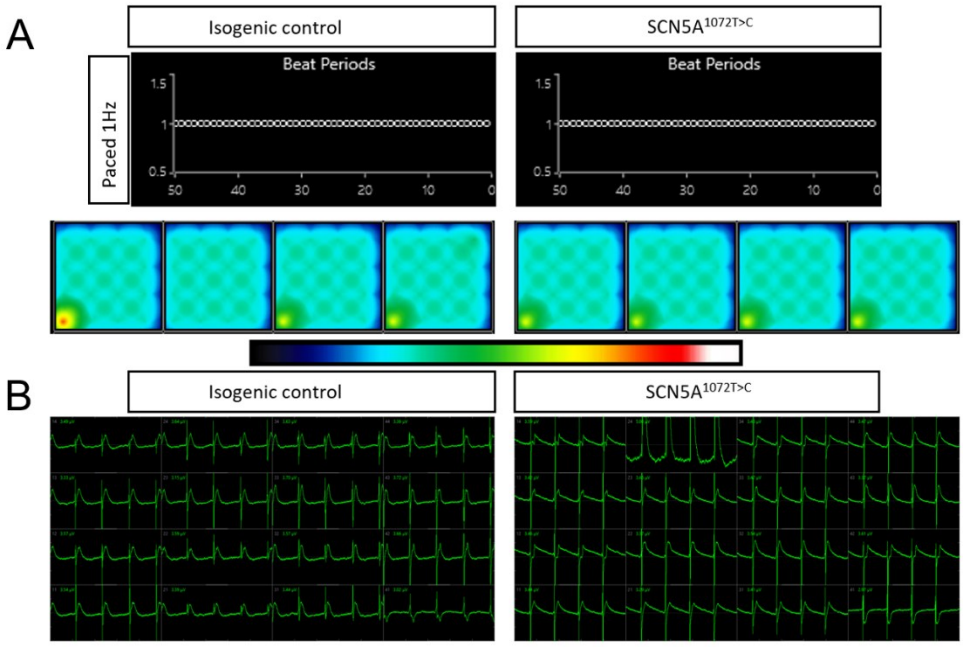

Figure 24: Demonstration of the recordings with multi-electrode array plate. (A) Beating periods of isogenic control and patient SCN5A$^{1072T>C}$ iPSC-derived cardiomyocytes. Diagram and color-coded map of wells show the regular beating at 1Hz. (B) Overview of signals obtained during recording.

3.11. SCN5A$^{1072T>C}$ iPSC-derived cardiomyocytes show an impaired conduction velocity in comparison to isogenic control cells

To analyze the electrical impulses of the cells during one action potential, field potentials of the cells were investigated. The field potential, similar to the action potential, indicates the electrical potential that can be recorded during cellular excitation (Figure 25 A, B). In contrast to the action potential, it can only be acquired extracellularly and does not indicate the potential of a cell alone, but the extracellular potential of the cells, recorded from one electrode of the MEA plate. This makes the field potential easier to derive, but also less accurate than the action potential. Because of the dependence of FPD (field potential duration) on beat frequency, not only FPD was measured, but also frequency-corrected FPD, corrected after the Fridericia formula (FPDc). In addition, the conduction velocity was investigated, which gives information about how fast the cells transmit the electrical signal to the next cell.

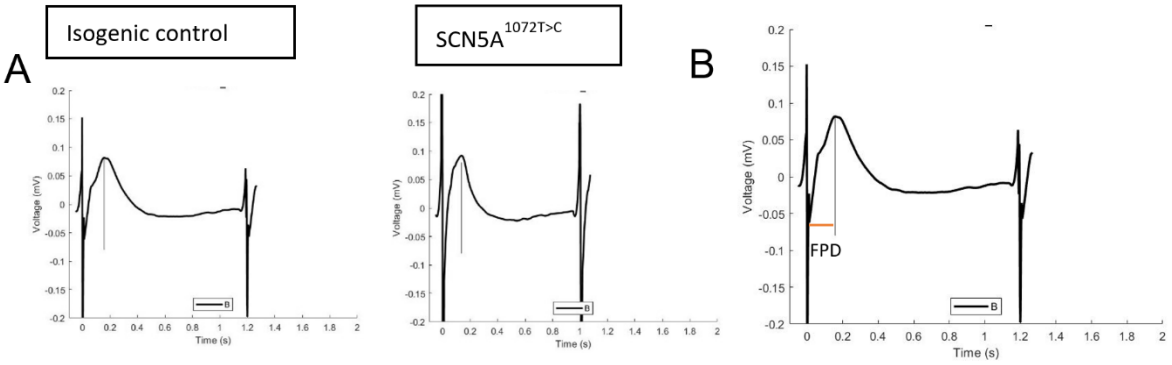

Figure 25: Field potential obtained with multi-electrode array (MEA) plate. (A) Field potential of isogenic control and patient SCN5A$^{1072T>C}$ iPSC derived cardiomyocytes. (B) Illustration of Field potential duration (FPD). mV=millivolt

Isogenic control (304,7±91) and SCN5A$^{1072T>C}$ (239,9±110,9) showed no significant differences in field potential duration (FPD) (N=8/11, p=0,1774) (Figure 26 A) and in FPDc (Fridericia) (isogenic control: 303,6±93,14; SCN5A$^{1072T>C}$: 238,4±112,4) (N=8/11, p=0,1518) (Figure 26 B). Conduction velocity was slightly decreased in the SCN5A$^{1072T>C}$ cells (isogenic control: 0,1742± 0,04121; SCN5A$^{1072T>C}$: 0,1092± 0,04887 (N=5/8, *p=0,0451) (Figure 26 C).

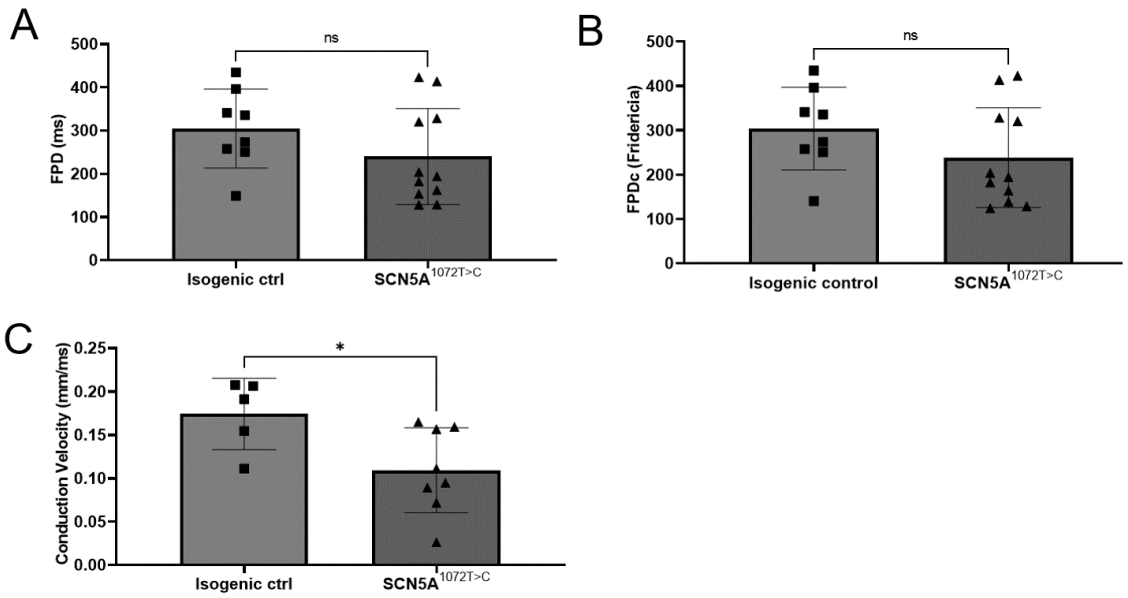

Figure 26: Statistical analysis of parameters obtained with multi-electrode array (MEA) plate. (A) Comparison of FPD (field potential duration) between isogenic control (304,7±91) and SCN5A$^{1072T>C}$ (239,9±110,9) (N=8/11, mean±S.D. Mann-Whitney test, p=0,1774). (B) Comparison of FPDc (frequency corrected field potential duration) between isogenic control (303,6±93,14) and SCN5A$^{1072T>C}$ (238,4±112,4) (N=8/11, mean±S.D. Mann-Whitney test, p=0,1518). (C) Comparison of Conduction velocity between isogenic control (0,1742± 0,04121) and SCN5A$^{1072T>C}$ (0,1092± 0,04887) (N=5/8, mean±S.D. Mann-Whitney test, *p=0,0451). ms=milliseconds, mm=millimeter

These findings provide initial evidence regarding the electrophysiological characteristics of the iPSC-derived CMs. While no statistically significant alterations in FPD and FPDc could be obtained in SCN5A$^{1072T>C}$ mutated cells, the subtle reduction in conduction velocity suggests the potential for underlying electrophysiological dysfunction associated with the SCN5A$^{1072T>C}$ mutation. To definitively characterize these effects, further investigations are necessary, including electrophysiological analyses of spontaneously active (non-paced) cells to avoid interference with intrinsic cellular processes, and assessment of intracellular action potentials of single cells.

3.12. ECG signals from zebrafish embryos can be effectively recorded and exhibit a morphology comparable to human

To study the effects of the SCN5A$^{1072T>C}$ mutation also *in vivo*, embryo zebrafish (Danio rerio) were used as an animal model. To study the SCN5A$^{1072T>C}$ mutation *in vivo*, a transgenic zebrafish line, overexpressing the mutated SCN5A (TgSCN5A$^{1072T>C}$) was used (Figure 27).

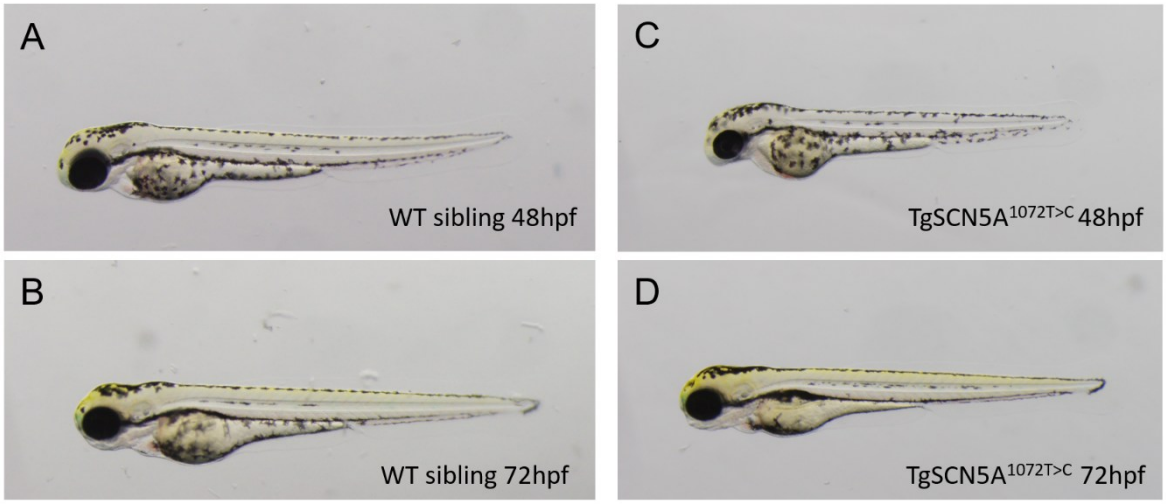

Figure 27: Images of embryo zebrafish. Wildtype sibling embryo zebrafish at 48hpf (hours post fertilization) (A) and 72hpf (B) and TgSCN5A$^{1072T>C}$ embryo zebrafish at 48hpf (C) and 72hpf (D).

To investigate whether these fish suffer from long QT syndrome, ECG of zebrafish embryos from a TÜAB wildtype line and the SCN5A$^{1072T>C}$ transgenic line were recorded by placing a thin glass capillary on the junction between the atrium and ventricle and deriving the electrical signals. QT duration was measured and compared between the two fish lines to investigate whether they exhibit QT interval prolongation. Since the mutated fish not only overexpress the SCN5A$^{1072T>C}$ gene but additionally express a GFP signal, GFP^{+} fish were selected for ECG recording in the mutated group (additional information and further characterization of the fish line can be found in Däuwels thesis).

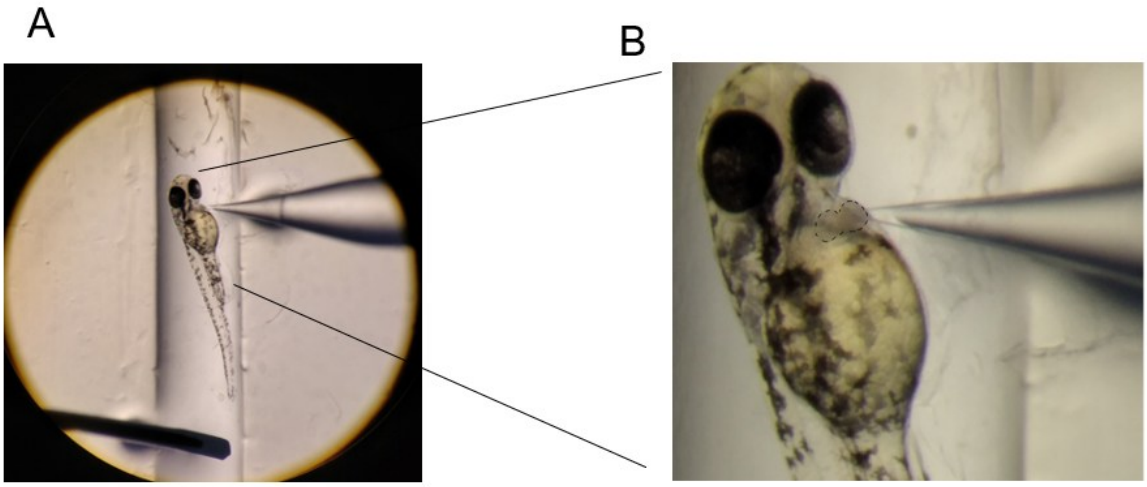

Figure 28: Position of ECG electrodes during ECG recording of embryo zebrafish. (A) Image of 48hpf (hours post fertilization) TÜAB wildtype embryo during ECG recording. Position of the recording electrode between atrium and ventricle on the skin surface of the embryo. Reference electrode in the surrounding media. (B) Magnified image with atrium and ventricle marked.

In most ECG recordings, I got a clear and rhythmic pattern of cardiac activity (Figure 29 A). Usually, I could identify the T wave and the QRS complex (Figure 29 B), which are well comparable to the human ECG (Figure 29 C). The P wave was not always clearly visible. However, this did not affect the integrity of the analysis.

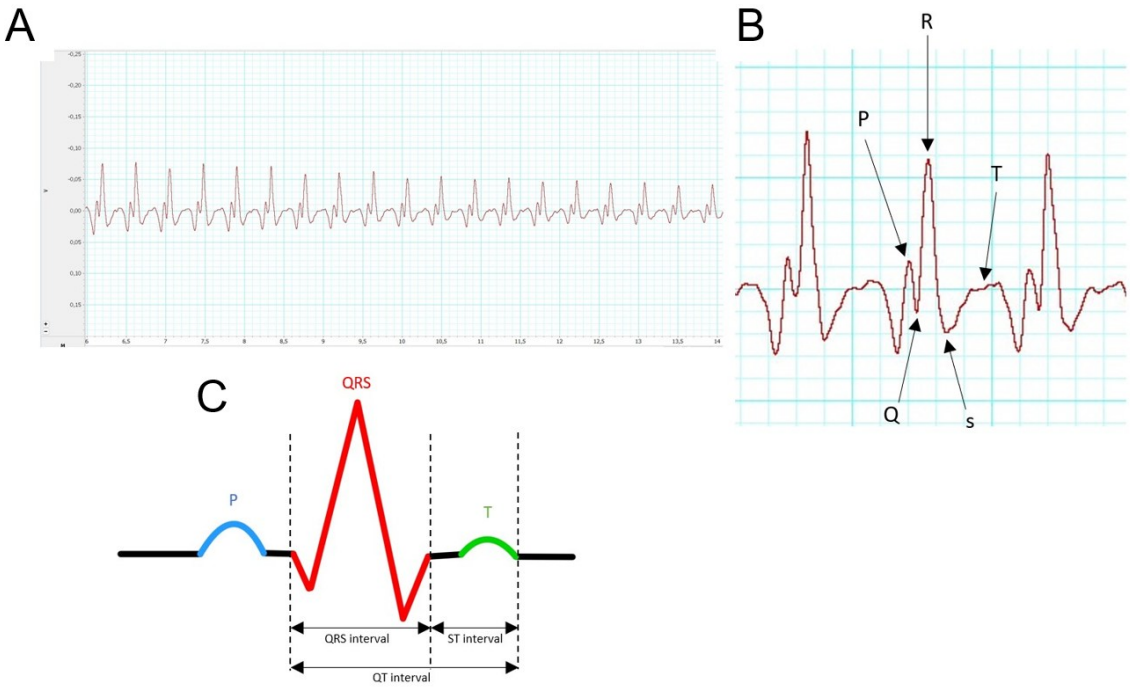

Figure 29: ECG recordings of embryo zebrafish and human. (A) ECG (electrocardiogram) of a 48hpf (hours post fertilization) TÜAB wildtype embryo. (B) Magnified ECG of a 48hpf TÜAB wildtype embryo with labeling of the important waves and peaks. (C) Typical human ECG shape with labeling of the different waves, peaks and intervals.

3.13. TgSCN5A$^{1072T>C}$ zebrafish embryos do not show QT-prolongation at 48hpf compared to TÜAB wildtype fish

To gain insight into the characteristics of the cardiac activity in embryonic zebrafish, ECG were recorded at 48hpf, which was the earliest time point possible to get a clear ECG signal (Figure 30). Beating frequency was determined and QT time was measured in ECG of TgSCN5A$^{1072T>C}$ and wildtype embryos. QT time was corrected for frequency (QTc), because the QT duration depends on the beating rate. It was used the Fridericia formula (QTc (Fridericia)=QT-time/(RR^(1/3)), which is a formula recommended for frequencies above 80bpm and produces more accurate results for QTc calculation at high frequencies than the Bazett formula, which is commonly used for diagnosis in humans.

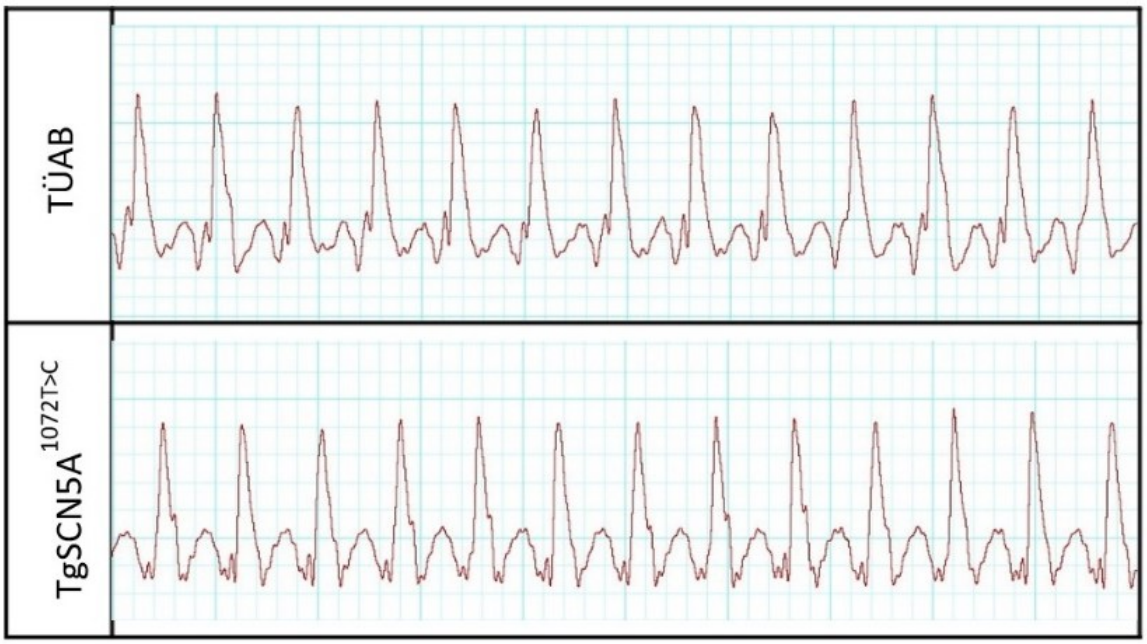

Figure 30: ECG recorded at 48hpf (hours post fertilization). On the top TÜAB wildtype (WT) zebrafish embryos and below TgSCN5A$^{1072T>C}$ zebrafish embryos.

In ECG recorded from 48hpf embryo zebrafish, we could observe that TgSCN5A$^{1072T>C}$ showed a slightly higher heart frequency (beats per minutes, bpm) (171,8±19,58) compared to the wildtype embryos (160,9±26,22) (N=13/23, *p=0,0496) (Figure 31 A). QTc showed no significant differences at 48hpf (TÜAB: 465,2±54,26; TgSCN5A$^{1072T>C}$: 460,8±46,1) (N=13/23, p=0,9224) (Figure 31 B), suggesting that, at this point of time the zebrafish embryos do not exhibit a phenotypic manifestation of long QT syndrome (LQTS).

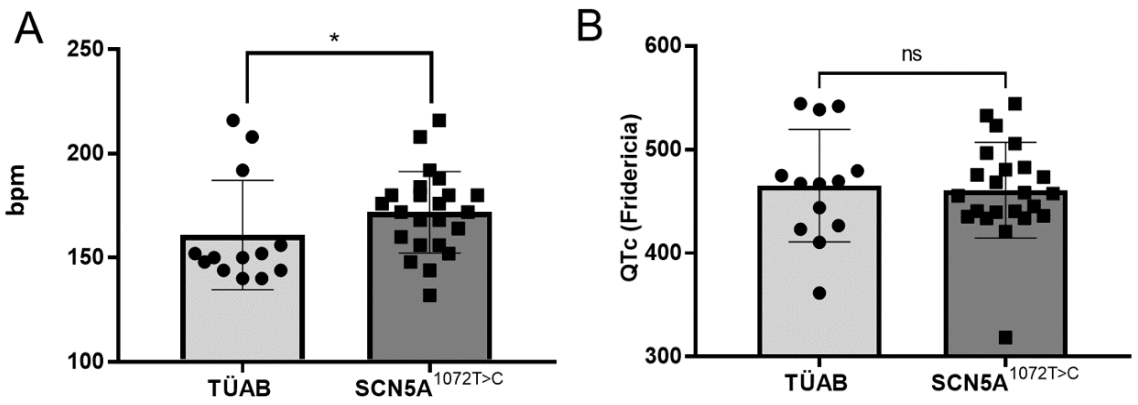

Figure 31: Heart rate and QTc (QT corrected) of embryo zebrafish at 48hpf (hours post fertilization). (A) Heart rate (in bpm=beats per minute) of TgSCN5A$^{1072T>C}$ (171,8±19,58) embryos is slightly higher than that of TÜAB wildtypes (160,9±26,22) at 48hpf (N=13/23, mean ± S.D. Mann-Whitney test, *p=0,0496). (B) QTc calculated after Fridericia shows no significant difference between TÜAB wildtypes (465,2±54,26) and TgSCN5A$^{1072T>C}$ (460,8±46,1) in 48hpf embryos (N=13/23, mean ± S.D. Mann-Whitney test, p=0,9224).

At this point, except for the slightly increased heart rate in TgSCN5A$^{1072T>C}$ embryo zebrafish, we had no evidence for a difference in cardiac electrical activity in TgSCN5A$^{1072T>C}$ embryos at 48hpf.

3.14. TgSCN5A$^{1072T>C}$ zebrafish embryos show QT prolongation at 72hpf

Because the embryonic zebrafish heart is still developing at 48hpf, we also examined TgSCN5A$^{1072T>C}$ zebrafish at a later time point at 72hpf (Figure 32 A).

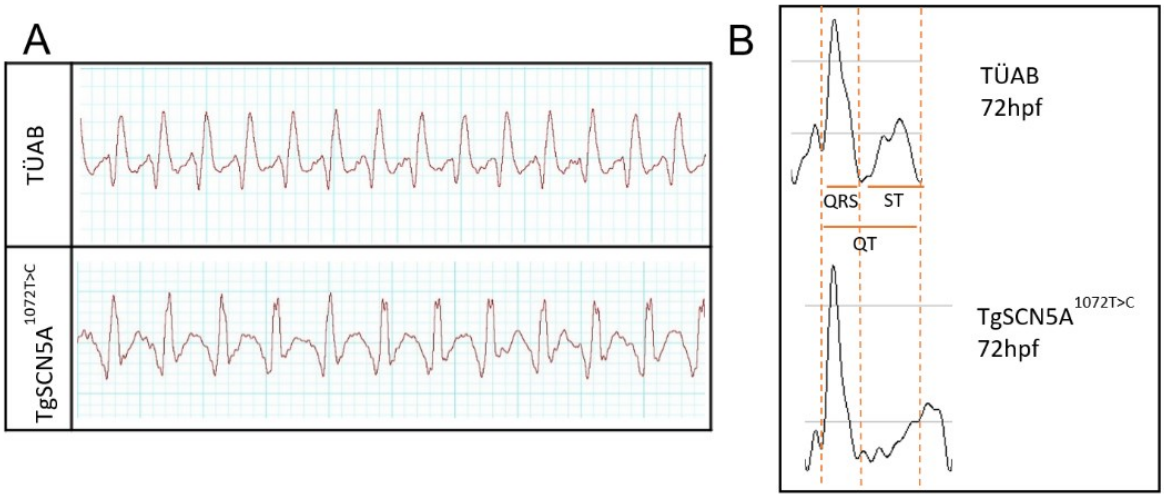

Figure 32: ECG recordings of embryo zebrafish at 72hpf (hours post fertilization). (A) ECG recorded at 72hpf from TÜAB wildtypes and TgSCN5A$^{1072T>C}$ embryo zebrafish. (B) Illustration of comparison of different ECG intervals, TÜAB wildtype and TgSCN5A$^{1072T>C}$.

In these 72h old embryo zebrafish, we could see differences regarding the QT time in the ECG (Figure 32 B). We found that TgSCN5A$^{1072T>C}$ zebrafish had a decreased heart rate (TÜAB: 179,3±12,27; TgSCN5A$^{1072T>C}$: 162±18,1) (N=17/20, **p=0,0018) (Figure 33 A), and prolonged QTc (Fridericia) compared with TÜAB wildtypes (TÜAB: 442,4±35,55; TgSCN5A$^{1072T>C}$: 489,3±36,5) (N=17/20, ***p=0,0008) (Figure 33 B), indicating that, at this time point, a phenotypic manifestation of LQTS has developed in TgSCN5A$^{1072T>C}$ zebrafish.

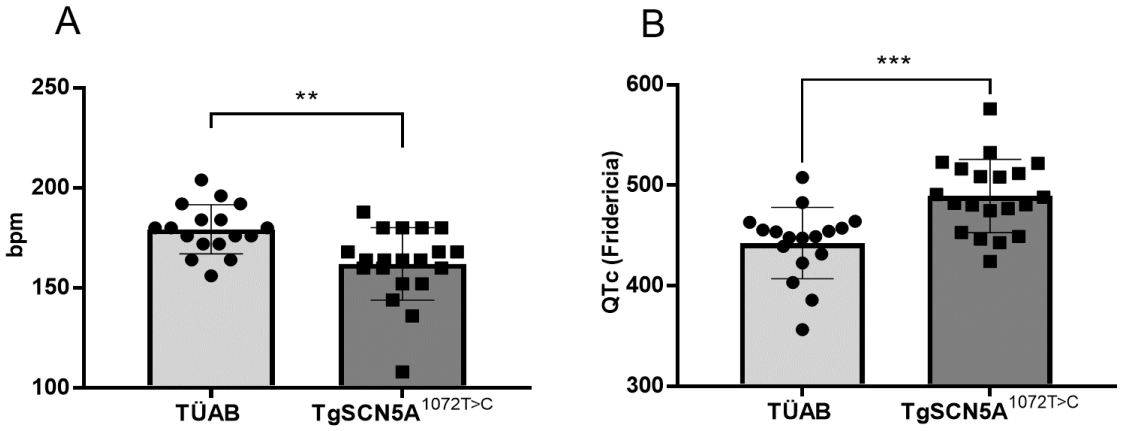

Figure 33: Heart rate and QTc (QT corrected) of embryo zebrafish at 72hpf (hours post fertilization). (A) TgSCN5A$^{1072T>C}$ (162±18,1) show lower heart rate (beats per minute) than TÜAB wildtype embryos (179,3±12,27) at 72hpf (N=17/20, mean ± S.D. Mann-Whitney test, **p=0,0018) (B) QTc (Fridericia) of TgSCN5A$^{1072T>C}$ embryos (489,3±36,5) was prolonged compared to TÜAB wildtype embryos (442,4±35,55) at 72hpf (N=17/20, mean ± S.D. Mann-Whitney test, ***p=0,0008).

In ECG, ST interval represents the repolarization process. As a result of the SCN5A$^{1072T>C}$ mutation, we would expect sodium current changes that would lead to a prolonged plateau phase in cardiac action potential and therefore to an impaired repolarization. Because QRS duration represents depolarization and ST duration represents repolarization, QT duration was subdivided in QRS complex duration and ST interval duration, to make more detailed statements about whether the depolarization or the repolarization process is impaired in the TgSCN5A$^{1072T>C}$ zebrafish. QRS duration was comparable in TgSCN5A$^{1072T>C}$ and WT fish (TÜAB: 137,3±27,49; TgSCN5A$^{1072T>C}$: 144±27,96) (N=16/20, p=0,6653) (Figure 34 A), but ST interval duration was prolonged in TgSCN5A$^{1072T>C}$ (TÜAB: 183,6±31,44; TgSCN5A$^{1072T>C}$: 211,9±30,11) (N=16/20, **p=0,0073) (Figure 34 B).

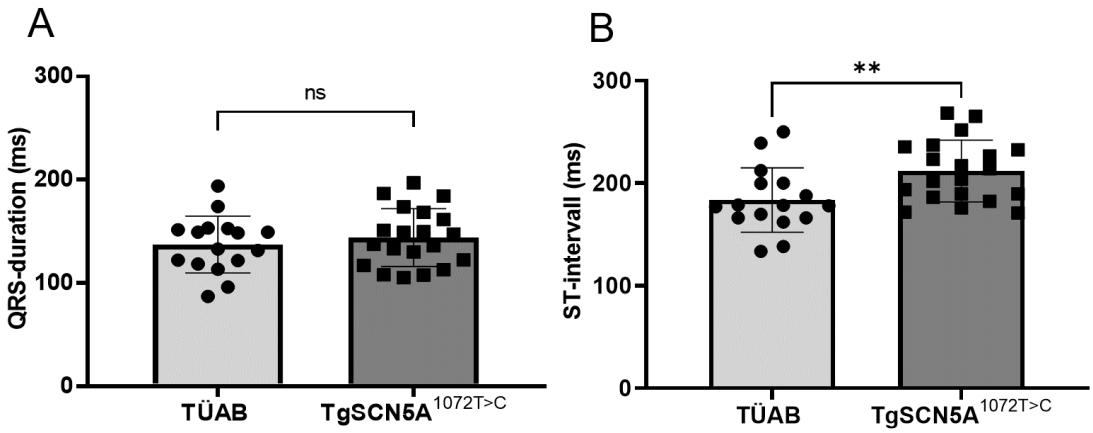

Figure 34: Comparison of QRS duration and ST interval duration of embryo zebrafish at 72hpf (hours post fertilization). (A) QRS duration showed no difference between TÜAB wildtype (137,3±27,49) and TgSCN5A$^{1072T>C}$ embryos (144±27,96) at 72hpf (N=16/20, mean ± S.D., Mann-Whitney test, p=0,6653). (B) ST interval was prolonged in TgSCN5A$^{1072T>C}$ embryos (211,9±30,11) compared to TÜAB wildtype embryos (183,6±31,44) at 72hpf (N=16/20, mean ± S.D. Mann-Whitney test, **p=0,0073). ms=milliseconds

These results indicate that especially ST duration is altered in the TgSCN5A$^{1072T>C}$ fish, which suggests an impaired repolarization process, whereas the depolarization process, represented by the QRS complex, appears normal. The results from the ECG of 72h old fish embryos support our hypothesis of altered repolarization, caused by the SCN5A$^{1072T>C}$ mutation, and we can summarize that the TgSCN5A$^{1072T>C}$ fish show a long QT syndrome.

3.15. TgSCN5A$^{1072T>C}$ +MO injected zebrafish show a long QT phenotype already at 48hpf

Zebrafish possess two different SCN5A genes, SCN5laa and SCN5lab. This experiment aimed to investigate if by knocking down the endogenous SCN5laa and SCN5lab genes in the TgSCN5A$^{1072T>C}$ zebrafish embryos, the phenotypic manifestation of LQTS would appear already at an earlier developmental stage (48hpf), due to reduced expression of SCN5laa and SCN5lab, which might lead to a reduced ability to compensate the SCN5A$^{1072T>C}$ mutation. To determine whether the knockdown of the endogenous SCN5laa and SCN5lab genes in the TgSCN5A$^{1072T>C}$ zebrafish results in a manifestation of a long QT phenotype already

at 48hpf, two splice-blocking morpholinos (MO) against SCN5laa and SCN5lab, 80µM each, were injected in TgSCN5A$^{1072T>C}$ oocytes in one cell state (prove of knockdown of SCN5laa and SCN5lab by using morpholinos was investigated by Däuwel and is described in her thesis). ECG was recorded from MO injected TgSCN5A$^{1072T>C}$ fish at 48hpf and compared to ECG from 72hpf old TgSCN5A$^{1072T>C}$ zebrafish, of which we already know, that they phenotypically exhibit a long QT syndrome (Figure 35).



Figure 35: ECG recorded from TgSCN5A$^{1072T>C}$ (72 hours post fertilization) and TgSCN5A$^{1072T>C}$ + morpholino (MO) injection (48 hours post fertilization).

QTc and beat frequency were compared between 48hpf TgSCN5A$^{1072T>C}$ zebrafish +MO and 72hpf TgSCN5A$^{1072T>C}$ zebrafish with a long QT syndrome, already known. The idea was that the ECG recordings of the 48hpf TgSCN5A$^{1072T>C}$ +MO fish, should resemble those of the 72hpf TgSCN5A$^{1072T>C}$ zebrafish, if they were to exhibit a long QT syndrome phenotype. ECG analysis showed, that zebrafish injected with morpholinos (TgSCN5A$^{1072T>C}$ +MO; 48hpf) had comparable QTc (Fridericia) to TgSCN5A$^{1072T>C}$ (72hpf) (TgSCN5A$^{1072T>C}$: 489,3±36,5; TgSCN5A$^{1072T>C}$ +MO: 507,6±31,77) (N=20/11, p=0,2788) (Figure 36 B). Similar results were also obtained for the beat frequency (TgSCN5A$^{1072T>C}$: 162±18,1; TgSCN5A$^{1072T>C}$ +MO: 158,4±16,89) (N=20/10, p=0,5462) (Figure 36 A), suggesting that after knockdown of the endogenous SCN5laa and SCN5lab the TgSCN5A$^{1072T>C}$ zebrafish already show a LQTS phenotype at 48hpf in contrast to

TgSCN5A$^{1072T>C}$ zebrafish not injected with morpholinos, which do not show a LQTS phenotype until 72hpf.

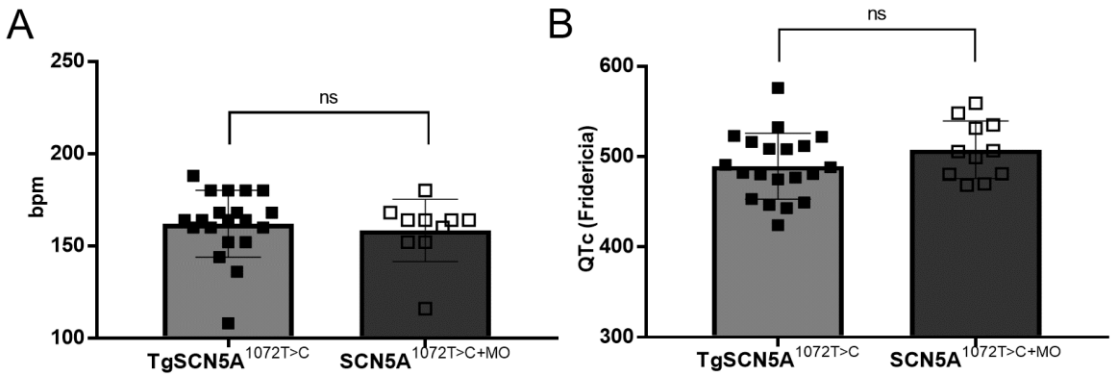

Figure 36: Comparison of beats per minute (bpm) and QTc (QT corrected) of TgSCN5A$^{1072T>C}$ 72hpf (hours post fertilization) and TgSCN5A$^{1072T>C}$ + morpholino (MO) injection 48hpf. (A) In heart rate (beats per minute) no significant difference could be seen between TgSCN5A$^{1072T>C}$ (72 hpf) (162±18,1) and TgSCN5A$^{1072T>C}$ +morpholino (MO) (48hpf) (158,4±16,89) (N=20/10, mean ± S.D. Mann-Whitney test, p=0,5462). (B) In QTc (Fridericia) no significant difference could be seen between TgSCN5A$^{1072T>C}$ (72hpf) (489,3±36,5) and TgSCN5A$^{1072T>C}$ +MO (507,6±31,77) (N=20/11, mean ± S.D Mann-Whitney test, p=0,2788).

These results reveal that by knocking down the endogenous fish SCN5laa and SCN5lab genes, the long QT phenotype manifests already after 48 hours, whereas the TgSCN5A$^{1072T>C}$ fish without MO injection exhibit this phenotype only after 72 hours. These results indicate that the endogenous SCN5laa and SCN5lab genes of the fish may help to prevent the appearance of the long QT phenotype at 48hpf, but do not protect the fish at 72hpf from getting long QT syndrome.

In summary, the generation of iPSC-derived cardiomyocytes from patient cells carrying the SCN5A$^{1072T>C}$ mutation, as well as from CRISPR/Cas9-corrected cells, was successful. The maturation of the cardiomyocytes was confirmed via immunostaining. Western blot analysis of protein expression revealed no significant differences in the total amount of the membrane fraction SCN5A proteins. The expression of the SCN5A protein was detected exclusively in the membrane fraction and not in the cytosolic fraction, suggesting that the protein remains primarily localized to the cell membrane in the SCN5A$^{1072T>C}$ mutant cells and is therefore not mislocalized as a result of the mutation. Immunostaining further demonstrated that the SCN5A$^{1072T>C}$ mutation did not lead to major impairments in sarcomere

structure. Additionally, mRNA expression levels of the SCN5A gene were not altered by the SCN5A$^{1072T>C}$ mutation. However, calcium imaging revealed a significantly altered calcium transient shape in the SCN5A$^{1072T>C}$ mutant cardiomyocytes compared to controls. Electrophysiological assessment using multi-electrode array (MEA) recordings showed a slightly reduced conduction velocity in the SCN5A$^{1072T>C}$ mutant cardiomyocytes.

Electrocardiograms (ECGs) were successfully recorded from the TgSCN5A$^{1072T>C}$ zebrafish embryos. At 48 hours post fertilization (hpf), no QT prolongation was observed in the mutants. However, at 72hpf, TgSCN5A$^{1072T>C}$ zebrafish exhibited a significantly lower heart rate and a significantly prolonged corrected QT interval (QTc) compared to wildtype zebrafish. When endogenous SCN5A expression was knocked down in the TgSCN5A$^{1072T>C}$ zebrafish using morpholinos, QTc prolongation was already evident at 48hpf, indicating an earlier onset of the electrophysiological phenotype in the absence of SCN5A compensation.

Taken together a functional impairment in both, SCN5A$^{1072T>C}$ iPSC-derived cardiomyocytes and TgSCN5A$^{1072T>C}$ embryonic zebrafish could be observed due to the mutation. No effects of the SCN5A$^{1072T>C}$ mutation were found on the sarcomere structure or gene expression in the investigations conducted here.

4. Discussion

4.1. Clinical and experimental background of a known SCN5A mutation in comparison to the novel SCN5A$^{1072T>C}$ mutation

Many cardiac diseases are associated with SCN5A mutations. LQTS 3, Brugada syndrome, sick sinus syndrome, conduction disturbances, atrial standstill, dilated cardiomyopathy and atrial fibrillation, are disorders that are or may be caused by SCN5A mutations [68]. Interestingly, the same SCN5A mutation can cause different diseases. The phenomenon when a specific SCN5A mutation causes different disease entities, which can also occur in the same individual as a mixed phenotype, is called overlap syndrome [62, 68]. One of the largest and best described families with overlap syndrome is described by Postema et al. [63]. They reported about a dutch family in which the SCN5A 1795insD mutation occurs, causing an overlap syndrome with different disease entities like LQTS, Brugada syndrome and conduction diseases [63]. Subsequently, the mutation was further investigated in mice, carrying the mice equivalent, the SCN5A 1798insD mutation, and the presence of an overlap syndrome could be confirmed in this animal model [67]. Moreover, in a computational simulation model of ventricular myocytes, it could be shown that the 1795insD SCN5A mutation may cause Brugada syndrome or LQTS, depending on the heart rate [17].

In this dissertation, starting with the clinical case of a patient who suffered from LQTS and had a positive family history, genetic testing revealed a SCN5A mutation not previously described in literature. The heterozygote genotype of the patient showed one SCN5A allele mutated in exon 9 c.1072T>C. The mutation is leading to an amino acid exchange from phenylalanine (PHE) to leucine (LEU) at position 358, in the intracellular region in chain A of the alpha subunit of NaV1.5.

In this case, the clinical entity was not definitively known from the outset. First, the patient was suspected to have DCM caused by the SCN5A mutation, prompting initial experiments to investigate DCM, while later it was clinically revealed to be rather a LQTS and I extended my investigations accordingly.

4.2. SCN5A$^{1072T>C}$ mutated patient iPSC-derived ventricular cardiomyocytes do not show structural abnormalities

In the last years modeling of inherited cardiac diseases with human induced-pluripotent stem cells (iPSC) has gained great importance and is becoming a powerful tool for the investigation of patient-specific mutations and personalized medicine. For example, iPSC can be used to create personalized disease models, as the cells are derived from the patient´s own tissue, or serve as a drug screening platform. Furthermore, there are approaches that utilize autologous iPSC for personalized cell-based therapies . Many different mutations and forms of LQTS have already been modeled using iPSC-derived cardiomyocytes. As commonly practiced, generation of iPSC and differentiation of cardiomyocytes was performed successfully and the different iPSC-lines did not differ in cell culture handling and behavior [52]. The mutation, carried from the index patient, did not affect the reprogramming process and the differentiation into cardiomyocytes. Maturity of the iPSC-derived CMs through NKX-2.5 staining could be detected in the SCN5A$^{1072T>C}$ iPSC-derived CMs on the same day as observed in the control cells. Immunostaining analysis of the cell morphology with a-actinin did not show a disturbed or less organized sarcomere structure caused by the mutation, and an identical localization of the SCN5A protein in the cardiomyocytes in mutated and control cells. Intracellular patterns of sarcomeric structure in a-actinin staining and localization of NaV1.5 in mutated and control cells in this research are comparable to the findings of Ma et al. [48], who investigated the heterozygous missense mutation SCN5A c.5287G>A in iPSC-derived CMs, obtained from a 7-year old girl, suffering from LQTS3. They also found similar patterns of sarcomeric structure in patient and control cells and an identical intracellular localization of NaV1.5 in patient and control cells [48]. Also in mice iPSC-derived CMs, heterozygous for KPQ deletion of SCN5A, immunostaining showed similar SCN5A Na^+ channel distribution and well-organized sarcomere structure in the cardiomyocytes [50]. Even in NaV1.5-knockout iPSC-derived CMs the sarcomeric structure is unaffected [60]. In relation to the findings of this study, this indicates that the investigated SCN5A$^{1072T>C}$ mutation behaves similarly to other mutations in the SCN5A gene and does not induce major impairments in sarcomeric structure. Furthermore, the analysis of SCN5A gene expression, determined by protein levels and mRNA

expression, revealed no difference between SCN5A$^{1072T>C}$ iPSC-derived CMs and control iPSC-derived CMs in this research. In the investigations from Malan et al. [50] who studied iPSC-derived CMs, heterozygous for KPQ deletion of SCN5A, relative SCN5A gene expression also did not differ between SCN5A mutants and WT at all three time points that were investigated, day 0, 9 and 14 [50]. These findings are comparable to the results of Ma et al., investigating the heterozygous missense mutation SCN5A c.5287G>A, who found similar levels of total SCN5A expression in their control and patient cells [48]. Consistent findings are also observed in the results of this study, where no difference in SCN5A expression could be detected, suggesting that also SCN5A$^{1072T>C}$ mutation does not lead to an altered SCN5A expression. Also, for other mutations such as a heterozygous CALM1-F142L mutation, which is associated with LQTS, no differences in sarcomere structure, organization and gene expression were observed [69]. Moreover, this study examined the expression of various genes involved either in calcium homeostasis or in the pathogenesis of long QT syndrome (LQTS). Among these were SCN5A, as well as SERCA and RyR, both of which play critical roles in the regulation of calcium homeostasis in cardiomyocytes and functionally interact with Calmodulin, expressed by the genes CALM1-3. None of these gene expressions were significantly altered in CALM1-mutated cells [69]. Given that significant differences in calcium dynamics were identified in the SCN5A$^{1072T>C}$ mutated cardiomyocytes in this study, we aimed to investigate whether key genes involved in calcium regulation might exhibit altered expression and could thus potentially be affected by the SCN5A$^{1072T>C}$ mutation. This investigation was conducted due to the significant differences in calcium dynamics, despite the lack of scientific evidence suggesting a direct interaction between SCN5A and SERCA or RyR genes so far. Similarly, to unchanged expression of these genes in CALM1-F142L mutated cells, no differences in the expression of SERCA2a and RyR were detected in SCN5A$^{1072T>C}$ mutated cells, which implies that, at least at the expression level, the SERCA2a and RyR genes are not affected by the SCN5A$^{1072T>C}$ mutation and that the differences in calcium dynamics observed in SCN5A$^{1072T>C}$ cells must have an alternative underlying cause. These results suggest that the heterozygote SCN5A$^{1072T>C}$ mutation, does not cause major structural impairments, like disruptions in sarcomere structure and distribution of SCN5A, as well as gene

expression of SCN5A, SERCA2a and RyR, despite significant differences in calcium dynamics.

Since I only investigated the mutation in heterozygosity, it would be interesting to investigate the same mutation in cells, homozygotic for the mutation. Homozygous conditions could result in new structural or functional problems because the cells no longer have a healthy allele that still encodes the wildtype channel. In my heterozygous condition, it is possible that the healthy wildtype allele may still be able to maintain physiological function of the NaV1.5 channel in ventricular iPSC-derived cardiomyocytes to the extent that I could not make pathological observations in my experiments. The observation that only the homozygous state, but not the heterozygous state, of certain SCN5A mutations leads to a pathological phenotype has been observed, for example, in the SCN5A missense mutation (p.I230T). A family was studied in which only the homozygous carriers of the mutation exhibited early cardiac arrhythmia, conduction disease, and severe ventricular arrhythmias [56]. Additionally, it has been described for another mutation (SCN5A-R814Q) that a homozygous mutation in a patient led to ventricular tachycardia and structural heart abnormalities, while the other family members, who were heterozygous for the mutation, remained asymptomatic [25]. To investigate whether the SCN5A$^{1072T>C}$ mutation, in its homozygous form, exerts stronger pathological effects under *in vitro* conditions, in the next step the mutation will be induced into the second, so far still wildtype allele, and the experiments will be repeated again.

4.3. Patient iPSC-derived ventricular CMs do not show major electrophysiological abnormalities but altered Ca^{2+} dynamics

Most SCN5A mutations leading to LQTS3 interrupt the inactivation process of the fast sodium influx or increase sodium window current in the cardiomyocyte action potential and thereby prolong the duration of the action potential, making cardiomyocytes more susceptible to early afterdepolarizations and arrhythmias [66, 102].

Because Ca^{2+} plays an important role in the cardiomyocyte action potential and excitation-contraction coupling, altered Na^{+} currents could also affect Ca^{2+} currents and homeostasis [66]. To analyze the calcium currents, I performed Calcium Imaging, in which Ca^{2+} dynamics are made visible by using Fura-2AM. Time of peak,

half width, rise time and decay time of the calcium waves were measured. The determinations of all 4 parameters showed significant differences between control iPSC-derived CMs and SCN5A$^{1072T>C}$ iPSC-derived CMs, with a significant decrease in the mutated cells for every parameter. In contrast to Calcium Imaging analyses in iPSC-derived CMs with mutations in the KCNQ1 gene, causing LQTS1, in which arrhythmias, expressed as double spikes or small events between spikes could be detected regularly [39], I did not detect arrhythmic events in SCN5A mutant cells in my Calcium Imaging analyses regularly. Interestingly, the Calcium Imaging analysis shows similar results to the Ca^{2+} analysis of Pierre et al., in which NaV1.5-knockout iPSC-derived CMs were studied [60]. Pierre et al. showed a reduced amplitude, duration, half time to peak and decay speed in their calcium transient characteristics [60], which are comparable results to the results obtained here. Furthermore, the insights gained here are comparable to the findings of Moureen [54], who also studied iPSC-derived CMs with LQTS caused by SCN5A mutations. Except for the spontaneous beat frequency, which was decreased in the analysis of this study and found increased by Moureen [54], all parameters show the same results. Time of peak/duration, half with, rise time and decay time are reduced in the SCN5A mutated cells. Except for rise time, the reduction is significant, in comparison to the wildtype SCN5A iPSC-derived CMs, comparable to the results presented here. These results are contrary to what I would actually expect in LQTS, because according to the prolonged action potential duration in LQTS cells, the Ca^{2+} transients should be prolonged, as described by Spencer et al. [87]. It would also be possible that our SCN5A mutation causes simultaneous presence of LQTS and Brugada syndrome, comparable to the SCN5A E1784K mutation [49, 90], which could explain why my electrophysical findings do not match with the typical results for LQTS [8].

To further explore electrophysiology, the field potential of iPSC-derived CMs by MEA was determined. Comparison of field potential duration (FPD) and corrected field potential duration (FPDc) showed no significant differences between control and SCN5A$^{1072T>C}$ cells. I only detected a significant difference in the conduction velocity, which was lower for the SCN5A mutant cells than for the control cells.

These results also do not match the typical electrophysiological presentation of a LQTS. In LQTS the FPD would have to be prolonged according to the action potential duration (APD), as it was shown for LQTS1 by Egashira et al. [21], for

LQTS2 in KCNH2-knockout hESC-derived CMs by Chang et al. [14], for other SCN5A mutations with a LQTS phenotype [32] and for mixed long-QT/Brugada syndrome phenotype [58]. Also, in the analysis of a APD, which has been shown to be comparable to FPD in different parameters such as rise time and duration [30], Ma et al. reported a APD prolongation in LQTS iPSC-derived CMs, especially in ventricular-like iPSC-derived CMs [48]. Other studies show no significant prolongation but a tendency to prolonged APD [22]. However, because my analyses were performed with a relatively small number of cells, the results need to be confirmed in larger analyses.

Because our laboratory has no expertise in the Patch-Clamp technique required to perform the measurement of single cell currents and action potentials, the examinations will be carried out by our collaborators in Marburg (AG Prof. Dr. Decher). Another issue that must always be considered when analyzing iPSC-derived cardiomyocytes is the immaturity of the cardiomyocytes [82]. One way to make the iPSC-derived CMs more representative of the adult phenotype is to keep the cells in culture for a long time before performing the experiments. Nevertheless, the iPSC-derived CMs do not fully exhibit an adult phenotype and always show embryonic characteristics as well. This circumstance could mean that diseases that only occur at a later age can only be modeled to a limited extent with iPSC-derived CMs. This fact should be considered, when the experimental results are interpreted and discussed.

For further differentiation, however, more detailed electrophysiological studies, are necessary. In order to make more differentiated observations, the single different ionic currents at the cardiomyocyte cell membrane could be measured. Also, the Na^+ current itself can be investigated more specifically and can be differentiated into a peak and a late Na^+ current. These studies would provide more detailed information about the behavior of the Na^+ currents and give more specific ideas of the pathophysiology of the $SCN5A^{1072T>C}$ mutation and how it is affecting the functionality of the NaV1.5 channel [31].

4.4. SCN5A$^{1072T>C}$ mutation causes QT-prolongation in embryo zebrafish at 72hpf

Since zebrafish and human heart electrophysiology are quite comparable, to study our SCN5A mutation in vitro and to assess the effects on whole heart electrophysiology, ECG were recorded on transgenic zebrafish embryos, overexpressing SCN5A$^{1072T>C}$. In earlier developmental stages at the time of 48hpf, the transgenic fish line showed only a slightly increased heart rate compared to wildtype zebrafish of the same age, whereas the QTc (Fridericia) were very similar to each other. At 72hpf, the SCN5A transgenic zebrafish showed significantly longer QTc (Fridericia) than the wildtype control fish, and likewise, a decreased heart rate was found in the mutants. The methodology of recording ECG in embryonic zebrafish has already been performed by others, such as from Frouhouhar et al. [24], who report the technique in detail, and Dhillon et al. [20], who optimized the technique and went into more detail on the analysis of QT time by examining the effects of QT time-prolonging drugs on the ECGs of zebrafish embryos. ECG of embryonic zebrafish have already been described for LQTS2 by Tanaka et al. [93], who studied the E637K mutation in the KCNH2 gene, in 72hpf zebrafish embryos by knocking down KCNH2 with Morpholinos. KCNH2 knockdown caused a prolongation of QTc that could be reversed by the injection of WT cRNA but not mutated KCNH2 cRNA.

Several ECG studies on zebrafish, for different SCN5A mutations, have already been reported in the literature. In the studies of Huttner et al. [36] the D1275N mutation in SCN5A was investigated. Huttner et al. studied mainly adult zebrafish. Comparable to my analysis, they found a reduced heart rate in their fish. In contrast to our findings, Huttner et al. showed an unaltered QTc time, but a prolonged PR interval and a widened QRS duration. Furthermore, models exist for LQTS triggered by SCN5A mutations in mice. Tian et al. [96] showed a QTc prolongation in mice ECG due to the SCN5A N1325S mutation, but no change in QRS complex duration, fitting our results.

To have more consistent results, the ECG recorded on TÜAB embryos overexpressing SCN5A$^{1072T>C}$ will be compared to ECG recorded on TÜAB embryos overexpressing the human WT SCN5A gene. In addition, it would be interesting to investigate whether the application of different drugs could reverse the LQTS

phenotype and to explore in further steps whether mutation-specific and personalized therapy will eventually be possible.

4.5. Conclusion and comparative analysis of *in vitro* and *in vivo* results

In synopsis, the results from the *in vitro* analyses in iPSC-derived CMs and the *in vivo* analyses in embryonic zebrafish are considered here in the context of each other. Structural differences could not be detected in the iPSC-derived CMs in the heterozygous state. The structural effects of the mutation on the hearts of zebrafish embryos, were investigated by Maximiliane Däuwel [19] from our laboratory and can be found in her thesis. She also studied SCN5A gene expression of zebrafish embryos. Concerning the gene expression of the patient iPSC-derived ventricular CMs, SCN5A, SERCA2a and RyR showed no expression differences in comparison to isogenic control iPSC-derived ventricular CMs.

Comparing the functional aspects, it is notable that the reduced beating frequency at the timepoint when QT-time prolongation manifests in SCN5A$^{1072T>C}$ transgenic zebrafish coincides with the reduced beating frequency of iPSC-derived CMs in Calcium Imaging. Zebrafish at 72hpf, like iPSC-derived ventricular CMs, show reduced beating frequency. The analysis of calcium dynamics on the zebrafish heart was also performed by Maximiliane Däuwel [19]. For the iPSC-derived ventricular CMs we can summarize that there is a decrease in time of peak, half width, rise time and decay time for the patient iPSC-derived ventricular CMs compared to the isogenic control. Since the electrophysiological experiments of the embryo zebrafish heart that go beyond Calcium Imaging still need to be carried out by our collaborators in Marburg we can only say that in MEA analysis of iPSC-derived ventricular CMs I did not observe major impairments of FPD, FPD and Conduction Velocity.

In summary, I could show that there are functional effects, especially in Calcium cycling, by the SCN5A$^{1072T>C}$ mutation in heterozygotic conditions. For further specification, the final statement about a causal role in long QT syndrome and the revealing of the exact mechanisms, more research is necessary.

5. Summary

Mutations in the sodium voltage-gated channel alpha subunit 5 (SCN5A) gene, encoding the voltage-gated sodium channel NaV1.5 primarily found in cardiac tissue, have been implicated in various cardiac disorders, including long QT syndrome type 3 (LQTS3). This dissertation investigates the potential causative role of the SCN5A$^{1072T>C}$ mutation in the development of LQTS, by utilizing induced pluripotent stem cells (iPSC) derived from a patient with clinically diagnosed LQTS. Using Clustered Regularly Interspaced Short Palindromic Repeats/CRISPR-associated protein 9 (CRISPR/Cas9), an isogenic control cell line was generated by correcting the mutation and replacing it with the wildtype base. In addition, a transgenic SCN5A$^{1072T>C}$ zebrafish line was used to study the electrophysiology of the embryos' hearts by recording electrocardiograms (ECG).

I was able to show that the fibroblasts of the patient could be successfully reprogrammed to iPSC, showing that the mutation does not interfere with the reprogramming procedure. Moreover, differentiation to iPSC-derived ventricular cardiomyocytes was also sufficient and not affected by the mutation. No major structural impairments in the sarcomere structure and no modified localization of NaV1.5 were induced by the mutation. Similarly, protein expression of SCN5A did not differ between the mutant and control iPSC-derived ventricular cardiomyocytes. In addition, no altered localization was detected and SCN5A protein was shown to be localized in the cell membrane in both cell lines. These results were also confirmed by quantitative reverse transcription polymerase chain reaction (qRT-PCR), which showed no significant differences in the expression levels of SCN5A but also the sarcoplasmic/endoplasmic reticulum Ca^{2+}-ATPase 2a (SERCA2a), and ryanodine receptor (RyR) expression levels were unaltered, when comparing mutant and corrected iPSC-derived ventricular cardiomyocytes (CMs). Thus, structural impairments due to the SCN5A$^{1072T>C}$ mutation could not be observed in these studies. However, differences were detected in the functional analysis, for which Calcium Imaging was performed. Calcium currents were impaired in the mutant iPSC-derived ventricular CMs and also the beating frequency was significantly decreased in the mutant cells compared with the corrected wildtype iPSC-derived ventricular CMs. In contrast, electrophysiological analysis of field potentials did not reveal major differences between the mutant and corrected iPSC-derived ventricular CMs. The ECG of embryonic zebrafish did not yet show distinct

differences compared with wildtype at 48 hours post fertilization (hpf), but at 72hpf they showed a significantly prolonged QT time, mainly caused by ST-interval prolongation. In accordance with this, the mutant fish showed a reduced beating frequency at the age 72hpf, which would fit the clinical presentation of a LQTS.

Overall, I found that the SCN5A$^{1072T>C}$ mutation did not lead to significant structural differences, nor did it affect the expression of the SCN5A gene. However, significant alterations were observed, particularly in the dynamics of calcium currents and in the QT interval in the TgSCN5A$^{1072T>C}$ zebrafish ECG, where a clear QT prolongation could be detected.

6. Bibliography

1. Adler A, Novelli V, Amin AS, Abiusi E, Care M, Nannenberg EA, Feilotter H, Amenta S, Mazza D, Bikker H, Sturm AC, Garcia J, Ackerman MJ, Hershberger RE, Perez MV, Zareba W, Ware JS, Wilde AAM, Gollob MH (2020) An International, Multicentered, Evidence-Based Reappraisal of Genes Reported to Cause Congenital Long QT Syndrome. Circulation 141:418–428. doi: 10.1161/CIRCULATIONAHA.119.043132

2. Agrotis A, Ketteler R (2015) A new age in functional genomics using CRISPR/Cas9 in arrayed library screening. Front Genet 6:300. doi: 10.3389/fgene.2015.00300

3. Aljabali AAA, El-Tanani M, Tambuwala MM (2024) Principles of CRISPR-Cas9 technology: Advancements in genome editing and emerging trends in drug delivery. J Drug Deliv Sci Technol 92:105338. doi: 10.1016/j.jddst.2024.105338

4. Aronsen JM, Swift F, Sejersted OM (2013) Cardiac sodium transport and excitation–contraction coupling. J Mol Cell Cardiol 61:11–19. doi: 10.1016/j.yjmcc.2013.06.003

5. Auman HJ, Coleman H, Riley HE, Olale F, Tsai H-J, Yelon D (2007) Functional Modulation of Cardiac Form through Regionally Confined Cell Shape Changes. PLoS Biol 5:e53. doi: 10.1371/journal.pbio.0050053

6. Bagnall RD, Weintraub RG, Ingles J, Duflou J, Yeates L, Lam L, Davis AM, Thompson T, Connell V, Wallace J, Naylor C, Crawford J, Love DR, Hallam L, White J, Lawrence C, Lynch M, Morgan N, James P, Du Sart D, Puranik R, Langlois N, Vohra J, Winship I, Atherton J, McGaughran J, Skinner JR, Semsarian C (2016) A Prospective Study of Sudden Cardiac Death among Children and Young Adults. N Engl J Med 374:2441–2452. doi: 10.1056/NEJMoa1510687

7. Bakkers J (2011) Zebrafish as a model to study cardiac development and human cardiac disease. Cardiovasc Res 91:279–288. doi: 10.1093/cvr/cvr098

8. Baroudi G, Chahine M (2000) Biophysical phenotypes of *SCN5A* mutations causing long QT and Brugada syndromes. FEBS Lett 487:224–228. doi: 10.1016/S0014-5793(00)02360-7

9. Bedada FB, Wheelwright M, Metzger JM (2016) Maturation status of sarcomere structure and function in human iPSC-derived cardiac myocytes. Biochim Biophys Acta Mol Cell Res 1863:1829–1838. doi: 10.1016/j.bbamcr.2015.11.005

10. Ben Jehuda R, Shemer Y, Binah O (2018) Genome Editing in Induced Pluripotent Stem Cells using CRISPR/Cas9. Stem Cell Rev and Rep 14:323–336. doi: 10.1007/s12015-018-9811-3

11. Bennett PB, Yazawa K, Makita N, George AL (1995) Molecular mechanism for an inherited cardiac arrhythmia. Nature 376:683–685. doi: 10.1038/376683a0

12. Burkhard S, Van Eif V, Garric L, Christoffels V, Bakkers J (2017) On the Evolution of the Cardiac Pacemaker. J Cardiovasc Dev Dis 4:4. doi: 10.3390/jcdd4020004

13. Calvet C, Seebeck P (2023) What to consider for ECG in mice—with special emphasis on telemetry. Mamm Genome 34:166–179. doi: 10.1007/s00335-023-09977-0

14. Chang Y, Li Y, Bai R, Wu F, Ma S, Saleem A, Zhang S, Jiang Y, Dong T, Guo T, Hang C, Lu W, Jiang H, Lan F (2021) hERG-deficient human embryonic stem cell-derived cardiomyocytes for modelling QT prolongation. Stem Cell Res Ther 12:278. doi: 10.1186/s13287-021-02346-1

15. Charpentier E, Doudna JA (2013) Rewriting a genome. Nature 495:50–51. doi: 10.1038/495050a

16. Cho SW, Kim S, Kim JM, Kim J-S (2013) Targeted genome engineering in human cells with the Cas9 RNA-guided endonuclease. Nat Biotechnol 31:230–232. doi: 10.1038/nbt.2507

17. Clancy CE, Rudy Y (2002) Na(+) channel mutation that causes both Brugada and long-QT syndrome phenotypes: a simulation study of mechanism. Circulation 105:1208–1213. doi: 10.1161/hc1002.105183

18. Cong L, Ran FA, Cox D, Lin S, Barretto R, Habib N, Hsu PD, Wu X, Jiang W, Marraffini LA, Zhang F (2013) Multiplex Genome Engineering Using CRISPR/Cas Systems. Science 339:819–823. doi: 10.1126/science.1231143

19. Däuwel, M: (unpublished findings)

20. Dhillon SS, Dóró É, Magyary I, Egginton S, Sík A, Müller F (2013) Optimisation of Embryonic and Larval ECG Measurement in Zebrafish for Quantifying the Effect of QT Prolonging Drugs. PLoS One 8:e60552. doi: 10.1371/journal.pone.0060552

21. Egashira T, Yuasa S, Suzuki T, Aizawa Y, Yamakawa H, Matsuhashi T, Ohno Y, Tohyama S, Okata S, Seki T, Kuroda Y, Yae K, Hashimoto H, Tanaka T, Hattori F, Sato T, Miyoshi S, Takatsuki S, Murata M, Kurokawa J, Furukawa T, Makita N, Aiba T, Shimizu W, Horie M, Kamiya K, Kodama I, Ogawa S, Fukuda K (2012) Disease characterization using LQTS-specific induced pluripotent stem cells. Cardiovasc Res 95:419–429. doi: 10.1093/cvr/cvs206

22. Fatima A, Kaifeng S, Dittmann S, Xu G, Gupta MK, Linke M, Zechner U, Nguemo F, Milting H, Farr M, Hescheler J, Šarić T (2013) The Disease-Specific Phenotype in Cardiomyocytes Derived from Induced Pluripotent Stem Cells of Two Long QT Syndrome Type 3 Patients. PLoS One 8:e83005. doi: 10.1371/journal.pone.0083005

23. Food and Drug Administration I Precision Medicine. https://www.fda.gov/medical devices/in-vitro-diagnostics/precision-medicine. Accessed 18 Mar 2023

24. Forouhar AS, Hove JR, Calvert C, Flores J, Jadvar H, Gharib M (2004) Electrocardiographic Characterization of Embryonic Zebrafish. Conf Proc IEEE Eng Med Biol Soc 2004:3615–3617. doi: 10.1109/IEMBS.2004.1404016

25. Frigo G, Rampazzo A, Bauce B, Pilichou K, Beffagna G, Danieli GA, Nava A, Martini B (2007) Homozygous SCN5A mutation in Brugada syndrome with monomorphic ventricular tachycardia and structural heart abnormalities. EP Europace 9:391–397. doi: 10.1093/europace/eum053

26. Funakoshi S, Yoshida Y (2021) Recent progress of iPSC technology in cardiac diseases. Arch Toxicol 95:3633–3650. doi: 10.1007/s00204-021-03172-3

27. GBD 2017 Causes of Death Collaborators (2018) Global, regional, and national age-sex specific mortality for 282 causes of death in 195 countries and territories, 1980-2017: a systematic analysis for the Global Burden of Disease Study 2017. Lancet 392:1736–1788. doi: 10.1016/S0140-6736(18)32203-7

28. Goetz LH, Schork NJ (2018) Personalized medicine: motivation, challenges, and progress. Fertil Steril 109:952–963. doi: 10.1016/j.fertnstert.2018.05.006

29. Goldenberg I, Moss AJ, Zareba W (2006) QT Interval: How to Measure It and What Is “Normal.” Cardiovasc Electrophysiol 17:333–336. doi: 10.1111/j.1540-8167.2006.00408.x

30. Halbach M, Egert U, Hescheler J, Banach K (2003) Estimation of Action Potential Changes from Field Potential Recordings in Multicellular Mouse Cardiac Myocyte Cultures. Cell Physiol Biochem 13:271–284. doi: 10.1159/000074542

31. Han D, Tan H, Sun C, Li G (2018) Dysfunctional Nav1.5 channels due to SCN5A mutations. Exp Biol Med 243:852–863. doi: 10.1177/1535370218777972

32. Hayama E, Furutani Y, Kawaguchi N, Seki A, Nagashima Y, Okita K, Takeuchi D, Matsuoka R, Inai K, Hagiwara N, Nakanishi T (2021) Induced Pluripotent Stem Cell-Derived Cardiomyocytes with SCN5A R1623Q Mutation Associated with Severe Long QT Syndrome in Fetuses and Neonates Recapitulates Pathophysiological Phenotypes. Biology 10:1062. doi: 10.3390/biology10101062

33. Hosen A, Nishat MNH, Soaib MdMH, Sharkar OS, Sahabuddin Md, Sharif IH, Bhajan SK (2025) A Review: CRISPR Cas System and the Mechanism With an Inhibition of Binding of CRISPR Cas-9. Nano Sel 6:e202400009. doi: 10.1002/nano.202400009

34. Howe K, Clark MD, Torroja CF, Torrance J, Berthelot C, Muffato M, Collins JE, Humphray S, McLaren K, Matthews L, McLaren S, Sealy I, Caccamo M, Churcher C, Scott C, Barrett JC, Koch R, Rauch G-J, White S, Chow W, Kilian B, Quintais LT, Guerra-Assunção JA, Zhou Y, Gu Y, Yen J, Vogel J-H, Eyre T, Redmond S, Banerjee R, Chi J, Fu B, Langley E, Maguire SF, Laird GK, Lloyd D, Kenyon E, Donaldson S, Sehra H, Almeida-King J, Loveland J, Trevanion S, Jones M, Quail M, Willey D, Hunt A, Burton J, Sims S, McLay K, Plumb B, Davis J, Clee C, Oliver K, Clark R, Riddle C, Elliott D, Threadgold G, Harden G, Ware D, Begum S, Mortimore B, Kerry G, Heath P, Phillimore B, Tracey A, Corby N, Dunn M, Johnson C, Wood J, Clark S, Pelan S, Griffiths G, Smith M, Glithero R, Howden P, Barker N, Lloyd C, Stevens C, Harley J, Holt K, Panagiotidis G, Lovell J, Beasley H, Henderson C, Gordon D, Auger K, Wright D, Collins J, Raisen C, Dyer L, Leung K, Robertson L, Ambridge K, Leongamornlert D, McGuire S, Gilderthorp R, Griffiths C, Manthravadi D, Nichol S, Barker G, Whitehead S, Kay M, Brown J, Murnane C, Gray E, Humphries M, Sycamore N, Barker D, Saunders D, Wallis J, Babbage A, Hammond S, Mashreghi-Mohammadi M, Barr L, Martin S, Wray P, Ellington A, Matthews N, Ellwood M, Woodmansey R, Clark G, Cooper JD, Tromans A, Grafham D, Skuce C, Pandian R, Andrews R, Harrison E, Kimberley A, Garnett J, Fosker N, Hall R, Garner P, Kelly D, Bird C, Palmer S, Gehring I, Berger A, Dooley CM, Ersan-Ürün Z, Eser C, Geiger H, Geisler M, Karotki L, Kirn A, Konantz J, Konantz M, Oberländer M, Rudolph-Geiger S, Teucke M, Lanz C, Raddatz G, Osoegawa K, Zhu B, Rapp A, Widaa S, Langford C, Yang F, Schuster SC, Carter NP, Harrow J, Ning Z, Herrero J, Searle SMJ, Enright A, Geisler R, Plasterk RHA, Lee C, Westerfield M, De Jong PJ, Zon LI, Postlethwait JH, Nüsslein-Volhard C, Hubbard TJP, Crollius HR, Rogers J, Stemple DL (2013) The zebrafish reference genome sequence and its relationship to the human genome. Nature 496:498–503. doi: 10.1038/nature12111

35. Hryhorowicz M, Lipiński D, Zeyland J, Słomski R (2017) CRISPR/Cas9 Immune System as a Tool for Genome Engineering. Arch Immunol Ther Exp 65:233–240. doi: 10.1007/s00005-016-0427-5

36. Huttner IG, Trivedi G, Jacoby A, Mann SA, Vandenberg JI, Fatkin D (2013) A transgenic zebrafish model of a human cardiac sodium channel mutation exhibits bradycardia, conduction-system abnormalities and early death. J Mol Cell Cardiol 61:123–132. doi: 10.1016/j.yjmcc.2013.06.005

37. Jervell A, Lange-Nielsen F (1957) Congenital deaf-mutism, functional heart disease with prolongation of the Q-T interval, and sudden death. Am Heart J 54:59–68. doi: 10.1016/0002-8703(57)90079-0

38. Jinek M, Chylinski K, Fonfara I, Hauer M, Doudna JA, Charpentier E (2012) A Programmable Dual-RNA–Guided DNA Endonuclease in Adaptive Bacterial Immunity. Science 337:816–821. doi: 10.1126/science.1225829

39. Kiviaho AL, Ahola A, Larsson K, Penttinen K, Swan H, Pekkanen-Mattila M, Venäläinen H, Paavola K, Hyttinen J, Aalto-Setälä K (2015) Distinct electrophysiological and mechanical beating phenotypes of long QT syndrome type 1-specific cardiomyocytes

carrying different mutations. Int J Cardiol Heart Vasc 8:19–31. doi: 10.1016/j.ijcha.2015.04.008

40. Kleinsorge M, Cyganek L (2020) Subtype-Directed Differentiation of Human iPSCs into Atrial and Ventricular Cardiomyocytes. STAR Protoc 1:100026. doi: 10.1016/j.xpro.2020.100026

41. Kumar A, Avishay DM, Jones CR, Shaikh JD, Kaur R, Aljadah M, Kichloo A, Shiwalkar N, Keshavamurthy S (2021) Sudden cardiac death: epidemiology, pathogenesis and management. Rev Cardiovasc Med 22:147. doi: 10.31083/j.rcm.2021.01.207

42. Kyle JW, Makielski JC (2014) Diseases Caused by Mutations in Nav1.5 Interacting Proteins. Cardiac Electrophysiol Clin 6:797–809. doi: 10.1016/j.ccep.2014.08.007

43. Lahrouchi N, Behr ER, Bezzina CR (2016) Next-Generation Sequencing in Post-mortem Genetic Testing of Young Sudden Cardiac Death Cases. Front Cardiovasc Med 3:13. doi: 10.3389/fcvm.2016.00013

44. Leong IUS, Skinner JR, Shelling AN, Love DR (2010) Zebrafish as a model for long QT syndrome: the evidence and the means of manipulating zebrafish gene expression. Acta Physiol 199:257–276. doi: 10.1111/j.1748-1716.2010.02111.x

45. Li W, Yin L, Shen C, Hu K, Ge J, Sun A (2018) SCN5A Variants: Association With Cardiac Disorders. Front Physiol 9:1372. doi: 10.3389/fphys.2018.01372

46. Li Y, Nguyen HV, Tsang SH (2016) Skin Biopsy and Patient-Specific Stem Cell Lines. Methods Mol Biol 1353:77–88. doi: 10.1007/7651_2015_225

47. London B (2001) Cardiac Arrhythmias: From (Transgenic) Mice to Men. J Cardiovasc Electrophysiol 12:1089–1091. doi: 10.1046/j.1540-8167.2001.01089.x

48. Ma D, Wei H, Zhao Y, Lu J, Li G, Sahib NBE, Tan TH, Wong KY, Shim W, Wong P, Cook SA, Liew R (2013) Modeling type 3 long QT syndrome with cardiomyocytes derived from patient-specific induced pluripotent stem cells. Int J Cardiol 168:5277–5286. doi: 10.1016/j.ijcard.2013.08.015

49. Makita N, Behr E, Shimizu W, Horie M, Sunami A, Crotti L, Schulze-Bahr E, Fukuhara S, Mochizuki N, Makiyama T, Itoh H, Christiansen M, McKeown P, Miyamoto K, Kamakura S, Tsutsui H, Schwartz PJ, George AL, Roden DM (2008) The E1784K mutation in SCN5A is associated with mixed clinical phenotype of type 3 long QT syndrome. J Clin Invest 118:2219–2229. doi: 10.1172/JCI34057

50. Malan D, Friedrichs S, Fleischmann BK, Sasse P (2011) Cardiomyocytes Obtained From Induced Pluripotent Stem Cells With Long-QT Syndrome 3 Recapitulate Typical Disease-Specific Features In Vitro. Circ Res 109:841–847. doi: 10.1161/CIRCRESAHA.111.243139

51. Mali P, Yang L, Esvelt KM, Aach J, Guell M, DiCarlo JE, Norville JE, Church GM (2013) RNA-Guided Human Genome Engineering via Cas9. Science 339:823–826. doi: 10.1126/science.1232033

52. Marotta D, Rao C, Fossati V (2022) Human Induced Pluripotent Stem Cell (iPSC) Handling Protocols: Maintenance, Expansion, and Cryopreservation. Methods Mol Biol 2454:1–15. doi: 10.1007/7651_2021_358

53. McGrath S, Ghersi D (2016) Building towards precision medicine: empowering medical professionals for the next revolution. BMC Med Genomics 9:23. doi: 10.1186/s12920-016-0183-8

54. Moureen FS (2019) Study of calcium dynamics in hiPSC -derived cardiomyocytes. Master´s Thesis, University of Helsinki

55. Nemtsas P, Wettwer E, Christ T, Weidinger G, Ravens U (2010) Adult zebrafish heart as a model for human heart? An electrophysiological study. J Mol Cell Cardiol 48:161–171. doi: 10.1016/j.yjmcc.2009.08.034

56. Neu A, Eiselt M, Paul M, Sauter K, Stallmeyer B, Isbrandt D, Schulze-Bahr E (2010) A homozygous SCN5A mutation in a severe, recessive type of cardiac conduction disease. Hum Mutat 31:E1609–E1621. doi: 10.1002/humu.21302

57. NHS England, Medical Directorate. Medicines, Diagnostics and Personalized Medicine Unit, Graham E I Improving Outcomes trough Personalized Medicine. https://www.england.nhs.uk/wp-content/uploads/2016/09/improving-outcomes-personalised-medicine.pdf. Accessed 10 Mar 2023

58. Okata S, Yuasa S, Suzuki T, Ito S, Makita N, Yoshida T, Li M, Kurokawa J, Seki T, Egashira T, Aizawa Y, Kodaira M, Motoda C, Yozu G, Shimojima M, Hayashiji N, Hashimoto H, Kuroda Y, Tanaka A, Murata M, Aiba T, Shimizu W, Horie M, Kamiya K, Furukawa T, Fukuda K (2016) Embryonic type Na+ channel β-subunit, SCN3B masks the disease phenotype of Brugada syndrome. Sci Rep 6:34198. doi: 10.1038/srep34198

59. Patten BM (1949) Initiation and early changes in the character of the heart beat in vertebrate embryos. Physiol Rev 29:31–47. doi: 10.1152/physrev.1949.29.1.31

60. Pierre M, Djemai M, Poulin H, Chahine M (2021) NaV1.5 knockout in iPSCs: a novel approach to study NaV1.5 variants in a human cardiomyocyte environment. Sci Rep 11:17168. doi: 10.1038/s41598-021-96474-6

61. Poon KL, Brand T (2013) The zebrafish model system in cardiovascular research: A tiny fish with mighty prospects. Glob Cardiol Sci Pract 2013:9-28. doi: 10.5339/gcsp.2013.4

62. Porretta AP, Probst V, Bhuiyan ZA, Davoine E, Delinière A, Pascale P, Schlaepfer J, Superti-Furga A, Pruvot E (2022) SCN5A overlap syndromes: An open-minded approach. Heart Rhythm 19:1363–1368. doi: 10.1016/j.hrthm.2022.03.1223

63. Postema PG, Van Den Berg MP, Van Tintelen JP, Van Den Heuvel F, Grundeken M, Hofman N, Van Der Roest WP, Nannenberg EA, Krapels IPC, Bezzina CR, Wilde AAM (2009) Founder mutations in the Netherlands: SCN5a 1795insD, the first described arrhythmia overlap syndrome and one of the largest and best characterised families worldwide. Neth Heart J 17:422–428. doi: 10.1007/BF03086296

64. Ramaswami R, Bayer R, Galea S (2018) Precision Medicine from a Public Health Perspective. Annu Rev Public Health 39:153–168. doi: 10.1146/annurev-publhealth-040617-014158

65. Remme CA (2023) SCN5A channelopathy: arrhythmia, cardiomyopathy, epilepsy and beyond. Phil Trans R Soc B 378:20220164. doi: 10.1098/rstb.2022.0164

66. Remme CA, Bezzina CR (2010) Sodium Channel (dys)function and cardiac arrhythmias. Cardiovasc Ther 28:287–294. doi: 10.1111/j.1755-5922.2010.00210.x

67. Remme CA, Verkerk AO, Nuyens D, Van Ginneken ACG, Van Brunschot S, Belterman CNW, Wilders R, Van Roon MA, Tan HL, Wilde AAM, Carmeliet P, De Bakker JMT, Veldkamp MW, Bezzina CR (2006) Overlap Syndrome of Cardiac Sodium Channel Disease in Mice Carrying the Equivalent Mutation of Human *SCN5A* -1795insD. Circulation 114:2584–2594. doi: 10.1161/CIRCULATIONAHA.106.653949

68. Remme CA, Wilde AAM, Bezzina CR (2008) Cardiac Sodium Channel Overlap Syndromes: Different Faces of SCN5A Mutations. Trends Cardiovasc Med 18:78–87. doi: 10.1016/j.tcm.2008.01.002

69. Rocchetti M, Sala L, Dreizehnter L, Crotti L, Sinnecker D, Mura M, Pane LS, Altomare C, Torre E, Mostacciuolo G, Severi S, Porta A, De Ferrari GM, George AL, Schwartz PJ, Gnecchi M, Moretti A, Zaza A (2017) Elucidating arrhythmogenic mechanisms of long-QT syndrome CALM1-F142L mutation in patient-specific induced pluripotent stem cell-derived cardiomyocytes. Cardiovasc Res 113:531–541. doi: 10.1093/cvr/cvx006

70. Ryan SD, Dolatabadi N, Chan SF, Zhang X, Akhtar MW, Parker J, Soldner F, Sunico CR, Nagar S, Talantova M, Lee B, Lopez K, Nutter A, Shan B, Molokanova E, Zhang Y, Han X, Nakamura T, Masliah E, Yates JR, Nakanishi N, Andreyev AY, Okamoto S, Jaenisch R, Ambasudhan R, Lipton SA (2013) Isogenic Human iPSC Parkinson's Model Shows Nitrosative Stress-Induced Dysfunction in MEF2-PGC1α Transcription. Cell 155:1351–1364. doi: 10.1016/j.cell.2013.11.009

71. Sala L, Yu Z, Ward-van Oostwaard D, Van Veldhoven JP, Moretti A, Laugwitz K, Mummery CL, IJzerman AP, Bellin M (2016) A new hERG allosteric modulator rescues genetic and drug-induced long-QT-syndrome phenotypes in cardiomyocytes from isogenic pairs of patient induced pluripotent stem cells. EMBO Mol Med 8:1065–1081. doi: 10.15252/emmm.201606260

72. Savio-Galimberti E, Argenziano M, Antzelevitch C (2018) Cardiac Arrhythmias Related to Sodium Channel Dysfunction. Handb Exp Pharmacol 246:331–354. doi: 10.1007/164_2017_43

73. Sayed N, Liu C, Wu JC (2016) Translation of Human-Induced Pluripotent Stem Cells. J Am Coll Cardiol 67:2161–2176. doi: 10.1016/j.jacc.2016.01.083

74. Schwartz PJ, Ackerman MJ, George AL, Wilde AAM (2013) Impact of Genetics on the Clinical Management of Channelopathies. J Am Coll Cardiol 62:169–180. doi: 10.1016/j.jacc.2013.04.044

75. Schwartz PJ, Crotti L, Insolia R (2012) Long-QT Syndrome: From Genetics to Management. Circ Arrhythm Electrophysiol 5:868–877. doi: 10.1161/CIRCEP.111.962019

76. Schwartz PJ, Moss AJ, Vincent GM, Crampton RS (1993) Diagnostic criteria for the long QT syndrome. An update. Circulation 88:782–784. doi: 10.1161/01.CIR.88.2.782

77. Schwartz PJ, Priori SG, Spazzolini C, Moss AJ, Vincent GM, Napolitano C, Denjoy I, Guicheney P, Breithardt G, Keating MT, Towbin JA, Beggs AH, Brink P, Wilde AAM, Toivonen L, Zareba W, Robinson JL, Timothy KW, Corfield V, Wattanasirichaigoon D, Corbett C, Haverkamp W, Schulze-Bahr E, Lehmann MH, Schwartz K, Coumel P, Bloise R (2001) Genotype-Phenotype Correlation in the Long-QT Syndrome: Gene-Specific Triggers for Life-Threatening Arrhythmias. Circulation 103:89–95. doi: 10.1161/01.CIR.103.1.89

78. Schwartz PJ, Stramba-Badiale M, Crotti L, Pedrazzini M, Besana A, Bosi G, Gabbarini F, Goulene K, Insolia R, Mannarino S, Mosca F, Nespoli L, Rimini A, Rosati E, Salice P, Spazzolini C (2009) Prevalence of the Congenital Long-QT Syndrome. Circulation 120:1761–1767. doi: 10.1161/CIRCULATIONAHA.109.863209

79. Sedmera D, Reckova M, deAlmeida A, Sedmerova M, Biermann M, Volejnik J, Sarre A, Raddatz E, McCarthy RA, Gourdie RG, Thompson RP (2003) Functional and morphological evidence for a ventricular conduction system in zebrafish and *Xenopus* hearts. Am J Physiol Heart Circ Physiol 284:H1152–H1160. doi: 10.1152/ajpheart.00870.2002

80. Semsarian C, Ingles J, Wilde AAM (2015) Sudden cardiac death in the young: the molecular autopsy and a practical approach to surviving relatives. Eur Heart J 36:1290–1296. doi: 10.1093/eurheartj/ehv063

81. Shi Y, Inoue H, Wu JC, Yamanaka S (2017) Induced pluripotent stem cell technology: a decade of progress. Nat Rev Drug Discov 16:115–130. doi: 10.1038/nrd.2016.245

82. Sinnecker D, Goedel A, Laugwitz K-L, Moretti A (2013) Induced Pluripotent Stem Cell-Derived Cardiomyocytes: A Versatile Tool for Arrhythmia Research. Circ Res 112:961–968. doi: 10.1161/CIRCRESAHA.112.268623

83. Skinner JR, Winbo A, Abrams D, Vohra J, Wilde AA (2019) Channelopathies That Lead to Sudden Cardiac Death: Clinical and Genetic Aspects. Heart Lung Circ 28:22–30. doi: 10.1016/j.hlc.2018.09.007

84. Song M, Ramakrishna S (2018) Genome Editing in Stem Cells for Disease Therapeutics. Mol Biotechnol 60:329–338. doi: 10.1007/s12033-018-0072-9

85. Song W, Shou W (2012) Cardiac Sodium Channel Nav1.5 Mutations and Cardiac Arrhythmia. Pediatr Cardiol 33:943–949. doi: 10.1007/s00246-012-0303-y

86. Spence R, Gerlach G, Lawrence C, Smith C (2008) The behaviour and ecology of the zebrafish, Danio rerio. Biol Rev 83:13–34. doi: 10.1111/j.1469-185X.2007.00030.x

87. Spencer CI, Baba S, Nakamura K, Hua EA, Sears MAF, Fu C, Zhang J, Balijepalli S, Tomoda K, Hayashi Y, Lizarraga P, Wojciak J, Scheinman MM, Aalto-Setälä K, Makielski JC, January CT, Healy KE, Kamp TJ, Yamanaka S, Conklin BR (2014) Calcium Transients Closely Reflect Prolonged Action Potentials in iPSC Models of Inherited Cardiac Arrhythmia. Stem Cell Rep 3:269–281. doi: 10.1016/j.stemcr.2014.06.003

88. Stainier DYR (2001) Zebrafish genetics and vertebrate heart formation. Nat Rev Genet 2:39–48. doi: 10.1038/35047564

89. Stainier DYR, Lee RK, Fishman MC (1993) Cardiovascular development in the zebrafish I. Myocardial fate map and heart tube formation. Development 119:31–40. doi: 10.1242/dev.119.1.31

90. Sumitomo N (2014) E1784K Mutation in SCN5A and overlap syndrome. Circ J 78:1839–1840. doi: 10.1253/circj.CJ-14-0564

91. Takahashi K, Tanabe K, Ohnuki M, Narita M, Ichisaka T, Tomoda K, Yamanaka S (2007) Induction of Pluripotent Stem Cells from Adult Human Fibroblasts by Defined Factors. Cell 131:861–872. doi: 10.1016/j.cell.2007.11.019

92. Takahashi K, Yamanaka S (2006) Induction of Pluripotent Stem Cells from Mouse Embryonic and Adult Fibroblast Cultures by Defined Factors. Cell 126:663–676. doi: 10.1016/j.cell.2006.07.024

93. Tanaka Y, Hayashi K, Fujino N, Konno T, Tada H, Nakanishi C, Hodatsu A, Tsuda T, Nagata Y, Teramoto R, Yoshida S, Nomura A, Kawashiri M, Yamagishi M (2019) Functional analysis of KCNH2 gene mutations of type 2 long QT syndrome in larval zebrafish using microscopy and electrocardiography. Heart Vessels 34:159–166. doi: 10.1007/s00380-018-1231-4

94. Terns MP, Terns RM (2011) CRISPR-based adaptive immune systems. Curr Opin Microbiol 14:321–327. doi: 10.1016/j.mib.2011.03.005

95. Tester DJ, Ackerman MJ (2014) Genetics of Long QT Syndrome. Methodist Debakey Cardiovasc J 10:29-33. doi: 10.14797/mdcj-10-1-29

96. Tian XL YS Wan X, Wu L, Chung MK, Tchou PJ, Rosenbaum DS, van Wagoner DR, Kirsch GE, Wang Q (2004) Mechanisms by which SCN5A mutation N1325S causes cardiac arrhythmias and sudden death in vivo. Cardiovasc Res 61:256–267. doi: 10.1016/j.cardiores.2003.11.007

97. Verstraelen TE, Ter Bekke RMA, Volders PGA, Masclee AAM, Kruimel JW (2015) The role of the SCN5A-encoded channelopathy in irritable bowel syndrome and other gastrointestinal disorders. Neurogastroenterol Motil 27:906–913. doi: 10.1111/nmo.12569

98. Vornanen M, Hassinen M (2016) Zebrafish heart as a model for human cardiac electrophysiology. Channels 10:101–110. doi: 10.1080/19336950.2015.1121335

99. Wallace E, Howard L, Liu M, O'Brien T, Ward D, Shen S, Prendiville T (2019) Long QT Syndrome: Genetics and Future Perspective. Pediatr Cardiol 40:1419–1430. doi: 10.1007/s00246-019-02151-x

100. Wang AYL, Aviña AE, Liu Y-Y, Kao H-K (2025) Pluripotent Stem Cells: Recent Advances and Emerging Trends. Biomedicines 13:765. doi: 10.3390/biomedicines13040765

101. Ward OC (1964) A new familial cardiac syndrome in children. J Ir Med Assoc 54:103–106.

102. Wilde AAM, Amin AS (2018) Clinical Spectrum of SCN5A Mutations. JACC Clin Electrophysiol 4:569–579. doi: 10.1016/j.jacep.2018.03.006

103. Wilde AAM, Amin AS, Postema PG (2022) Diagnosis, management and therapeutic strategies for congenital long QT syndrome. Heart 108:332–338. doi: 10.1136/heartjnl-2020-318259

104. Wilde AAM, Brugada R (2011) Phenotypical Manifestations of Mutations in the Genes Encoding Subunits of the Cardiac Sodium Channel. Circ Res 108:884–897. doi: 10.1161/CIRCRESAHA.110.238469

105. Wong CX, Brown A, Lau DH, Chugh SS, Albert CM, Kalman JM, Sanders P (2019) Epidemiology of Sudden Cardiac Death: Global and Regional Perspectives. Heart Lung Circ 28:6–14. doi: 10.1016/j.hlc.2018.08.026

106. Yamanaka S (2020) Pluripotent Stem Cell-Based Cell Therapy—Promise and Challenges. Cell Stem Cell 27:523–531. doi: 10.1016/j.stem.2020.09.014

107. Ye L, Chang Y-H, Xiong Q, Zhang P, Zhang L, Somasundaram P, Lepley M, Swingen C, Su L, Wendel JS, Guo J, Jang A, Rosenbush D, Greder L, Dutton JR, Zhang J, Kamp TJ, Kaufman DS, Ge Y, Zhang J (2014) Cardiac Repair in a Porcine Model of Acute Myocardial Infarction with Human Induced Pluripotent Stem Cell-Derived Cardiovascular Cells. Cell Stem Cell 15:750–761. doi: 10.1016/j.stem.2014.11.009

108. Yu J, Vodyanik MA, Smuga-Otto K, Antosiewicz-Bourget J, Frane JL, Tian S, Nie J, Jonsdottir GA, Ruotti V, Stewart R, Slukvin II, Thomson JA (2007) Induced Pluripotent Stem Cell Lines Derived from Human Somatic Cells. Science 318:1917–1920. doi: 10.1126/science.1151526

109. Zipes DP, Camm AJ, Borggrefe M, Buxton AE, Chaitman B, Fromer M, Gregoratos G, Klein G, Moss AJ, Myerburg RJ, Priori SG, Quinones MA, Roden DM, Silka MJ, Tracy C, ESC Committee for Practice Guidelines, Priori SG, Blanc J-J, Budaj A, Camm AJ, Dean V, Deckers JW, Despres C, Dickstein K, Lekakis J, McGregor K, Metra M, Morais J, Osterspey A, Tamargo JL, Zamorano JL, ACC/AHA Task Force Members, Smith SC, Jacobs AK, Adams CD, Antman EM, Anderson JL, Hunt SA, Halperin JL, Nishimura R, Ornato JP, Page RL, Riegel B (2006) ACC/AHA/ESC 2006 guidelines for management of patients with ventricular arrhythmias and the prevention of sudden cardiac death: A report of the American College of Cardiology/American Heart Association Task Force and the European Society of Cardiology Committee for Practice Guidelines (Writing Committee to Develop Guidelines for Management of Patients With Ventricular Arrhythmias and the Prevention of Sudden Cardiac Death) Developed in collaboration with the European Heart

Rhythm Association and the Heart Rhythm Society. Europace 8:746–837. doi: 10.1093/europace/eul108

7. Acknowledgements

Die Danksagung wurde aus Gründen des Datenschutzes entfernt.

8. Curriculum Vitae

Der Lebenslauf wurde aus Gründen des Datenschutzes entfernt.